

Data-driven design of organic electronic materials

Présentée le 5 octobre 2023

Faculté des sciences de base
Laboratoire de design moléculaire computationnel
Programme doctoral en chimie et génie chimique

pour l'obtention du grade de Docteur ès Sciences

par

Jacob Terence BLASKOVITS

Acceptée sur proposition du jury

Prof. K. Sivula, président du jury
Prof. A.-C. Corminboeuf, directrice de thèse
Prof. R. Tykwinski, rapporteur
Prof. D. Casanova, rapporteur
Prof. F. Nüesch, rapporteur

[She] was just beginning to understand that the boys she knew, however incompetent they might seem, were going to turn into men, and be allowed to do things that you would think required a lot more talent and authority than they could have.

— Alice Munro, *Who Do You Think You Are?* (1978)

Computational papers such as this are of no value to science [...] and they should be discouraged.

— Reviewer 3, *Submission to Energy & Environmental Science* (2020)

To my wife

Acknowledgements

I am indebted to a number of people for the successful completion of this thesis.

Firstly, my advisor, Prof. Clémence Corminboeuf, for taking me on as a student, for her availability and efficient feedback on papers, projects, and presentations, despite her mind-boggling work schedule, and for her understanding when I was stuck in various and sundry locales during the COVID days. Most importantly, she provided me with the freedom to explore the research topics which interested me and to mold them according to my own ideas. Only after interacting with many other PhD students does one recognize the value of an advisor who enables that. This led to multiple projects, many of which are not presented in this thesis¹⁻⁵, in topics as diverse as my research interests.

Secondly, the postdocs and senior graduate students who guided, advised and assisted me in matters technical, conceptual, aesthetic, philosophical and political at various points throughout my thesis (in order of my first scientific interaction): Dr. Benjamin Meyer, Dr. Maria Fumanal, Dr. Sergi Vela, Dr. Shubhajit Das, Dr. Raimon Fabregat, Dr. Kun-Han Lin, Dr. Rubén Laplaza and Dr. Marc Garner. Whatever I've learned, it was thanks to the excellent researchers who surrounded me and imparted their wisdom upon me, specifically: Benjamin for machine learning; Maria for excited states; Sergi for dataset construction and management; Shubhajit for catalysis and skills in the arcane world of Gaussian keywords; Raimon for the computer science expertise and artistic talents; Kun-Han for all things materials science; Rubén for Python and data science; Marc for orbitals and symmetry.

Véronique Bujard, who provided administrative assistance from day one, and Dr. Daniel Jana, who dispensed software and cluster mastery in matters far beyond my technical abilities, made the PhD experience far less painful than I would have expected.

I thank the lab members with whom I supervised students' projects - Kun-Han, Raimon, Maria, Sergi, and Rubén - for edifying pedagogical experiences and, of course, the hard-working and eager students who carried out those projects: Iwona Swiderska, Hélène Wu, Yuri Cho, and Luca Schaufelberger. I probably ended up learning as much as they did.

Beyond the academic aspect, which occupies the remaining 98% of this document, I acknowledge and recall for posterity: Benjamin for taking me running in the mountains and vineyards in the early days of my PhD and sharing his alpine routes; Veronika for her advice in navigating reports, teaching, course credits (and other doctoral school matters I would never have found out about on my own) and for organizing various activities, especially the *caves ouvertes*

Acknowledgements

outings in Valais; the inhabitants of the Greater Morges Metropolitan Area (both security council and rotating members) for meetings by the lake and many fine evenings around the dinner table at *Château Postdoc*; the Folkmann-Garner for the hikes, walks, dinners and pumpkin-carving; Rubén and Shubhajit for the long conversations and career advice, especially over Friday afternoon drinks; the BCH building staff for the occasional early-morning and late-night conversations, and for doing the invisible yet vital work of ensuring our research premises remain a pleasant place to study; Dr. Antonio Prlj for my first invited seminar, in my ancestral homeland no less; Prof. Katalin É. Kiss for lending me a computer screen during the first COVID lockdown, when I was stuck in Budapest; Yuri for the daily (q)(w/u)or(l)dle and remembering the capital of Burkina Faso; the members of the *Orchestre de chambre des étudiant(e)s de Lausanne* and the *Sinfonietta de Genève* for all the music-making.

I thank all other lab members, past and present, for discussions and contributing to a pleasant working environment: Matt, Alberto, Boodsarin, Simone, Ksenia, Frédéric, Puck, Alexandre, Juliette, Yannick, Matthieu, Liam, Osvaldo, Sara; as well as all MSc students and visiting scholars: Eurne, Théo, Sinjini, Manuel, Alan, Dune, David, Pit, Miyeon, Ella, Bruna, Yanan, Hanna, Patricia, Thanapat, Alexander, Malte, Matthew. I hope I have not forgotten anyone.

My current work in organic electronic materials builds on the training I received by working with another excellent group of scientists. I am indebted to my former lab members - Prof. Mario Leclerc, Thomas, Philippe, Pierre-Olivier, Francois, Jean-Rémi, Amélie, Nicolas, Maxime, Carl, Karine, Sepideh, Éliane, Mathieu, Catherine, Josyane, Serge and Rodica - for three years of learning in Québec.

Of course, the most thanks are owed to those who have supported me throughout my studies and beyond: my family. My wife Lena for her love, care and patience; my parents Janice and Rick, who instilled in me a desire to learn and work hard; Irena, Mikalai and Veronika for their hospitality and willingness to travel so far to visit us; and all those who for years have supported me from near and far, across countries and time zones: Alice, Irene, Ken, Sally, Mary-Ann, Simone, Ronald, Claire, and all the others. Whenever I find myself thinking these four PhD years have passed quickly, I need only reflect on how many family members and friends were around when I began but are no longer. I owe everything to those surrounding me. On a lighter note, I must not forget the little dog Jack, the mental health officer, who could fit in the palm of your hand at the beginning of this thesis, but by now already has grey hair on his muzzle and questionable political opinions.

I am grateful to Prof. Kevin Sivula (EPFL), Prof. Frank Nüesch (EPFL/EMPA), Prof. Rik Tykwinski (University of Alberta), and Prof. David Casanova (Donostia International Physics Center/IKERBASQUE) for agreeing to serve on my thesis committee and for their valuable feedback. Finally, I acknowledge the EPFL for financial support and the allocation of computational resources.

Lonay, April 2023

Abstract

Singlet fission (SF) is a multiexciton-generating process whereby an excited state singlet (S_1) is converted into two lower-energy triplets (T_1). The inclusion of a SF-capable material into a photovoltaic device offers the potential for the absorption of photons above the bandgap of traditional solar cell materials, thus increasing the theoretical limit of power conversion efficiency. However, the number of reported SF-capable materials remains remarkably low, and trends pointing towards new molecules have not yet been established. Intramolecular SF (iSF) enables the tuning of bi-chromophoric systems and offers an appealing alternative to the intermolecular SF process, which relies heavily on geometric factors. We show that the building-block approach to conjugated donor-acceptor (D-A) polymer synthesis provides fertile ground to formulate simple and robust design rules for iSF based on the energy ($E(S_1) \geq 2 \times E(T_1)$) and character of the S_1 and T_1 states. The suitability of the proposed guidelines, which are evaluated using descriptors extracted from time-dependent density functional theory (TDDFT), is validated by the correct identification of some of the few polymers that have previously been shown to exhibit SF experimentally. When used in concert with statistical models, these guidelines provide a cost-effective screening protocol for the identification of promising D-A units for iSF from a curated database of 117K reported crystal structures. This dataset is then used to address the (almost) inverse challenge: the search for molecules with inversion of the S_1 and T_1 states ($E(S_1) < E(T_1)$). This property unlocks high-efficiency organic light-emitting diode (OLED) emitters in which fluorescence from S_1 is no longer impeded by population transfer to the thermodynamically-favored T_1 state. Such inversions have been identified in only one class of molecules to date. Following a pre-screening based on TDDFT, approximate second-order and equations-of-motion coupled-cluster methods are employed to refine the excited state energies. Compounds with known inversions are recovered, confirming the validity of the screening methodology, and a new molecular class with this behavior is identified. This class consists of non-alternant hydrocarbons whose pentalene-like cores are aromatically stabilized in a D_{2h} symmetry by their peripheral polycyclic connectivities, which imbues them with the inverted character of the normally unstable and antiaromatic D_{2h} -pentalene. Put together, these virtual screening methodologies significantly enrich the palette of both SF and OLED emitter materials. The building blocks discovered show promise for the next generation of efficiency improvements in devices.

Keywords: singlet fission, donor-acceptor materials, fragment-based design, chemical building blocks, organic solar cells, Hund's rule, thermally-activated delayed fluorescence, organic light-emitting diodes, statistical models, computational chemistry

Résumé

La fission singlet (FS) est un processus à génération de multiples excitons où un état excité de spin singulet (S_1) est converti en deux états triplets excités de plus basse énergie (T_1). L'inclusion d'un matériau capable d'effectuer la FS dans un dispositif photo-voltaïque permettrait d'absorber des photons au-delà de la largeur de la bande interdite des matériaux traditionnels utilisées comme couche active dans des cellules solaires, ce qui mènerait à une hausse de la limite théorique de l'efficacité de conversion énergétique. Cependant, le nombre de matériaux rapportés pouvant effectuer la FS demeure étonnamment bas et des principes de base pouvant guider la conception de nouveaux candidats moléculaires n'ont pas encore été établis jusqu'à maintenant. La FS intramoléculaire (FSi) rend possible la mise au point de systèmes bichromophores et propose un alternatif attrayant au processus de FS intermoléculaire, qui repose principalement sur des facteurs géométriques. Nous démontrons que l'approche des « blocs de construction moléculaires » provenant des voies de synthèse des polymères conjugués de type donneur-accepteur s'agit d'une source prometteuse afin d'élaborer des règles simples et robustes pour la FSi basé sur l'énergie ($E(S_1) \geq 2 \times E(T_1)$) et le caractère des états S_1 et T_1 . La pertinence des lignes directrices proposées, qui sont évaluées à partir de descripteurs extraits de calculs de la théorie de la fonctionnelle de la densité dépendante du temps (TFDDT), est validée en identifiant correctement quelques-uns des rares polymères qui ont manifesté le FS expérimentalement. Lorsqu'ils sont utilisés conjointement avec des modèles statistiques, ces lignes directrices servent de méthode de criblage efficace pour l'identification de candidats de type D-A pour la FSi à partir d'une base de données de 117 000 structures cristallines expérimentales.

Cette base de données est ensuite utilisée comme point de départ pour le défi inverse : la découverte de molécules ayant les états S_1 et T_1 inversés ($E(S_1) < E(T_1)$). Cette propriété engendrera une hausse importante de l'efficacité de diodes électroluminescentes organiques (DELOs) puisque le transfert de population de l'état S_1 vers l'état T_1 , un processus qui est en générale thermodynamiquement favorable, n'entravera plus la fluorescence. Ces inversions ont été rapportées au sein d'une seule catégorie de molécules jusqu'à présent. Un tri initial à partir de résultats TFDDT a été suivi de l'affinage des énergies des états excités par les méthodes de type cluster couplé, d'abord à deuxième ordre approximatif (CC2) et ensuite à deuxième ordre aux équations du mouvement (EOM-CCSD). On retrouve des composés déjà connus pour cette propriété - confirmant ainsi la validité de la méthodologie proposée - et on dévoile une nouvelle classe moléculaire. Celle-ci s'agit d'hydrocarbures cycliques non-alternants dont le coeur est composé d'une unité pentalène dans une symétrie de type D_{2h} .

Résumé

Ce coeur symétrique, qui engendre le caractère inversé des états excités, mais qui est normalement instable et anti-aromatique, est stabilisé par aromaticité grâce à la connectivité de la périphérie polycyclique. Mises ensemble, ces méthodologies de tri computationnel élargissent la palette de matériaux à disposition pouvant effectuer la FS dans les cellules solaires et la fluorescence dans les DELOs. Les blocs de construction présentés sont prometteurs pour la prochaine génération de dispositifs à performance accrue.

Mots-clés : fission singulet, matériaux de type donneur-accepteur, design à base de fragments, blocs de construction chimiques, cellules solaires organiques, règle de Hund, fluorescence retardée à déclenchement thermique, diodes électroluminescentes organiques, modèles statistiques, chimie computationnelle

Contents

Acknowledgements	i
Abstract	iii
Résumé	v
List of Figures	xi
1 Introduction	1
2 Theory	5
2.1 Theory of singlet fission	5
2.2 Requirements for singlet fission	10
2.3 Singlet fission in photovoltaic devices	12
2.4 Classes of singlet fission materials	15
2.5 Excited state analysis	19
3 Designing singlet fission candidates from donor–acceptor copolymers	21
3.1 Introduction	21
3.2 Methodology	23
3.2.1 Criteria to achieve iSF and design strategy	23
3.2.2 Database construction	24
3.2.3 Computational details	25
3.3 Results	26
3.3.1 BDT-TDO copolymer	26
3.3.2 Excited state energies	27
3.3.3 Excited state character	29
3.3.4 Charge transfer prediction	30
3.4 Screening protocol	32
3.5 Conclusion	34
4 Identifying the trade-off between intramolecular singlet fission requirements in donor–acceptor copolymers	37
4.1 Introduction	37
4.2 Database	39

Contents

4.3	Results	40
4.3.1	Trade-off	40
4.3.2	FMO model	42
4.3.3	Functionalization	45
4.4	Conclusion	47
4.5	Computational details	48
5	Heteroatom oxidation controls singlet–triplet energy splitting in singlet fission building blocks	49
5.1	Introduction	49
5.2	Methods	51
5.3	Results	51
5.3.1	Excited state energies	51
5.3.2	State character	52
5.3.3	Oxidized units in donor-acceptor systems	54
5.4	Conclusion	55
6	Data-driven discovery of organic electronic materials enabled by hybrid top-down/bottom-up design	57
6.1	Introduction	57
6.2	Results and discussion	60
6.2.1	Dataset	61
6.2.2	Prediction of optical properties	64
6.2.3	Discovery of materials for singlet fission	65
6.3	Methods	70
6.3.1	Quantum chemistry computations	70
6.3.2	Dataset	71
6.3.3	Automated cross-coupling	71
6.3.4	Statistical models	72
6.4	Conclusion	73
7	Symmetry-Induced Singlet-Triplet Inversions in Non-Alternant Hydrocarbons	75
7.1	Introduction	75
7.2	Results	76
7.2.1	Screening protocol	76
7.2.2	Azaphenalenenes	78
7.2.3	Zwitterions	78
7.2.4	Non-alternant hydrocarbons	78
7.3	Discussion	79
7.4	Conclusion	81
8	Conclusions and Outlook	83
8.1	Conclusions	83

8.2 Outlook	84
A Appendix A: Three-minute thesis	87
Bibliography	89
Curriculum Vitae	115

List of Figures

2.1	General overview of the singlet fission process in a simplified 2-electron/2-orbital-type (i.e., HOMO/LUMO on each chromophore) active space scheme. The y-axis gives an approximate energy scale for the processes involved. When a SF-capable layer is used in a solar cell in conjunction with a semiconductor, the triplet energies match closely with that material's bandgap. No competing pathways are shown.	6
2.2	Electronic configurations contributing to the 1TT state in a simplified scheme comprised of the HOMO and LUMO of each monomer. The subscripts T_+ , T_- , and T_0 refer to the spins of the monomers' microstates.	7
2.3	Comparison of possible singlet fission mechanisms between two equivalent chromophores (above) and within a donor-acceptor-type system (below), in a simplified HOMO/LUMO scheme. At each step, the global state is shown above.	10
2.4	Classes of molecules in which singlet fission has been reported experimentally.	16
3.1	Mechanisms for SF after absorption: direct S_1 to 1TT conversion following the blue arrows, or indirect conversion mediated by charge transfer (CT) states following the brown arrows.	22
3.2	Fundamental design for strong donor-acceptor-type iSF polymers, in which absorption leading to S_1 on the strong donor (SD, in blue) provides enough charge transfer character (denoted with $\delta+$ and $\delta-$) to efficiently generate local T_1 on the adjacent strong acceptors (SA, in red). ⁶	24
3.3	Library of acceptors and donors. Dotted lines denote the bonding positions for D-A polymer chains. Common abbreviations for the cores, when available, are given in parentheses. Structures discussed in section 3.3.1 are highlighted in red and blue.	25
3.4	ΔE_{ST}^{vert} and ΔE_{ST}^{adia} values associated with the 81 donor-acceptor dimers, colored based on the acceptor. These are computed with TDDFT (TDA) at the ω B97X-D/6-31G* level. The vertical and adiabatic cutoffs established as the energy conservation criterion are shown as dotted lines at -1.0 and 0.0 eV, respectively.	28
3.5	Adiabatic donor-to-acceptor charge-transfer contribution of S_1 ($\Omega_{D \rightarrow A}^{S_1}$) and vertical local acceptor contribution of T_1 ($\Omega_{A \rightarrow A}^{T_1}$) obtained for the 81 dimers, colored based on the acceptor. Evaluated with TheoDORE using results from computations with TDDFT (TDA) at the ω B97X-D/6-31G* level.	30

List of Figures

3.6	Schematic representation of the dependence of $\Omega_{D \rightarrow A}^{S1}$ in the dimer with the FMOs (HOMO, LUMO) of the monomers. The local excitations in the donor (blue) and acceptor (red) compete with the CT excitation (green).	31
3.7	FMO ratios of the 81 donor-acceptor monomer pairs included in our dataset (<i>top</i>), see section 3.2.2), and of 25 substituted bithiophene-BT monomer pairs (<i>bottom</i>). Cutoffs for discarding poor CT dimers are represented by the dotted lines. The structures of the reference (nonsubstituted) dimer and the dimers with the highest and lowest $\Omega_{D \rightarrow A}^{S1}$ values are shown. In both plots, the $\Omega_{D \rightarrow A}^{S1}$ of the resulting dimer is given by the color gradient.	33
3.8	(left) Compounds retained following steps 1-3 of the screening protocol, ordered following the ranking criterion of $\Omega_{D \rightarrow A}^{S1}$ as defined in step 4 and colored based on acceptor. (right) The best four potential DA copolymer candidates flagged for iSF	34
4.1	Library of acceptor cores, donor cores, side-chains (R) and functional groups (X) used to create the database studied here. Dotted lines denote the sites for linkages to adjacent donor/acceptor cores.	39
4.2	Relationship between the donor-to-acceptor charge-transfer character of S_1 ($\Omega_{D \rightarrow A}^{S1}$, x-axis) and the local acceptor character of T_1 ($\Omega_{A \rightarrow A}^{T1}$, y-axis) for the 2944 dimers in our database, colored based on (a) the vertical singlet-triplet splitting in the dimer (ΔE_{ST}^{vert}) and (b) the acceptor core, only for those systems with $\Delta E_{ST}^{vert} > -1$. (c) Best dimer candidates with a given acceptor core in the trade-off regime. All structures and their relevant dimer and monomer excited state properties may be visualized interactively at https://www.materialscloud.org/discover/isf	41
4.3	The competition between charge transfer (green), local donor (blue) and local acceptor (red) transitions leads to four regimes in the FMO dimer model.	43
4.4	Monomer FMO criteria D_{crit} and A_{crit} , colored according to the descriptors: (a) $\Omega_{D \rightarrow A}^{S1}$, (b), $\Omega_{A \rightarrow A}^{T1}$. The gray background indicates the region of FMO space where both descriptors show optimal values.	43
4.5	Monomer FMO criteria D_{crit} and A_{crit} , colored according to ΔE_{ST} . The gray background indicates the region of FMO space where $\Omega_{D \rightarrow A}^{S1}$ and $\Omega_{A \rightarrow A}^{T1}$ show optimal values (see Figure 4.4).	44
4.6	Histograms showing the change in the descriptors (a) $\Omega_{D \rightarrow A}^{S1}$ (b) $\Omega_{A \rightarrow A}^{T1}$ (c) ΔE_{ST} upon different acceptor functionalization. ΔX is evaluated as the difference between a substituted dimer with respect to the dimer with H in the substituted position.	46
5.1	Proposed strategies to increase singlet-triplet splitting (ΔE_{ST}) in organic chromophores.	50
5.2	(a) Examples of building blocks studied in this work. (b) Five oxidized derivatives of 2,2'-bithiophene.	51

5.3	(a) Vertical and adiabatic S_1 , T_1 , and ΔE_{ST} energies of bithiophene and its oxidized derivatives. Grey line indicates the ΔE_{ST} cut-off. (b) Summary of the change of adiabatic S_1 , T_1 , and ΔE_{ST} upon S-, S,S- and N-oxidation for all compounds, showing averages (white points), 1st-3rd quartiles (black bars), and maximal/minimal values (whiskers). See ESI for details.	52
5.4	Projected density of states (PDOS), key molecular orbitals and vertical excitation energies for thiophene (Th) and its two S-oxidized derivatives (Th-1O and Th-2O). Transitions between the states most involved in the T_1 and S_1 excitations are marked with black and red arrows, respectively. The molecular orbitals contributing to the charge transfer (CT) character of certain excitations and the atoms on which they are centered are highlighted in green. All energies are given in eV. BB = carbon backbone.	53
5.5	Donor-to-acceptor charge-transfer character of S_1 ($\Omega_{D \rightarrow A}^{S_1}$, x-axis) and local acceptor character of T_1 ($\Omega_{A \rightarrow A'}^{T_1}$, y-axis) in dimers, colored by the dihedral between the donor and acceptor (φ_{D-A}).	56
6.1	General view of the (a) <i>bottom-up</i> (purple) and (b) <i>top-down</i> (green) philosophies of high-throughput virtual screening, with with end-goals in yellow. Requirements for the different stages of a successful screening campaign are indicated in italics and datasets are shown as blocks, whose widths represent the datasets' sizes relative to one another. (c) The <i>hybrid</i> screening methodology described in this work, with the union of top-down (green) and bottom-up (purple) elements enabled by statistical models and automated fragment coupling (orange).	59
6.2	Overview of the preparation of the FORMED dataset, consisting of a top-down screening of the CSD, extensive refinement based on structure and composition, and subsequent evaluation of electronic, structural and topological properties.	61
6.3	(a) S_1 and T_1 excitation energies across the FORMED dataset; points are colored according to the frontier molecular orbital gap. The yellow region defines both the thermodynamically feasible regime for singlet fission and T_1 energies well-matched to the bandgap of conventional semiconductors (to the right of the vertical dashed grey line). The dotted grey line indicates the hard thermodynamic cutoff for singlet fission ($S_1 \geq 2T_1$), while the solid black line is the same cutoff but relaxed to the Franck-Condon regime ($S_1 - 2^*T_1 > -1 eV$) based on linear trends between vertical and adiabatic excitation energies reported previously ^{7,8} (see section S7). (b) Dimensionality reduction plot of the molecules in the FORMED and QM9 datasets using the t-distributed stochastic neighbor embedding algorithm generated from the 3D structures encoded using the spectrum of London and Axilrod-Teller-Muto potentials ⁹ representation (see Methods section for details).	62

List of Figures

- 6.4 Bottom-up application of the FORMED dataset, including the automated unsaturated C-H site identification, topological analysis of coupling sites, and cross-coupling of molecular building blocks, followed by property prediction on the resulting dimer space. 64
- 6.5 Workflow for the generation of diverse dimers from the FORMED dataset. Details are provided in section S5. 65
- 6.6 Charge-transfer-mediated intramolecular singlet fission in donor-acceptor systems. Upon photoexcitation, charge transfer (green) from the donor (blue) to the acceptors (red) mediates the formation of triplets on neighboring acceptors. 67
- 6.7 Largest (green) and smallest (red) coefficients to the multilinear regression $\xi = c_i n_i + c_j n_j + c_k n_k + \dots$, where each coefficient c_i corresponds to the contribution of functional group i to the score function ξ and n_i is the number of instances of the functional group i in each given molecule. Representative examples of molecules containing some of the most favorable substructures for singlet fission are presented. The number of occurrences of each substructure in FORMED is given in black; substructures with fewer than five occurrences in the dataset are not shown. *Dipp* = 2,6-diisopropylphenyl; *TMS* = trimethylsilyl. 68
- 6.8 (a) Predicted excited state energies of the million donor-acceptor dimers generated by automated fragment coupling, colored according to the ξ score function (see section S7). Compounds with the highest score are located in the dashed box. Contour lines give the shape of the score function, with positive and negative contours shown as solid and dotted lines, respectively. The full FORMED dataset, containing the building blocks from which the dimers were constructed, is shown in grey in the background for comparison. (b) Leading candidates of D-A dimers generated through automated cross-coupling and proposed to have favourable energetics for singlet fission. Donor and acceptor cores are colored blue and red, respectively, and are shown alongside their CSD names; dotted lines indicate possible linkages to adjacent repeating units in a polymer. 69
- 7.1 Schematic of three excited states, color-coded to indicate state pairs of identical electron configuration. a) Three pairs of excited states that obey Hund's rule, i.e., each triplet is of lower energy than the singlet of the same configuration. b) The S_1 and S_2 states violate Hund's rule by having lower energy than the equivalent triplet states, T_1 and T_3 76
- 7.2 Three-step protocol for screening compounds in the FORMED database (top) for excited-state violations of Hund's rule with increasingly complex methods. 77

7.3	Survey of three classes of compounds exhibiting Hund's rule violations identified through screening: azaphenalenenes, zwitterions, and polycyclic aromatic hydrocarbons with high symmetry induced by aromaticity. The energy splitting labels correspond to singlet-triplet pairs of the same configuration. Structures are labeled according to their Cambridge Structural Database codes. Excitation energies were obtained with EOM-CCSD/aug-cc-pVDZ using ground state geometries optimized at the ω B97X-D/def2-TZVP level.	78
7.4	Key molecular orbitals, ground-state ring aromaticity (aromatic in green, antiaromatic in magenta) as determined from nucleus-independent chemical shifts (blue), and bond lengths (in Å, black) of ground-state COLDEM, the ground-state (C_{2h}) and high-symmetry (D_{2h}) geometries of pentalene, and ground-state BIVZIP01. Geometries were optimized at the ω B97X-D/def2-TZVP level; SCF orbitals and excitation energies were obtained at the EOM-CCSD/aug-cc-pVDZ level.	80
A.1	Slide serving as a visual aid for my three-minute thesis presentation.	87

1 Introduction

This thesis concerns the data-driven design of organic molecules for the efficient generation and use of energy. For each of these two applications, we focus on a process which shows immense potential for applications in organic optoelectronic materials: *singlet fission* (SF) to improve solar cell efficiencies, and *singlet-triplet inversions* to improve organic light-emitting diode (OLED) efficiencies. In both cases, the promise of the process is overshadowed by the paucity of compounds that possess the requisite properties.

SF is a multiexciton-generating process which has demonstrated significant promise for boosting the power conversion efficiency (PCE) of solar cells by promoting the splitting of a photon-absorbing singlet exciton into two triplet excitons within a single molecule. Traditionally, SF is targeted as an intermolecular process, however its dependence on crystal packing makes molecular design difficult. Furthermore, almost all practical applications of SF materials (and indeed most fundamental research into the topic) are still based primarily on two or three classes of molecules.

In contrast, intramolecular SF (iSF) enables the exploration of tunable bichromophoric systems following well-defined structure-property relationships, thus reducing significantly the role of packing effects and intermolecular couplings. Among different possibilities, the modular strategy on which the chemistry of donor-acceptor (D-A) copolymers is based leads to materials which can undergo iSF in certain conditions. However, despite the breadth of literature on conjugated polymers, the number of reported iSF-capable D-A copolymers remains remarkably small, at fewer than five compounds. Furthermore, while SF chromophores have been incorporated in photovoltaic devices, efficiencies remain low.

Contrary to SF, which requires a large gap between the lowest excited singlet and triplet (at least $> 1\text{eV}$, depending on their absolute energies), OLED emitters usually require the smallest possible gap between these states. Here, holes and electrons are injected into an emissive material, where they combine to release a photon of visible light. One of the key limitations to device efficiency is the statistical ratio of three triplet excitons formed for every one singlet. While the desired fluorescent emission occurs from the S_1 state, the triplets are lost through

Introduction

phosphorescence or non-radiative decay unless they can be rapidly (re)converted into singlets. To promote population of S_1 , very small $S_1 - T_1$ gaps (on the order of ≤ 0.1 eV) have been targeted to enable reverse intersystem crossing from triplet to singlet via thermal activation, leading to the thermally-activated delayed fluorescence mechanism.

Molecules with *inversions* of the singlet and triplet excited-state energies - that is, $S_1 - T_1 < 0$ - are highly promising for the development of active materials for OLEDs, as fluorescence from the S_1 state would no longer be impeded by population transfer to the thermodynamically favored T_1 state. To date, azaphenalenenes are the sole class of molecules where these inversions have been identified unambiguously, and a functionalized azaphenalene has only recently been incorporated in an OLED for the first time. For this highly unusual property to be fully exploited as emitting materials, it will be necessary to identify chromophores which can emit at different wavelengths and with high intensity. This requires the discovery of new core motifs beyond azaphenalene derivatives.

Broadly, the thesis pursues three goals: (a) the establishment of chemical design principles relevant to the two processes in question; (b) the discovery of molecules and motifs that fulfill these design requirements; (c) the development of tools to accelerate the design and discovery process.

Point (a) is addressed by identifying relationships between the desired excited-state properties and practical chemical descriptors relating to the ground states of the molecules concerned. Ground-state properties have the advantage of being more intuitive than excited states. They are simpler to compute, meaning that they can be used for screening purposes. Point (b) is achieved by the bottom-up generation of combinatorial datasets from molecular fragments, the top-down screening of an existing experimental dataset, and the combination of both approaches. Computational screening workflows are then established in which the best candidates are located by means of the target descriptors identified in point (a). For such a workflow to be practical for a massive number of molecules, descriptors must be evaluated rapidly and accurately. To do this, in (c) we encode molecular structure using physics-based representations, and train machine learning models on the excited state properties computed for these datasets. This enables on-the-fly prediction of optical properties to high accuracy without resorting to *ab initio* computation, such that intensive computational efforts can be concentrated on the most promising candidates.

The thesis is structured as follows. In **Chapter 2**, the theory of singlet fission for solar energy applications is outlined. **Chapters 3-7** are published as articles or pre-prints. The overviews to each of these chapters is based on their abstracts in the respective publications.

In **Chapter 3**, we propose a set of parameters to screen conjugated D-A copolymer candidates with potential iSF behavior. We focus our analysis on the $E(S_1) \geq 2E(T_1)$ thermodynamic condition and on the appropriate charge transfer (CT) character of S_1 . We map the CT character with respect to the frontier molecular orbital (FMO) energies of the constituent monomers, providing a cost-effective protocol for an accelerated screening of promising iSF

D-A pairs, while minimizing the number of computations. These parameters are applied to a chemically diverse, curated library of 81 truncated dimers of synthetically feasible D-A copolymers. From our dataset, four candidates are flagged for iSF, two of which were previously experimentally reported. This protocol is envisioned to be scaled up for the high-throughput screening of large databases of D-A dimers for the design and identification of conjugated polymers capable of iSF.

In **Chapter 4**, we identify the trade-off between the main iSF requirements of the D-A strategy outlined in chapter 3, and formulate design rules that allow them to be tuned simultaneously in a fragment-based approach. Based on a library of 2944 D-A copolymers, we establish simple guidelines to build promising materials for iSF. These consist of (1st) selecting an acceptor core with high intrinsic singlet-triplet splitting, (2nd) locating a donor with a larger monomer frontier molecular orbital (FMO) gap than that of the acceptor, and (3rd) tuning the relative energy of donor and/or acceptor FMOs through functionalization to promote photoinduced charge transfer in the resulting polymer. Remarkably, systems containing benzothiadiazole and thiophene-1,1-dioxide acceptors, which have been shown to undergo iSF, fulfill all criteria simultaneously when paired with appropriate donors. This is due to their particular electronic features, which make them highly promising candidates in the quest for iSF materials.

In **Chapter 5**, we propose heteroatom oxidation as a robust strategy to achieve sufficient S_1/T_1 splitting to overcome the demanding energy splitting criterion that the S_1 energy must be at least twice that of T_1 , which has been a limiting factor in expanding the range of materials capable of SF. We demonstrate the potential of this approach for intramolecular SF and apply the screening protocol outlined in the two previous chapters to a pool of ring systems containing oxidized heteroatoms. This study was guided by the observation that prominent candidates for SF, both reported experimentally and proposed computationally, contained structurally similar yet rarely-discussed motifs of oxidized sulfur and nitrogen. Thus, this simple moiety must have a significant effect on energy levels.

The high-throughput exploration and screening of molecules for organic electronics involves either a 'top-down' curation and mining of existing repositories, or a 'bottom-up' assembly of user-defined fragments based on known synthetic templates, such as applied in the three previous chapters. Both are time-consuming approaches that require significant resources to compute electronic properties accurately. In **Chapter 6**, we generate a top-down set of almost 117K synthesized molecules containing their optimized structures, electronic and topological properties and chemical composition, and use these structures as a vast building block library for bottom-up fragment-based materials design. A tool is developed to automate the coupling of these building block units based on their available $C(sp^2/sp)$ -H bonds, thus providing a fundamental link between the two philosophies of dataset construction. Statistical models are trained on this dataset and a subset of the resulting hybrid top-down + bottom-up compounds, which enables on-the-fly prediction of key ground and excited state properties (frontier molecular orbital gaps, S_1 and T_1 energies) from molecular geometries with high accuracy across all known p -block organic compound space. With access to *ab initio*-quality optical

Introduction

properties in hand, it is possible to apply this bottom-up pipeline using existing compounds as building blocks to any materials design campaign. To illustrate this, we construct and screen over a million molecular candidates for intramolecular singlet fission, the leading candidates of which provide insight into the structural features that may promote this multiexciton-generating process.

In **Chapter 7**, we screen the curated database of organic crystal structures presented in the previous chapter to identify existing compounds for violations of Hund's rule in the lowest excited states. We identify two further classes with this behavior. The first, a class of zwitterions, has limited relevance to molecular emitters as the singlet-triplet inversions occur in the third excited singlet state. The second class consists of two D_{2h} -symmetry non-alternant hydrocarbons, a fused azulene dimer and a bicalicene, whose lowest excited singlet states violate Hund's rule. Due to the connectivity of the polycyclic structure, they achieve this symmetry through aromatic stabilization. These hydrocarbons show promise as the next generation of building blocks for OLED emitters.

Conclusions and an outlook on the fields discussed are provided in **Chapter 8**.

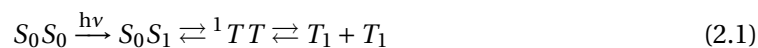
Finally, **Appendix A** contains the text and visual aid for a scientific popularization competition I participated in during my PhD, in which I summarized my thesis work in three minutes for a non-scientific audience.

2 Theory

This chapter outlines some of the theoretical background on singlet fission (SF) that is not covered explicitly in the following chapters (section 2.1). The necessary requirements both for SF to occur (section 2.2) and for it to be implemented in solar technologies (section 2.3) are discussed. The general classes of organic compounds in which SF has been studied are summarized (section 2.4). The chapter closes with a brief theoretical overview of the method used throughout this thesis for the analysis of excited state character (section 2.5).

2.1 Theory of singlet fission

SF was first discussed by Singh and coworkers at the National Research Council of Canada in 1963 in the context of a dark state which could undergo two-photon absorption.¹⁰ This state was found present in anthracene crystals but not in free anthracene, suggesting a multi-chromophore process, which led to the first description of that intermediate state as an excited spin-singlet comprised of two coupled triplet excitons which may dissociate.¹¹ Since that discovery, the following stepwise picture of SF has emerged:



Generally speaking, SF can be summarized by the following steps, as shown schematically in Figure 2.1: an organic chromophore in a singlet ground state is promoted to a higher-energy singlet state via photoexcitation ($h\nu$); this is converted through a spin-allowed process to a slightly lower energy triplet-pair state 1TT ; 1TT evolves into two triplets, each of approximately half the energy of the initial S_1 state, and each located on a different chromophoric center, for instance on adjacent molecules, or nearby segments on the same extended molecule.¹²⁻¹⁴ Through a process of spatial separation and spin decoherence, the individual triplet components of the triplet-pair disentangle until they behave as two fully independent triplet excitons $T_1 + T_1$.

The SF process is usually broken down into two key events: the generation of 1TT from the initial singlet, and the formation of independent triplets T_1 from the triplet pair. Experimentally, measurements of delayed fluorescence provide indirect evidence for SF, as a result of the formation and then recombination of the triplet excitons occurring on a timescale much longer than direct emission down from the S_1 state.¹⁵ The presence and time evolution of triplet states may be observed directly with transient absorption spectroscopy,^{16–18} and through the study of photocurrent as a function of a magnetic field. The SF rate can be modified through the effect of the magnetic field on the Zeeman interaction in the triplet-pair state.¹⁹ Quantum efficiencies are also used to quantify SF, as values above 100 % are the hallmark of a multiexciton-generating process at work. The external (internal) quantum efficiency EQE (IQE) describes the ratio of incident (absorbed) photons to collected charges (see section 2.3 below).

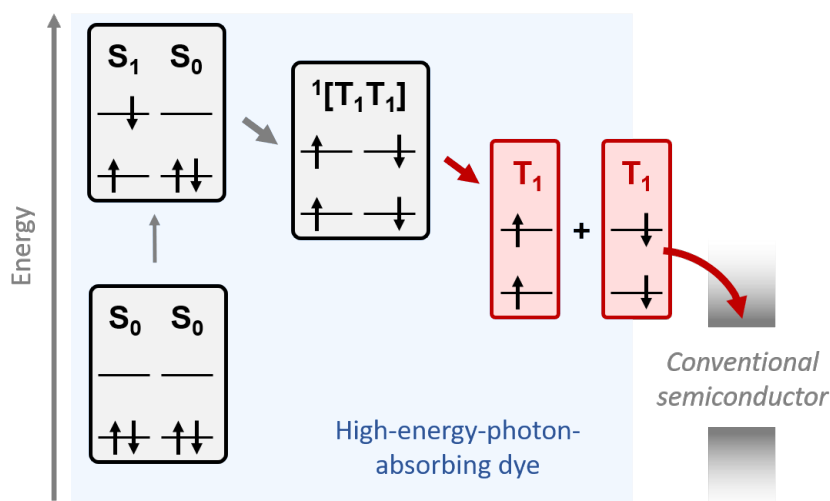


Figure 2.1: General overview of the singlet fission process in a simplified 2-electron/2-orbital-type (i.e., HOMO/LUMO on each chromophore) active space scheme. The y-axis gives an approximate energy scale for the processes involved. When a SF-capable layer is used in a solar cell in conjunction with a semiconductor, the triplet energies match closely with that material’s bandgap. No competing pathways are shown.

In this thesis, we will use the label ‘ S_1 ’ (and ‘ S_0S_1 ’ in a multichromophoric species, as in Equation 2.1) to describe the lowest excited state of singlet multiplicity, drawing from the nomenclature of molecular excited states, although this may be referred to elsewhere in the literature as the ‘local’ or Frenkel exciton, in contrast to the ‘multiexciton’ states. Furthermore, we note that in these figures, elsewhere in this thesis, and throughout the literature, the monomer excited states are schematized as purely single-particle excitations, for instance between the HOMO and LUMO.

We see that SF involves at least two distinct chromophore centers. These may be individual molecules within a crystal or thin film layer or separate centers in a molecular homodimer, which are perhaps separated by a bridging spacer unit. Although we indicate here that initial

singlet excitation (S_1) occurs in one center alone (or ‘monomer’), the exciton may be highly delocalized.²⁰ Although excitation to a higher state than S_1 is possible, (i.e., S_n , where $n > 1$), according to Kasha’s rule the system will quickly relax through internal conversion to S_1 .²¹ For this reason, we consider here the S_1 state to be the initial photoexcited state for SE. From this singlet exciton emerges a multiexcitonic triplet-pair state (1TT), which retains the overall configuration of a singlet. The full electronic structure description of the 1TT state is quite complex, involving six doubly-excited terms if we make the approximation that only the highest occupied and lowest unoccupied molecular orbitals (HOMO and LUMO) are involved in each transition (Figure 2.2).

$$|^1TT\rangle = \frac{1}{\sqrt{3}} \left(\begin{array}{c} \left(\begin{array}{|c|c|} \hline \uparrow & \downarrow \\ \hline \uparrow & \downarrow \\ \hline \end{array} \right) + \left(\begin{array}{|c|c|} \hline \downarrow & \uparrow \\ \hline \downarrow & \uparrow \\ \hline \end{array} \right) \\ |T_+^A T_-^B\rangle \quad |T_-^A T_+^B\rangle \end{array} + \frac{1}{2} \left(\begin{array}{c} \left(\begin{array}{|c|c|} \hline \downarrow & \uparrow \\ \hline \uparrow & \downarrow \\ \hline \end{array} \right) + \left(\begin{array}{|c|c|} \hline \uparrow & \downarrow \\ \hline \downarrow & \uparrow \\ \hline \end{array} \right) - \left(\begin{array}{|c|c|} \hline \downarrow & \downarrow \\ \hline \uparrow & \uparrow \\ \hline \end{array} \right) - \left(\begin{array}{|c|c|} \hline \uparrow & \uparrow \\ \hline \downarrow & \downarrow \\ \hline \end{array} \right) \end{array} \right) \right) \\ |T_0^A T_0^B\rangle \end{array}$$

Figure 2.2: Electronic configurations contributing to the 1TT state in a simplified scheme comprised of the HOMO and LUMO of each monomer. The subscripts T_+ , T_- , and T_0 refer to the spins of the monomers’ microstates.

The monomer triplet configurations shown in Figure 2.2, summarized as:

$$|^{1,0}TT\rangle = \frac{1}{\sqrt{3}} (|T_+^A T_-^B\rangle + |T_-^A T_+^B\rangle - |T_0^A T_0^B\rangle) \quad (2.2)$$

combine into a state of singlet spin multiplicity (hence the first superscript 1) and spin quantum number m_s of 0 (second superscript). As a result, $S_1 \rightleftharpoons ^1TT$ is a spin-conserving process. However, these microstate configurations may also couple to form states of overall triplet spins:

$$|^{3,-1}TT\rangle = \frac{1}{\sqrt{2}} (|T_-^A T_0^B\rangle - |T_0^A T_-^B\rangle) \quad (2.3)$$

$$|^{3,0}TT\rangle = \frac{1}{\sqrt{2}} (|T_+^A T_-^B\rangle - |T_-^A T_+^B\rangle) \quad (2.4)$$

$$|^{3,+1}TT\rangle = \frac{1}{\sqrt{2}} (|T_+^A T_0^B\rangle - |T_0^A T_+^B\rangle) \quad (2.5)$$

or quintet spins:

$$|^{5,-2}TT\rangle = |T_-^A T_-^B\rangle \quad (2.6)$$

$$|^{5,-1}TT\rangle = \frac{1}{\sqrt{2}} (|T_-^A T_0^B\rangle + |T_0^A T_-^B\rangle) \quad (2.7)$$

$$|^{5,0}TT\rangle = \frac{1}{\sqrt{6}} (|T_+^A T_-^B\rangle + |T_-^A T_+^B\rangle + 2|T_0^A T_0^B\rangle) \quad (2.8)$$

$$|^{5,+1}TT\rangle = \frac{1}{\sqrt{2}}(|T_+^A T_0^B\rangle + |T_0^A T_+^B\rangle) \quad (2.9)$$

$$|^{5,+2}TT\rangle = |T_+^A T_+^B\rangle \quad (2.10)$$

Although the 5TT states are usually assumed to be much higher in energy than the triplet-pairs of other configurations, it has been shown in tetracene dimers that the energy splitting of 5TT and 1TT can be as little as 10 meV.²² The 1TT state can couple with other singlet configurations of similar energy through configuration-interaction, thus stabilizing it.^{23,24} This energy difference between the triplet-pairs of singlet and quintet character can be used as an approximation for the binding energy $E_{binding}$ which must be overcome for the triplet dissociation into independent T_1 s to be possible²⁵:

$$E_{binding} = E(^5TT) - E(^1TT) \quad (2.11)$$

The coupling between S_1 and 1TT is a central requirement for the key process of SF to occur. In a limit of weak coupling between initial and final states i and f , the rate of a photophysical process can be approximated using Fermi's golden rule (k_{FGR}):

$$k_{FGR} = \frac{2\pi}{\hbar} |V_{if}|^2 \delta(E_f - E_i) \quad (2.12)$$

in the regime of weak coupling V_{if} between the states (that is, the nonadiabatic regime), where \hbar is the reduced Planck's constant and $\delta(E_f - E_i)$ is a delta function which ensure the conservation of energy between the states. δ_{if} is usually expressed as the Franck-Condon weighted density of states ρ^{FC} :²⁶

$$\delta_{if} \approx \rho_{if}^{FC} = \frac{1}{\sqrt{4\pi E_{reorg}^{ij} k_B T}} \exp\left[-\frac{(E_{reorg}^{ij} + \Delta G_0^{ij})^2}{4\pi E_{reorg}^{ij} k_B T}\right] \quad (2.13)$$

where E_{reorg}^{ij} is the reorganization energy, k_B is Boltzmann's constant, and T is the temperature. ΔG_0^{ij} is the energy difference between the free energy of the states (the driving force). The resulting rate constant is not valid in large coupling (adiabatic) regimes, in which case other rate expressions have been established which include outer-sphere dynamic effects caused by the transfer process.²⁷ Some ways by which the SF rate constant has been evaluated include the Landau-Zener formulation, which accounts for tunnelling effects,^{28,29} harmonic transition state theory,^{30,31} and kinetic approaches based on linear free energies.^{25,32}

The SF process may be either *direct* or *charge-transfer-mediated*. In the case of SF between two electronically equivalent chromophores, such as a homodimer, the direct mechanism would involve the direct coupling of the initial singlet state to the triplet-pair state. Equation

2.12 contains only the first-order term which accounts for the coupling between states i and f through the electronic Hamiltonian H_{el} , which would correspond to the rate for the direct SF process:

$$V_{if} = \langle S_1 S_0 | H_{el} | {}^1 T T \rangle \quad (2.14)$$

This corresponds to a single two-electron process, as shown by the brown arrows in the example in Figure 2.3a, which may be mediated by intermolecular vibrations.³³ Alternatively, charge transfer (CT) states may assist the process through a collection of indirect one-electron processes, given as anion-cation and cation-anion states with singlet spins (${}^1 AC$ and ${}^1 CA$) and shown between the green brackets in Figure 2.3a.³⁴ This mechanism follows the green arrows. The second-order expansion to the coupling is expressed as:

$$V_{if} = \sum_{m \neq i, f} \frac{V_{im} V_{mf}}{E_m - E_i} \quad (2.15)$$

in which m are the states that mediate the transition from i to f . These intermediary states become significant if the couplings V_{im} and V_{mf} between them and the initial and final states are large and their energy differences are small. In the CT-mediated example given in Figure 2.3a, the two sets of $V_{im} V_{mf}$ elements from Equation 2.15 correspond to:³⁵

$$V_{im} V_{mf} \approx \langle S_1 S_0 | H_{el} | {}^1 AC \rangle \langle {}^1 AC | H_{el} | {}^1 T T \rangle \quad (2.16)$$

$$V_{im} V_{mf} \approx \langle S_1 S_0 | H_{el} | {}^1 CA \rangle \langle {}^1 CA | H_{el} | {}^1 T T \rangle \quad (2.17)$$

These coupling terms can be evaluated in a number of ways, notably using a mutually orthogonal frozen orbital approach, in which the states are described by different populations of the frontier molecular orbital (HOMO/LUMO) pairs on each chromophore.³⁵⁻³⁷

The CT states may act as ‘real’ intermediates in the $S_1 S_0 \rightarrow {}^1 T T$ process if they are at an energy between the $S_1 S_0$ and ${}^1 T T$ states, although they may instead assist in the process as ‘virtual’ intermediates in a so-called superexchange mechanism if they are higher-lying than the others and therefore do not become populated.^{38,39} Finally, it is also possible that CT states which lie below the desired ${}^1 T T$ state may act as traps. In general, larger couplings in Equations 2.16 and 2.17 lead to higher SF rates in the CT-mediated mechanism compared to the coupling described by the two-electron process in the direct mechanism. However, couplings that are too strong may induce various deactivation channels, such as charge separation and excimer formation, or may enable the reverse process of triplet recombination to a singlet (${}^1 T T \rightarrow S_0 + S_1$).⁴⁰⁻⁴⁴

Given the importance of CT states in driving the process of SF, it would be desirable to design

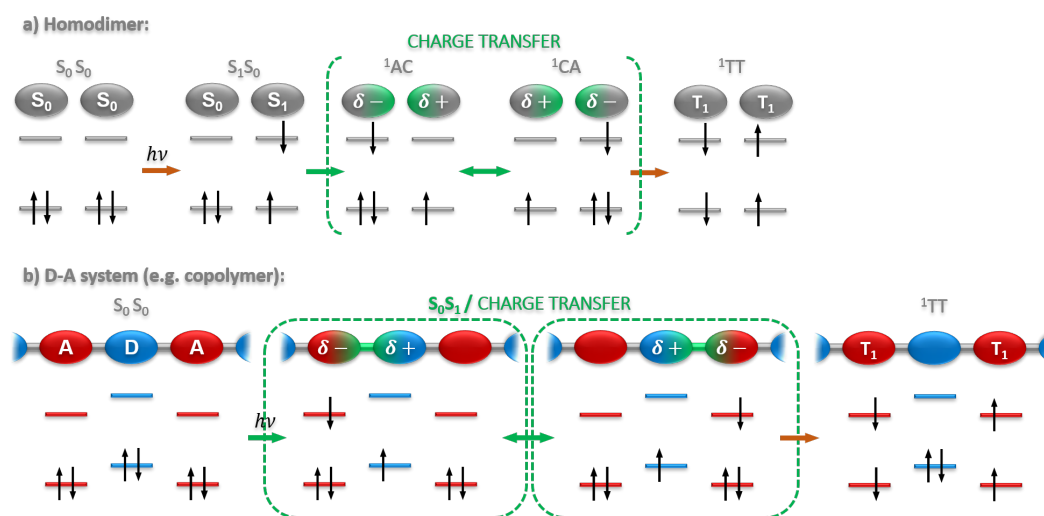


Figure 2.3: Comparison of possible singlet fission mechanisms between two equivalent chromophores (above) and within a donor-acceptor-type system (below), in a simplified HOMO/LUMO scheme. At each step, the global state is shown above.

chromophores in which strong coupling to these states is favourable. However, these couplings terms are highly sensitive to the interchromophore geometry,⁴⁵ which is difficult to control in a solid (crystalline or amorphous) medium. This has led to the tailored design of two classes of *intramolecular* SF materials based on covalently-bound chromophores: dimers and polymers, which are discussed in greater detail in section 2.4. Dimers are usually composed of two SF-capable chromophores separated by a linker. The linker provides the necessary orientation between chromophores to promote through-space coupling (an example is shown in Figure 2.4c). Polymers, on the other hand, may engage in either through-space coupling (between polymer chains) or through-bond coupling between the chemically-bound units within one chain. In that case, the degree of charge transfer may be sufficiently large that it becomes the defining feature of the S_1 state (Figure 2.3b, configurations in green boxes), rather than an intermediary state which couples to both the S_1 and 1TT states.

2.2 Requirements for singlet fission

The requirements for singlet fission may be summarized as follows (in order of the steps of the singlet fission process):

1. **The S_1 minimum should be at least twice as large as the T_1 minimum** ($\Delta E_{ST} \geq E(S_1) - 2E(T_1)$). This is commonly referred to as the 'thermodynamic' condition, and has been the subject of much study in the design of new singlet fission chromophores.^{35,36}
2. **The recombination (fusion) of the two T_1 states, for instance via $T_1 + T_1 \rightarrow T_2$ or $T_1 + T_1 \rightarrow Q_1$, must be disfavoured**, (where Q denotes a quintet state).^{35,36} Therefore, to

make such processes thermodynamically unfeasible, $E(T_2) > 2E(T_1)$ and $E(Q_1) > 2E(T_1)$ is ideal.

3. **The rate of intersystem crossing (ISC) directly into the triplet manifold $S_1 \rightarrow T_n$ must be smaller than that of the SF process.** Small ISC rates often exist in many organic chromophores, as ISC requires good spin-orbit coupling, which exists primarily when heavier atoms are present.
4. **$S_0 + S_1 \rightarrow {}^1TT$ must be efficient to overcome other deactivation pathways.** Direct fluorescence from the excited singlet state back to the ground state $S_1 \rightarrow S_0 + h\nu$, for instance, is in principle unavoidable, although rapid triplet-pair formation may reduce its likelihood.
5. **Non-radiative decay pathways $S_1 \xrightarrow{CI} S_0$ must be limited.** This may be an issue in highly flexible molecules, such as polyenes, which have readily available conical intersections (CI) down to the ground state,^{46,47} but is generally less of a concern in rigid structures.

It is important to note that the comparison of energies between states only provides an initial approximation of the possible decay pathways in that they are indicative of the thermodynamic feasibility of a given pathway. In practice, each photophysical process is described by a kinetic rate, and for SF to be competitive with other processes, the rate constant of 1TT formation from S_1 (requirement 4) must be larger than that of the reverse process (${}^1TT \rightarrow S_0 + S_1$) and fluorescence, while the rate constant of independent triplet formation from the triplet-pair state (${}^1TT \rightarrow T_1 + T_1$) must be larger than the reverse process of triplet recombination and direct relaxation of 1TT to the ground state. In a recent study of the kinetics of SF in a covalently-linked pentacene dimer in solution at room temperature using time-resolved optical and electron paramagnetic resonance spectroscopy, rate constants of 2×10^9 , 5×10^7 and $9 \times 10^7 \text{ s}^{-1}$ were obtained for the first three processes described above, showing that for that compound triplet-pair formation is indeed the favoured decay path for the S_1 state.²⁴ In the same study, a triplet-pair of overall quintet spin (5TT) evolves from 1TT with a rate constant of $1 \times 10^7 \text{ s}^{-1}$ and subsequent triplet separation from 5TT occurs at $6 \times 10^6 \text{ s}^{-1}$, while the reverse process of ${}^5TT \rightarrow {}^1TT$ and decay of 1TT to the ground state occur at the similar rates of 5×10^6 and $1 \times 10^7 \text{ s}^{-1}$, respectively.²⁴

The energy gap between states expressed in condition 1 is possible in organic chromophores due to the repulsive exchange interaction which is present in the singlet excited state but not in the triplet. Provided that both the S_1 and T_1 states are dominated by HOMO \rightarrow LUMO transitions, the gap between the lowest singlet and triplet excited states is approximately equal to twice the exchange integral between the HOMO and LUMO orbitals (K_{HL})⁴⁸:

$$E(S_1) - E(T_1) \approx 2K_{HL} \quad (2.18)$$

where the exchange integral is defined as

$$K_{HL} = \int \int \phi_{HOMO}(r_1)\phi_{LUMO}(r_2)\frac{1}{|r_2 - r_1|}\phi_{HOMO}(r_2)\phi_{LUMO}(r_1)dr_1dr_2 \quad (2.19)$$

in which ϕ_{HOMO} and ϕ_{LUMO} are the HOMO and LUMO orbitals, respectively. This repulsive exchange interaction present between the electron and hole in the singlet exciton leads to delocalization of the exciton through a large region of an extended π -conjugated chromophore (in a single molecule) or among many molecules (in a molecular crystal). The absence of this interaction in triplet excitons leads to larger binding energies and therefore localized excitations.⁴⁹

It has been shown that endoergic SF ($\Delta E_{ST} < 0$) is possible under certain circumstances, by overcoming the energy deficit through entropic gain brought about by this difference in singlet and triplet exciton sizes, due to the number of configurations available.^{25,31,50} Although even a small endoergic SF process would be highly desirable for increasing solar cell efficiencies⁵¹ (the discussion of which is provided below), it exists primarily in crystals, particularly in tetracene.³¹ It was proposed that this entropic gain, which occurs at both the triplet-pair formation and triplet separation steps, can also be achieved in intramolecular conjugated systems longer than dimers, leading to independent triplet formation.⁵² On the other hand, a ΔE_{ST} difference which is too positive (exoergic) lowers the SF rate and leads to competition with other reaction pathways.³⁵

2.3 Singlet fission in photovoltaic devices

One of the most significant limitations in a single-junction solar cell device issues from the matching of the energy of incident photons to the semiconductor bandgap (E_g): photons of lower energy than E_g are not absorbed, while excitons resulting from the absorption of higher energy photons thermalize to E_g , and therefore their excess energy is lost. As a result of these losses (and others, related to radiative recombination and thermodynamics), an inherent power-conversion efficiency (PCE) limitation exists ($\sim 31\%$). One of the main techniques by which to absorb photons of different energies while limiting thermal losses is by increasing the number of junctions, in which different materials with staggered bandgaps are layered on top of each other.⁵³ Using these tandem approaches leads to a theoretical PCE of $\sim 46\%$, although the inclusion of larger numbers of layers makes for a much more involved device manufacturing process, and challenges persist for scaling up to production-level solar cell fabrication.⁵⁴

Another approach is to include multiexciton-generating (MEG) processes to collect the otherwise wasted high-energy photons. The term 'MEG' has been discussed as a means to improve solar cell efficiencies in the context of inorganic semiconductors, such as quantum dots⁵⁵⁻⁵⁷, in which both excitons are formed within the same quantum dot. Hanna and Nozik have demonstrated that the theoretical PCE limit may be increased to 44% for single-junction photovoltaics through MEG processes.⁵⁸ However, quantum dots have nearly degenerate singlet

and triplet energies, and therefore MEG occurs according to an unrelated mechanism.^{59,60} Singlet fission can be considered the organic/molecular version of MEG, with the advantage of longer lifetimes of triplets excitons (μs), in contrast to electron-hole recombination which occurs on the picosecond scale in inorganic media.⁶¹

The main practical advantage of SF is as an efficiency-boosting material in solar cells. This would be done, for instance, by including a layer of an SF-capable dye which absorbs high-energy photons and injects the down-converted triplet excitons into the semiconductor (Figure 2.1). The key merit of this is the possibility of pushing quantum efficiencies above 100%, in that more charge carriers could be generated than photons absorbed. The expression for EQE is given by:

$$EQE(\lambda) = LHE(\lambda)\varphi_{injection}(\lambda)\varphi_{regeneration}\eta_{cc}(\lambda) \quad (2.20)$$

where $\varphi_{injection}$ is the electron injection quantum yield, $\varphi_{regeneration}$ is the dye regeneration quantum yield and η_{cc} is the efficiency of charge collection, all at a given wavelength λ . LHE is the light-harvesting efficiency, which relates to the absorbance A of the active layer and depends on the molar absorption coefficient of the dye and number of absorbing molecules (due to layer thickness, *etc.*):

$$LHE(\lambda) = 1 - 10^{-A(\lambda)} \quad (2.21)$$

By integrating the EQE over all wavelengths, we arrive at the expression for the device current (J_{sc}), which is a key metric for solar cell efficiencies:

$$J_{sc} = \int EQE(\lambda)q\Gamma(\lambda) dE \quad (2.22)$$

where q is the electronic charge and Γ is the photon flux. Regardless of the manner of triplet formation (in either an inter- or intra-molecular fashion, via either a direct or charge-transfer-mediated mechanism, *etc.*), once the triplet excitons are formed, they must reach an interface and undergo charge separation via electron transfer. We see from Equation 2.20 that the EQE is dependent on the injection quantum yield $\varphi_{injection}$. $\varphi_{injection}$ depends on the injection time τ_{inj} and the relaxation time τ_{relax} :

$$\varphi_{injection} = \frac{1}{1 + \frac{\tau_{inj}}{\tau_{relax}}} \quad (2.23)$$

τ_{inj} is the inverse of the rate of interfacial electron transfer (k_{iET}) from the chromophore 'donor' (here, the SF material) into the conduction band of the semiconductor 'acceptor'. This process follows a form of the standard Marcus theory⁶² expression for non-adiabatic charge

transfer established by Levich and Dogonadze⁶³, similar to Equation 2.13 above:

$$\frac{1}{\tau_{inj}} = k_{iET} = \frac{2\pi}{\hbar} \int_0^\infty dE \lambda \rho(\lambda) |V(\lambda)|^2 \frac{1}{\sqrt{4\pi E_{reorg} k_B T}} \exp\left[-\frac{(E_{reorg} + \Delta G_0 - E)^2}{4\pi E_{reorg} k_B T}\right] \quad (2.24)$$

in which E_{reorg} is the total reorganization energy upon charge transfer, E are the energies of acceptor states described by the density of states $\rho(\lambda)$, $V(\lambda)$ is the coupling between donor and acceptor (which also exists as a distribution, due to the range of local geometric arrangements at the donor-acceptor interface). ΔG_0 is the difference between the free energy of the states (the driving force). In this context, it is the difference between the conduction band of the acceptor and the ionization potential of the donor.

The solid-state morphology and interfacial effects contribute to the SF chromophore having different state energies than in the isolated molecule. Such variations may be crucial for the identification of chromophores that fulfill the energetic requirements for SF and charge injection into an acceptor. This is particularly the case in the initial S_1 state which has a delocalized character.

From this analysis, we may summarize that the following parameters are necessary for a SF chromophore to be effectively implemented in a solar cell, beyond the fundamental requirements outlined in the previous section:

1. The lowest excited singlet state must be absorptive (i.e., the $S_0 \rightarrow S_1$ transition must be optically active and have a non-negligible oscillator strength), and the compound should have a high absorption coefficient. A high absorbance across the range of wavelengths of interest means that a thinner chromophore layer can be used, while still having a high LHE (Equation 2.21). A thinner absorbing layer reduces the distance the triplet exciton must travel to reach the site of charge injection.
2. The chromophores are stable under environmental conditions (e.g., they do not photodegrade, dimerize, or oxidize). This may be challenging due to the ground-state diradical character, which is often larger in compounds where appropriate SF energetics are achieved, and may make the compound more susceptible to undergoing reactions.
3. The resulting free triplet excitons have sufficiently large diffusion lengths and lifetimes to move through the SF layer and reach the dye (donor) - semiconductor (acceptor) interface.
4. The interfacial energies between dye and semiconductor are well-aligned to enable efficient charge separation and the dye reorganization energy is low. The oxidation potential of the SF chromophore is therefore important.

5. The triplet excitons are of sufficiently high energy to be injected into the bandgap E_g of the semiconductor, i.e., $E_g=1.1$ eV for silicon and higher for other common high-performance inorganic semiconductors, such as gallium arsenide ($E_g=1.4$ eV) and cadmium telluride ($E_g=1.5$ eV).

Note that other losses contributing to the limits of solar cell efficiency beyond the SF material itself are not discussed here, such as those related to reflectance, thermal effects, and shading. To date, SF-capable molecules have been incorporated in inorganic, dye-sensitized and all-organic solar cells. While high quantum efficiencies have been achieved, PCEs remain low.⁶⁴ A number of classes of materials, notably derivatives of pentacene and tetracene, have been studied to address these device requirements, as is discussed below. A summary of the different broad classes of SF materials reported to date is given in Figure 2.4.

2.4 Classes of singlet fission materials

Pentacenes (Figure 2.4a) have been studied for the implementation of the SF process in light harvesting, first in donor-acceptor junctions.⁶⁵ Internal quantum efficiencies above 100% were initially reported using a pentacene absorber in a photodetector¹⁹; this was later achieved in an organic photovoltaic device with pentacene and poly(3-hexylthiophene) layers, although the PCE was less than 2%.⁶⁶ Triplet excitons in these settings were observed to have relatively long diffusion lengths.⁶⁵ It has been suggested that blended OPV morphologies lead to triplet-triplet annihilation.⁶⁷ Nanoparticles, such as PbS and PbSe, have also been used as triplet acceptors from pentacene to this effect. By tailoring the nanoparticle bandgap to the T_1 energy of the SF-capable acene, efficient exciton transfer is possible.⁶⁸ SF has also been observed through dye-sensitization of an indium-zinc oxide semiconductor with a pentacene dimer derivative, but not with a monomeric derivative.⁶⁹

Tetracene, which has a T_1 energy well-matched to silicon, has also been shown to undergo SF in solar cells (Figure 2.4a). This has occurred, for instance, (a) in combination with copper phthalocyanine and fullerene, such that SF occurs in tetracene and the triplet excitons separate into triplet charge carriers at the phthalocyanine/fullerene interface;⁷⁰ (b) using a conjugated tetracene-based polymer donor in a polymer/fullerene donor-acceptor junction;⁷¹ and (c) via direct sensitization of silicon through addition of a thin hafnium oxynitride to alleviate electron-hole pair quenching while still enabling efficient coupling between tetracene and silicon for energy transfer to occur.⁷² The 5,6,11,12-tetraphenyl derivative of tetracene (rubrene) has also been used in an OPV together with a S_1 exciton donor and a non-fullerene acceptor,⁷³ thereby using the SF material not for absorption but rather solely for triplet formation, and as the donor with a fullerene acceptor,⁷⁴ in which triplet-triplet annihilation was the main competing pathway.⁷⁵ Finally, beyond acenes, SF processes in quinoidal and radicaloid-type compounds with low T_1 energies have also been observed,^{76,77} including in a dye-sensitized solar cell scheme.⁷⁸

The push for new SF-capable chromophores has been motivated in part by the fact that the SF process is endothermic in anthracene and tetracene, while the T_1 energy is too low for solar cell applications in the longer acenes, pentacene and hexacene (Figure 2.4a). Other classes of materials are presented below in which SF has been reported but not yet studied in photovoltaic devices.

Rylene diimides, including derivatives of perylene and terylene (Figure 2.4b), exhibit concurrently higher triplet and singlet energies, and have multiple available sites for functionalization. In general, the R_1 site is used for functionalization with solubilizing side-chains or as a site to link with other chromophores, while the R_2 site has a more significant effect on the unit's electronic structure. Perylene diimides have shown efficient triplet formation upon appropriate substitution.⁷⁹ Slip-stacked conformations along the π -plane has been shown to be necessary for triplet formation, which has been achieved in the crystal structure through substitution⁸⁰, and in intramolecular dimers through the use of tailored linkers (such as in the example in Figure 2.4c) and solvent effects.⁸¹ However, face-to-face arrangements suppress SF by instead engendering a charge separation state. Trimers and tetramers of perylene (without the diimide) alternating with alkoxybenzene have shown that endothermic SF can occur in an intramolecular fashion when triplet formation has a number of possible chromophore sites, thereby increasing the entropy of the T_1+T_1 states.⁵²

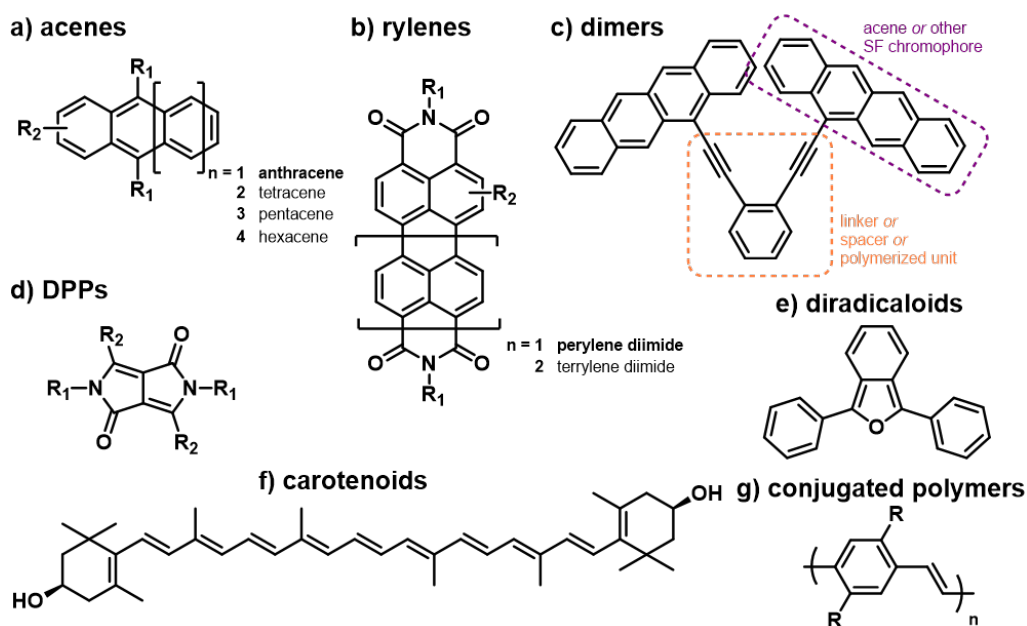


Figure 2.4: Classes of molecules in which singlet fission has been reported experimentally.

Diketopyrrolopyrrole (DPP, Figure 2.4d) is an inexpensive dye with a large absorption coefficient which, like rylene diimides, is solution-processable when substituted at the R_1 position with alkyl side-chains. The R_2 site is used for connections to other molecular building blocks, and thin films of DPP have exhibited SF when R_2 is thiophene-substituted, which is a small enough unit to be coplanar with the DPP core.⁸² SF was also observed in nanoparticles of

thiophene-substituted DPP, where smaller particles correlate with faster triplet formation but shorter exciton lifetimes.⁸³ Non-covalent assemblies of DPP hydrogen-bonded to rylene diimides have also been prepared as tailored architectures for SF.⁸⁴ One particularly interesting approach combines liquid-crystallinity with a donor-acceptor (D-A) approach, in which an electron-rich (D) and electron-poor (A) core are coupled together.⁸⁵ The acceptor-donor-acceptor trimer framework consisted of a central hexabenzocoronene donor, responsible for self-assembled stacking into liquid-crystal domains, flanked with DPP acceptors, and led to very high singlet fission yields and long T_1 lifetimes.

Another design approach for SF is to focus on fulfilling the thermodynamic conditions for SF through tuning of the diradical character of the molecular ground state.^{86,87} This is based on the spin-unrestricted computation of the occupation n of the highest occupied and lowest unoccupied natural orbitals (HONOs and LUNOs) and their energy-adjacent neighboring orbitals (HONO-1, LUNO+1, *etc.*):

$$T_i = \frac{n_{\text{HONO}-i} - n_{\text{LUNO}+i}}{2} \quad (2.25)$$

which relates to the expression for the multiradical character y_i via:

$$y_i = 1 - \frac{2T_i}{1 + T_i^2} \quad (2.26)$$

such that for a pure diradical character, $y_0 = 1$ and $y_1 = 0$, while for a pure tetraradical character, y_0 and y_1 are both 1. Based on these indices, it was proposed that condition 1 listed above ($\Delta E_{ST} \geq 0$) is not fulfilled if $y_0 \rightarrow 0$ or $y_0 \approx y_1$. Furthermore, a large tetraradical character y_1 leads to condition 2 ($E(S_{T_2}) > S_{T_1}$) not being met. Therefore, obtaining a reasonably high y_0 while maintaining a low y_1 leads to compounds fulfilling both energy-based conditions. This is the case for derivatives of diphenylisobenzofuran shown in Figure 2.4e.

Carotenoids (Figure 2.4f) are natural compounds with many alternating single and double bonds in an all-*trans* configuration. Their lowest excited singlet is a dark state with a double-excitation character³⁶, which corresponds to two local triplets in two distinct parts of the molecule, analogous to butadiene. This configuration may aid in the formation of the triplet-pair state, although it has been proposed that this state is not in fact involved in the SF process at all.^{88,89} Rather, the triplet-pair state may form directly from the lowest bright state to which the compound was excited. The identification of natural carotenoids has led to the design of a number of synthetic polyene analogs.⁹⁰ While carotenoids in biological environments^{91,92} (such as their parent light-harvesting complexes) were shown to exhibit SF, in solution the free carotenoid molecules undergo non-radiative decay back down to the S_0 ground state via the dark state.⁸⁹ This suggests that the conformational flexibility of the free molecules enables this non-productive relaxation, while the effect of the environment in their aggregated form is key for SF to occur,^{88,92} possibly due to the fact that it must occur in an intermolecular fashion.

This leads to the final class of conjugated polymers (Figure 2.3g), which are an extension of polyenes. Conjugated polymers exhibit a number of materials-specific advantages, such as broad absorption profiles, photo- and chemical stability, rapid triplet-pair formation, long T_1 lifetimes, the possibility of charge and exciton transport through the chain, and in the case of intramolecular electronic processes, little dependence on geometric arrangement for coupling between chromophores. The extended π -conjugated chain in a polymer offers many possible sites for triplet-pair and free T_1 positions, thus providing a driving force that would not be present in smaller systems. This has been given as a reason for rapid 1TT formation in benzodithiophene-DPP polymers but not in trimers composed of the same D and A units.⁹³ In general, due to the inclusion of fused rings in the building blocks, conjugated polymers also tend to be more rigid than polyenes, and non-radiative decay pathways are thus less accessible.

Many of the requirements for SF chromophores outlined above are fulfilled in conjugated polymers, making them a promising template for SF design. The optical, conformational and physical properties can also be tuned based on the choice of the comonomers and substituents. For instance, solubility (required for solution-based deposition techniques) can be manipulated based on the nature of the side-chains. High coplanarity between repeating units, which is determined by the local steric environment around the inter-monomer coupling site, increases conjugation and favours delocalized excitations, whereas large dihedrals between units lead to local excitations. Furthermore, photophysical processes in polymers may occur in an intra- or inter-chain fashion. Bulky side-chains reduce interchain interactions and therefore reduce intermolecular processes. It has been proposed that having fewer such interactions reduces charge carrier formation between chains, thus favouring triplet formation.⁹⁴

Polymers can be broadly classified into those with and without a significant D-A-type structure. In the former category, electron-rich and electron-poor moieties are copolymerized to form alternating $(D-A)_n$ structures. In the latter, either a single repeating unit is used, leading to such homopolymers as polydiacetylene⁹⁴, polyphenylene⁹⁵, polythiophene,⁹⁶ and polyfluorene,⁹⁷ or copolymers in which one of the monomers - usually a vinyl group - serves as a spacer to maintain planarity in the chain, such as in poly(phenylene-vinylene) (shown in Figure 2.4g).⁹⁸

In the D-A category, low-lying excitations may be described by significant charge transfer character. If this is the case, polar solvents may stabilize the S_1 energy below the thermodynamic requirement for SF, which may explain why some D-A polymers exhibit SF in thin film but not in solution.⁹³ By ensuring that S_1 is dominated by CT character, they do not act as trap states but rather assist in the SF process, as shown in Figure 2.3b. Due to the exchange interactions, the T_1 is likely to remain a localized state, in particular on the acceptor.⁹⁹ If this occurs, the triplets may not readily recombine, leading to long lifetimes.⁹³ Such a D-A polymer, based on thiophene-1,1-oxide acceptors, showed very high triplet quantum yields.⁹⁹

As a final note, polymers for SF derived from pentacene have also been reported, such as in

micelles,¹⁰⁰ and as side-chains on a non-conjugated polymer, in which SF is mediated by through-space interactions.¹⁰¹

2.5 Excited state analysis

To describe quantitatively the character of the excited states, we employ a wavefunction analysis scheme based on the following formalism¹⁰² and implemented in the TheoDORE program.¹⁰³

The transition density matrix $D^{i \rightarrow f}$ which describes the electronic transition between initial (i.e., ground) state i and final (excited) state f is written as:

$$D^{i \rightarrow f}(r_h, r_e) = n \int \dots \int \Psi_i(r_h, r_2, \dots, r_n) \Psi_f(r_e, r_2, \dots, r_n) dr_2 \dots dr_n \quad (2.27)$$

in which $\Psi_{i,f}$ are the wavefunctions of the initial and final states from which the hole and electron originate, respectively, and r_h and r_e are the coordinates of the excitonic hole and electron. In a basis of localized and orthogonal orbitals, when the ground state is described by a single determinant, the transition density matrix is the collection of one-electron excitation operators. This may be written as:

$$d_{ab}^{i \rightarrow f} = \langle \Psi_i | E_{ab} | \Psi_f \rangle \quad (2.28)$$

where E_{ab} is the excitation from occupied orbital a to unoccupied (virtual) orbital b . This $n_a * n_b$ matrix, where n is the number of orbitals of each kind in the system, is readily extracted from a TDDFT computation.

The collection of transition density matrix elements $D_{ab}^{i \rightarrow f}$ can be used to decompose the excitation into local and charge transfer contributions. A given element describes a local excitation on a particular molecular fragment A if both orbitals a and b are located on atoms within fragment A . By summing all elements located on fragment A , we arrive at an expression for the fraction of the total excitation f which is local to A (Ω_{AA}^f):

$$\Omega_{AA}^f = \frac{1}{2} \sum_{a,b \in A} (d_{ab}^{i \rightarrow f})^2 \quad (2.29)$$

Next, if orbitals a and b are on different fragments (i.e., A and B), that matrix element would describe a charge transfer character from fragment A to B . By summing over all orbitals a and b belonging to fragments A and B , respectively, we obtain a similar fraction Ω_{AB}^f , termed a 'charge transfer number':

$$\Omega_{AB}^f = \frac{1}{2} \sum_{a \in A} \sum_{b \in B} (D_{ab}^{i \rightarrow f})^2 \quad (2.30)$$

Although every atom in the system must be attributed to a fragment, the number of defined fragments is not limited. Once all local ($A = B$) and charge-transfer ($A \neq B$) combinations are considered, we observe that there are $n_{fragments}^2$ of Ω values contributing to a given excitation. The resulting Ω matrix, while evaluated in an atomic orbital basis, provides a convenient (and quantitative) description of the excitation in real space: diagonal elements denote local contributions to the transition, while all off-diagonal elements describe charge transfer between various fragments. The sum of all Ω values is equal to or slightly below 1 (i.e., 0.999).

It is important to note here that the partitioning of a chemical system into fragments is to one's discretion. For instance, a 'fragment' may be defined as the collection of subsets of atoms in one part of a molecule – such as the atoms in one monomer of a dimer or one particular ligand in a transition metal complex. Alternatively, it may be defined as all atoms of one molecule of a non-covalent assembly of molecules, such as a crystal or π -stacked structure. The appropriate definition of fragments provides a convenient means to locate the hole and electron within the system, and therefore to characterize the excitation. In the case of two associated molecules X and Y, a local state would have one large $\Omega_{X \rightarrow X}$ component, a charge transfer state (such as in a donor-acceptor system) would be dominated by one large contribution of $\Omega_{X \rightarrow Y}$, and a delocalized (Frenkel-type) exciton would have non-negligible contributions of $\Omega_{X \rightarrow X}$ and $\Omega_{Y \rightarrow Y}$, while a charge-resonance state (such as in some pentacene dimers) would exhibit equally large contributions of $\Omega_{X \rightarrow Y}$ and $\Omega_{Y \rightarrow X}$.

Finally, the approximate exciton size d_{exc}^f is obtained by summing over all atom pairs:

$$d_{exc}^f = \sqrt{\frac{1}{\Omega} \sum_{M,N} \Omega_{MN}^f (d_{MN})^2} \quad (2.31)$$

where where M and N are the indices of all atoms, Ω_{MN}^f is the charge transfer number between atoms (as computed above for fragments), d_{MN} is the distance between them, and Ω is simply a normalization factor, which is sum of all Ω_{MN} values. Note that this expression, unlike that of the charge transfer numbers, does not require an *a priori* definition of fragments.

3 Designing singlet fission candidates from donor–acceptor copolymers

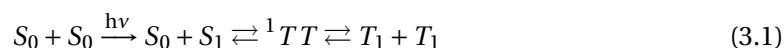
This chapter is published as:

Blaskovits, J. T.; Fumanal, M.; Vela, S.; Corminboeuf, C. Designing singlet fission candidates from donor–acceptor copolymers. *Chemistry of Materials*, **2020**, 32 (15), 6515–6524. <https://doi.org/10.1021/acs.chemmater.0c01784>

Details of database construction, benchmarking results, and supplementary figures pertaining to excited state character, tetramers, monomer properties and excitonic effects are made available in the Supporting Information of the original publication. All data discussed in this chapter are available in a Materials Cloud repository (<https://archive.materialscloud.org/record/2020.75>). The collection of all output files from Gaussian, Turbomole and TheoDORE computations is available at the same location.

3.1 Introduction

First described in 1965, singlet fission (SF) is the spin-allowed conversion of a high-energy singlet to two lower-energy triplets.¹¹ To be energetically possible, the excited singlet energy needs to be at least twice that of the triplet (i.e., $E(S_1) \geq 2E(T_1)$). By definition, SF is a multiexcitonic process: upon the absorption of light, the absorbing singlet splits into two independent triplets (T_1) through a correlated triplet-triplet pair (1TT) according to the following scheme²⁷:



In organic photovoltaic devices, this theoretically leads to a doubled photocurrent if both excitons are separated at a donor-acceptor interface. In this way, materials exhibiting quantum efficiencies above 100% and power conversion efficiencies (PCE) beyond the thermodynamic (detailed balance) limit of 33% become accessible.³⁶

SF involves two centers: following singlet excitation in one, there is energy transfer to the sec-

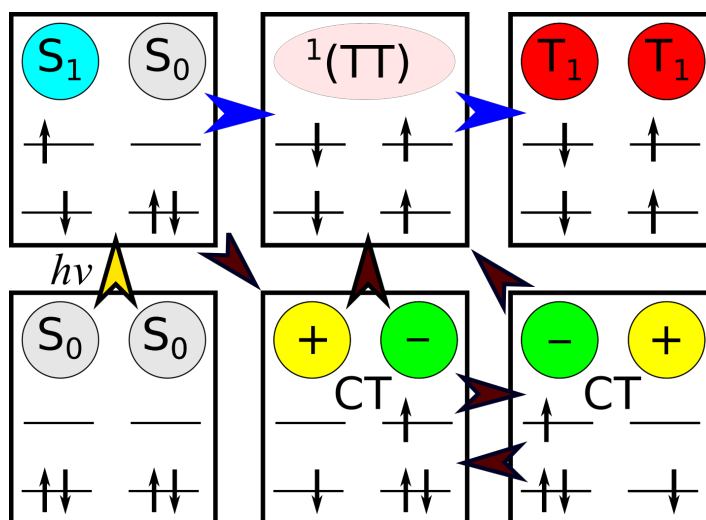


Figure 3.1: Mechanisms for SF after absorption: direct S_1 to 1TT conversion following the blue arrows, or indirect conversion mediated by charge transfer (CT) states following the brown arrows.

ond, such that one triplet is formed at each center.²⁷ Both direct^{104,105} and charge-transfer^{38,106–108} mechanisms have been proposed for this (Figure 3.1). The formation of the triplet pair can proceed through either an intermolecular or an intramolecular process. In the former case, the centers are located on two separate molecules, while in the latter the two centers are covalently bound to one another. Intermolecular SF has been extensively studied in molecular crystals.^{10,11,109–111} However, its success depends highly on the coupling between the separate units,¹¹² which ultimately relies on the molecular packing, and as such can be difficult to predict and control.^{27,104} This limitation is circumvented in intramolecular SF (iSF).^{34,113} Such is the case of covalently-linked dimers, in which synthetic modification of the linking units enables fine-tuning of the spatial orientation between the sites.^{114–117} However, precisely due to the proximity of the two implicated fragments, the triplets in these systems recombine quickly and rarely become independent. Molecules with extended conjugation, such as polyenes and carotenoids, have also shown iSF,⁹¹ but their large structural flexibility makes nonradiative decay pathways readily available.

A few studies have demonstrated iSF in conjugated polymers, particularly in donor-acceptor (D-A) copolymers, leading to some very promising candidates.^{6,99,118–120} On the one hand, Busby *et al.* designed a poly(benzodithiophene-*alt*-thiophene-1,1-dioxide) (BDT-TDO) copolymer with a triplet quantum yield of 170%, which highlighted the importance of i) strong intramolecular donor-acceptor interactions, and ii) an acceptor core with a low triplet energy. On the other hand, Zhai *et al.* reported SF character in thin films of poly(phenylene-*alt*-vinylene) albeit not in solution, indicating that for certain polymers SF may involve interchain processes.¹¹⁹ Given the limited number of copolymer-based materials undergoing iSF reported so far, clear performance trends could not be established.

To date, research exploring the mechanisms of SF has been restricted to the small number of materials in which this process was experimentally observed.^{27,34,113,121} Computations of iSF in polymers have been done retroactively to rationalize SF reported in existing materials^{6,122}, but there has been a lack of effort to locate new iSF copolymer materials using computational tools.¹²³ Only very recently a computational screening of intermolecular SF candidates, based on crystal structures, has been reported.¹²¹ Certainly, the discovery of novel iSF systems will largely benefit not only from large-scale screening but also from the development of new molecular design principles. In this work, we take advantage of the well-established modular chemistry of conjugated polymers, and their demonstrated potential for iSF, to explore their chemical space using computational screening techniques. Through systematic modulation of the donor and acceptor units in truncated dimers, we sought to establish design rules that link the monomer and dimer characteristics to the iSF potential of the resulting copolymer. In this way, we provide an accelerated computational screening framework that allows to explore a wide range of potential conjugated copolymers from *in silico* donor-acceptor combinations. From a curated database of 81 systems, we identify four promising iSF candidates; in two of these iSF has been previously reported.^{6,99} Altogether, we discuss both the rational and large-scale strategies of molecular design that will enable the discovery of new iSF materials.

3.2 Methodology

3.2.1 Criteria to achieve iSF and design strategy

The main conditions that SF candidates need to fulfill are the following: (1) the energy of S_1 is greater than or equal to twice the energy of T_1 ¹²³:

$$\Delta E_{ST} = E(S_1) - 2E(T_1) \geq 0 \quad (3.2)$$

(2) the coupling between the two chromophores involved is strong, to promote $S_1 \rightarrow {}^1TT$;³⁴
 (3) the correlated triplet pair (1TT) must evolve into two independent triplets (T_1) that can physically separate from one another and escape recombination. These criteria are referred to here as the (1) energetic, (2) coupling and (3) separation criteria, respectively.

Within the framework of donor-acceptor copolymers, the design strategy consists in combining a donor core, which acts as the main photon absorption site and whose S_1 has a dominant CT contribution to the acceptor, with an acceptor featuring a low-lying triplet state (see Figure 3.2).⁹⁹ In this way, the strong CT character of S_1 is expected to promote an efficient splitting to 1TT (coupling criterion), while the spatial separation between the two triplets on nearby acceptors, separated by the donor unit, is expected to diminish the possibility of triplet-triplet recombination (separation criterion).

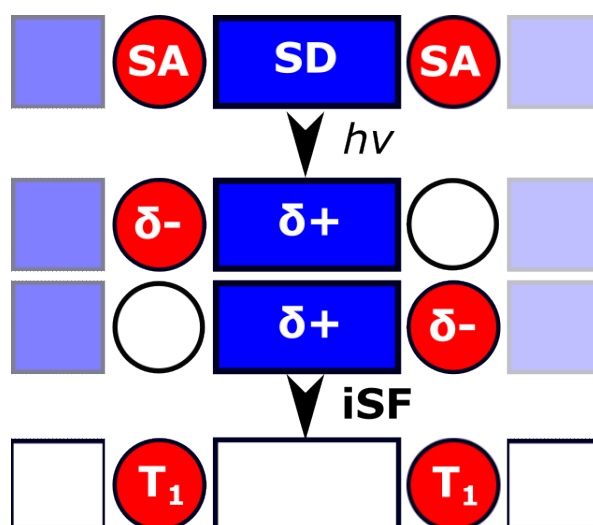


Figure 3.2: Fundamental design for strong donor-acceptor-type iSF polymers, in which absorption leading to S_1 on the strong donor (SD, in blue) provides enough charge transfer character (denoted with $\delta+$ and $\delta-$) to efficiently generate local T_1 on the adjacent strong acceptors (SA, in red).⁶

3.2.2 Database construction

Our database includes nine donors and nine acceptors that are commonly found in the literature of conjugated polymers.^{124–128} These contain cyclic, fused, and bridged derivatives of thiophene, benzene, pyrrole, and other heterocycles (see Figure 3.3). Well-established chemical motifs were prioritized to ensure that potential SF candidates that emerge from this database are synthetically feasible, as well as units that are amenable to multiple polymerization techniques and that can be synthesized with high atom economy in few steps.^{129–132} Units reported in previous works to display iSF in conjugated polymers were included: thiophene-1,1-dioxide (TDO)⁹⁹, benzodithiophene (BDT)¹¹⁸, phenylene¹¹⁹, vinylene¹¹⁹ (in the form of (*E*)-2-(2-(thiophen-2-yl)vinyl)thiophene), TVT), cyclopentadithiophene (CPDT)⁶, benzothiadiazole (BT)⁶ and isoindigo (il).¹²⁰

Each donor and acceptor core was encoded as a simplified molecular-input line-entry system (SMILES) string.¹³³ The dimer set was generated by linking the nine donors with the nine acceptors through a covalent carbon-carbon bond to form the 81 donor-acceptor pairs. The resulting SMILES strings of the dimer were then converted to Cartesian coordinates by using the gen3d operation in OpenBabel¹³⁴, which includes a conformational search and a geometry optimization at the force field level. Tighter convergence criteria were then applied by reoptimizing the geometries at the density functional theory (DFT) level. The full method used for dataset construction is detailed in section S1 of the Supporting Information, and all data are made available in the Materials Cloud repository.

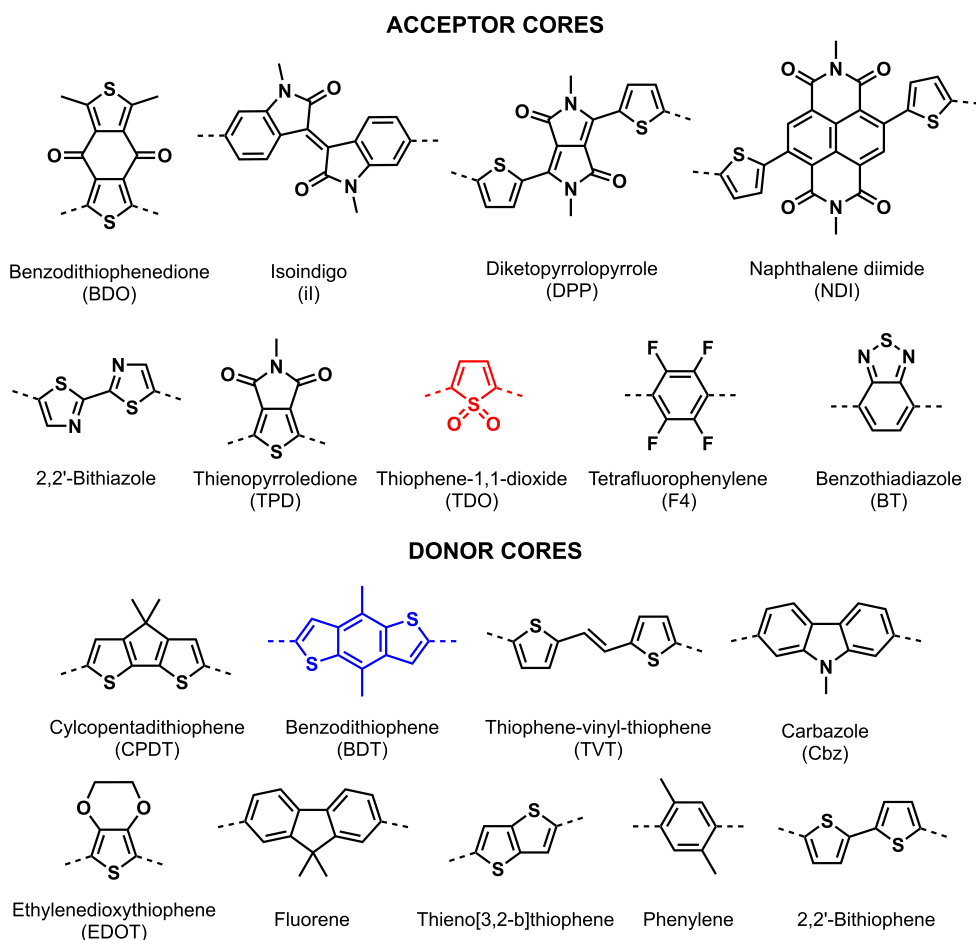


Figure 3.3: Library of acceptors and donors. Dotted lines denote the bonding positions for D-A polymer chains. Common abbreviations for the cores, when available, are given in parentheses. Structures discussed in section 3.3.1 are highlighted in red and blue.

3.2.3 Computational details

DFT computations were performed by using the Gaussian16 package (Revision A.03).¹³⁵ Ground and excited state geometries for the model copolymer described in section 3.3.1 were optimized at the ω B97X-D/TZVP level of theory.^{136,137} The 6-31G* basis set was used for subsequent database computations as it was shown to give very similar results to TZVP (see section S2). Normal mode analysis confirmed that the stationary points were minima with all real frequencies. To evaluate the energetic criterion, vertical excitations and excited-state geometry optimizations were computed by using time-dependent density functional theory (TD-DFT), within the Tamm-Dancoff approximation (TDA) to correct for the triplet instabilities reported in TD-DFT.¹³⁸ The range-separated hybrid functional ω B97X-D was used, given its accurate treatment of excited states, in particular with respect to its description of charge transfer (CT) character.^{139,140} The default range separation parameter ($\omega=0.2$) was used as this has been found to be the optimal value for conjugated systems of similar size to

Chapter 3. Designing singlet fission candidates from donor–acceptor copolymers

the present dimers.^{141,142} Full details of functional and basis set benchmarking are given in section S2. For computations with solvent, the solvent cavity reaction field (SCRF) was used with a conductor-like polarizable continuum model (CPCM), which was found to give nearly equivalent results to the SMD continuum model (see section S2.3 for a comparison of solvent models).

Gaussian output files were parsed with cclib¹⁴³ and TheoDORE (version 1.7.2)^{102,103} to assess the coupling and separation criteria by means of the local and CT character of the electronic transitions. This is done through the $\Omega_{i \rightarrow j}$ values, which quantify the amount of hole (h^+) and electron (e^-) transition density located in the different molecular fragments (i, j). In the present case, we considered two fragments: the donor (D) and the acceptor (A) cores of the donor-acceptor dimer. Accordingly, the electronic transition is decomposed into a matrix containing four Ω values, in which the diagonal elements ($\Omega_{D \rightarrow D}$ and $\Omega_{A \rightarrow A}$) quantify intrafragment contributions (i.e., the hole and electron are formed on the same fragment, $i=j$), while the off-diagonal elements are the charge-transfer components ($i \neq j$), in which the electron density is transferred from the donor fragment to the acceptor fragment ($\Omega_{D \rightarrow A}$) or vice versa ($\Omega_{A \rightarrow D}$). For each transition, the sum of the four Ω values is 1.

3.3 Results

The results are presented in four sections. In section 3.3.1 we analyze the excited state characteristics of the BDT-TDO copolymer, which previously exhibited iSF experimentally. In sections 3.3.2 and 3.3.3 we establish specific numerical thresholds to efficiently screen the energetic, coupling and separation criteria (as outlined in section 3.2.1) from the curated dataset of 81 donor-acceptor dimers described in section 3.2.2. Finally, in section 3.3.4 we map the CT character of S_1 with respect to the frontier molecular orbital (FMO) energies of the constituent monomers, and test it on 25 substituted bithiophene-benzothiadiazole pairs.

3.3.1 BDT-TDO copolymer

Copolymers made of the thiophene-1,1-dioxide acceptor (TDO, shown in red in Figure 3.3), and benzodithiophene donor (BDT, shown in blue in Figure 3.3) have shown good SF quantum yields and triplet pair lifetimes.⁹⁹ Given its status as a prototypical SF copolymer with excellent properties, we selected it as a representative test-case to establish a cost-effective computational strategy to evaluate iSF design criteria (section 3.2.1).

Vertical and adiabatic S_1 , T_1 , T_2 , and Q_1 energies were computed using the dimer (D-A) and tetramer (D-A-D-A) cluster models of the BDT-TDO copolymer (see Table S4). While the energetic criterion (1) is not fulfilled for the dimer model at the Franck-Condon point ($\Delta E_{ST}^{vert} = E(S_1) - 2E(T_1) = -0.72$ eV), this value becomes much closer to zero in the adiabatic picture ($\Delta E_{ST}^{adia} = -0.18$ eV), and even slightly positive for the extended tetramer model ($\Delta E_{ST}^{adia} = 0.04$ eV). This highlights the impact of adiabaticity in predicting potential SF behavior, while showing that

the dimer-to-tetramer extension has a much less meaningful impact on the energetic criterion.

Fragment-based decomposition analysis of hole and electron density in the excited states revealed that charge transfer from the donor core (BDT) to the acceptor (TDO) at the Franck-Condon point is the primary contribution to the S_1 excitation ($\Omega_{D \rightarrow A}^{S_1} = 0.46$), following the coupling criterion, whereas a local excitation within the acceptor dominates in T_1 state ($\Omega_{A \rightarrow A}^{T_1} = 0.42$), matching with the separation criterion (see section 3.2.1).¹⁴⁴ Similar values were obtained for the adiabatic states and, in all cases, the three other possible contributions to excitation character are smaller (see Tables S5-S6).

To be efficient, SF needs to overcome triplet-triplet annihilation (TTA) paths, that is, recombination of the two T_1 states to higher excited states such as T_2 or Q_1 . For the recombination paths to be energetically unfavourable, both $E(T_2) - 2E(T_1)$ and $E(Q_1) - 2E(T_1)$ should be positive.³⁴ While low-lying T_2 or Q_1 states do not necessarily prevent the singlet splitting, they may reduce the rate of SF. The computed adiabatic energy of T_2 resulted in 0.4 eV below S_1 when evaluated in gas phase conditions. Remarkably, this difference is significantly reduced to 0.1 eV when including polar solvent effects (see Table S4). This decrease originates in the strong CT character of S_1 , which has negligible contributions to the mainly local T_1 and T_2 states. Finally, we found that Q_1 is consistently above both S_1 and T_2 in all cases.

In summary, our computations correctly predict (1) thermodynamic adequacy, (2) donor-to-acceptor CT character as the largest contribution to S_1 , and (3) T_1 being primarily localized on the acceptor in the BDT-TDO copolymer. Adiabaticity plays an important role in the ΔE_{ST} prediction and thus, empirical rules to correct cost-effective vertical energies of D-A dimers are required. In the next section, we exploit this approach using a curated database of D-A dimers.

3.3.2 Excited state energies

Threshold for the energetic criterion. We sought to establish a computationally efficient method to evaluate ΔE_{ST} (i.e., the energetic criterion), which bypasses the structural optimization of S_1 and T_1 . To do so, the S_1 and T_1 energies of 81 donor-acceptor dimers in our dataset (see section 3.2.2) were evaluated at the S_0 geometry and at their excited state minima to establish an empirical trend. We found that the relationship between the vertical and adiabatic energies for both S_1 and T_1 is linear (see Figures S9 and S10), and thus the correlation between the vertical and adiabatic ΔE_{ST} is also linear (see Figures 3.4 and S11). The vertical T_1 energies are found to be consistently higher than those obtained from adiabatic computations. As a result, all dimers with $\Delta E_{ST} \geq 0$ eV in adiabatic computations are also above -1 eV when computed vertically (shown as dotted lines in Figure 3.4). It is therefore possible to approximate the energy conservation criterion computed adiabatically to:

$$\Delta E_{ST}^{adia} \geq 0 \text{ eV} \iff \Delta E_{ST}^{vert} \geq -1 \text{ eV}$$

In this way, all the systems with $\Delta E_{ST}^{vert} \geq -1$ will be selected as potentially promising for iSF.

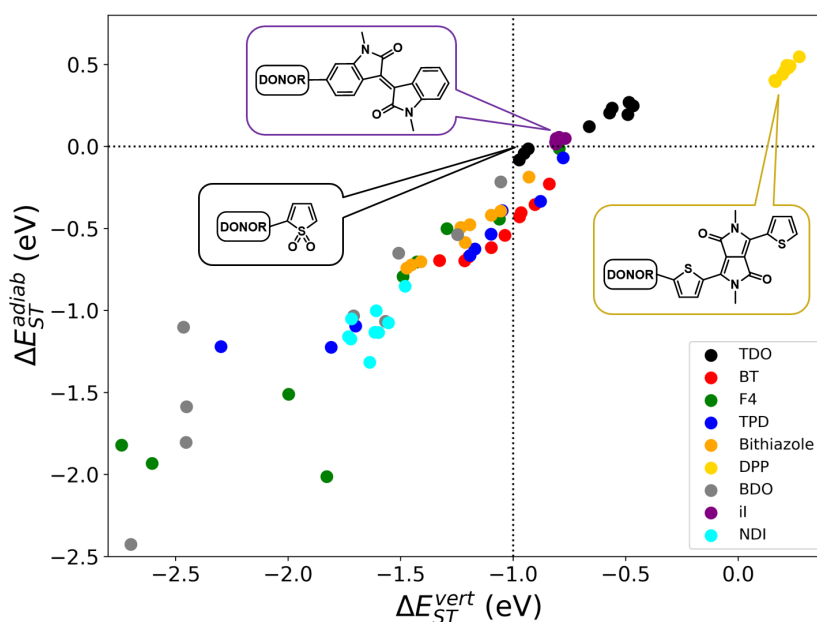


Figure 3.4: ΔE_{ST}^{vert} and ΔE_{ST}^{adia} values associated with the 81 donor-acceptor dimers, colored based on the acceptor. These are computed with TDDFT (TDA) at the ω B97X-D/6-31G* level. The vertical and adiabatic cutoffs established as the energy conservation criterion are shown as dotted lines at -1.0 and 0.0 eV, respectively.

This provides a simple and cheap method to estimate ΔE_{ST} from vertical computations by means of systematically shifting the threshold value corresponding to the energetic criterion. It is noted that the linear relationship between the vertical and adiabatic values fails when ΔE_{ST}^{vert} is below -2 eV. However, this will not bias our identification of potential iSF candidates based on this criterion, as this loss of correlation occurs well below the established threshold of -1 eV.

The computed ΔE_{ST}^{vert} and ΔE_{ST}^{adia} values of the 81 D-A dimers are represented with respect to their acceptor unit in Figure 3.4. Considering the nine sets of same-acceptor pairs, the dimers can be classified into two categories: those in which the energetic criterion mainly depends on the acceptor unit (acceptor-dependent), and those which have a broad distribution of ΔE_{ST} depending on both the donor and acceptor constituents (donor-tuning). In the former category, all dimers containing the same acceptor (DPP, il, TDO and NDI) have approximately the same energy splitting values regardless of the donor. In the latter category are the dimers containing BT, F4, TPD, bithiazole, and BDO acceptors, for which certain donors modulate the excited state energy levels toward favorable splitting. In particular, the donors TVT, CPDT, 2,2'-bithiophene, thienothiophene and BDT, which all include thiophene moieties, shift ΔE_{ST} to more positive values, while the donors that do not have thiophene motifs (Cbz, fluorene and phenylene) are systematically detrimental to the energy conservation condition. Smaller

values of ΔE_{ST} originate in nonplanar dihedral angles between the donor and acceptor units in dimers linked via a benzene ring. This leads to a weaker effective conjugation and, generally, to higher T_1 excitation energies (see section S5).

To assess whether dimer models are representative of larger oligomeric (and polymeric) systems, we evaluated (i) the vertical and adiabatic excited state energies, (ii) the structure, and (iii) the excited state character, of a subset of 21 tetramers. We considered systems that span the entire range of excitation energies and Ω values, with each donor and acceptor moiety represented at least once. The correlation between the dimer and tetramer vertical excitation energies is linear for the entire range of excitation energies and the y-intercept is close to zero (see Figures S15-S16). Consequently, negligible deviations in ΔE_{ST}^{vert} and ΔE_{ST}^{adia} between the two cluster models are obtained (see Figures S17-S18). Also, the excited states' character remains very similar in the vertical and adiabatic pictures for both the dimer (Figure S12 and S13) and tetramer models (see Figures S19-S22), likely due to the small changes in D-A conjugation upon excited state geometry optimization (see Figures S23-S25). A comparison of the S_0 and S_1 minima structures for the dimer and tetramer models can be found in section S7. Note that two of the 81 cases deviate significantly from the vertical versus adiabatic $\Omega_{D \rightarrow A}^{S1}$ trend (Figure S12). This indicates that the vertical approach may not always be valid for evaluating $\Omega_{D \rightarrow A}^{S1}$, while the iSF potential of donor-acceptor polymeric systems in terms of ΔE_{ST} and $\Omega_{A \rightarrow A}^{T1}$ can be efficiently captured through vertical excitation computations on D-A model dimers.

3.3.3 Excited state character

To identify how the excitation energies and thus, ΔE_{ST} , are affected by the different state character of S_1 and T_1 , we performed a fragment-based analysis of the main local and CT contributions. We focused on the donor-to-acceptor CT component to S_1 ($\Omega_{D \rightarrow A}^{S1}$) and on the local acceptor contribution to T_1 ($\Omega_{A \rightarrow A}^{T1}$) as key requirements for efficient iSF that will potentially favour singlet splitting and prevent fast TTA, respectively (criteria 2 and 3, section 3.2.1). These are represented for the 81 dimers in Figure 3.5. The dimers BDT-TDO (discussed in section 3.3.1) and CPDT-BT, for which iSF has been reported,^{6,99} fulfill both criteria, with the key contributions ($\Omega_{A \rightarrow A}^{T1}$ and $\Omega_{D \rightarrow A}^{S1}$) both above 0.4. The reported bithiophene-ii system¹²⁰ fulfills the separation criterion with $\Omega_{A \rightarrow A}^{T1}$ above 0.4, but not the coupling criterion as it is characterized by a small $\Omega_{D \rightarrow A}^{S1}$ of 0.1. For that reason, we tentatively select a $\Omega_{A \rightarrow A}^{T1}$ of 0.4 as threshold for screening purposes and classify the remaining systems according to their $\Omega_{D \rightarrow A}^{S1}$. Remarkably, with the exception of one BDO-containing dimer, all other dimers found in the $\Omega_{D \rightarrow A}^{S1} > 0.4$ region have BT as acceptor, which systematically generates very promising candidates for iSF. In fact, the classification into acceptor-dependent and donor-tuning D-A dimers discussed for the energy splitting values remains valid for $\Omega_{A \rightarrow A}^{T1}$ and $\Omega_{D \rightarrow A}^{S1}$. In particular, DPP- and ii-containing dimers, which systematically show positive ΔE_{ST} , lead to large $\Omega_{A \rightarrow A}^{T1}$ and small $\Omega_{D \rightarrow A}^{S1}$ in all cases (due to large $\Omega_{A \rightarrow A}^{S1}$ values). Despite fulfilling the energetic criterion, the fact that S_1 and T_1 are both characterized by a local excitation

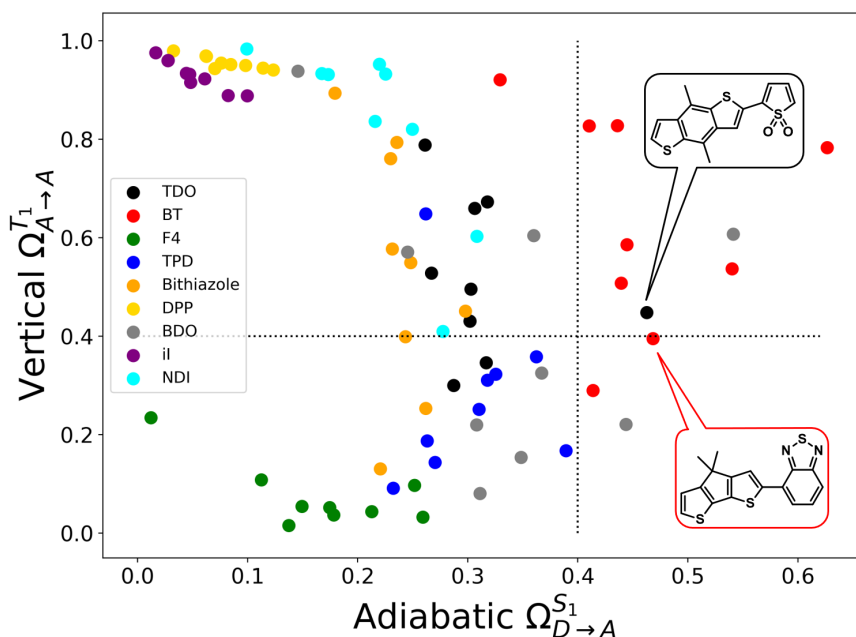


Figure 3.5: Adiabatic donor-to-acceptor charge-transfer contribution of S_1 ($\Omega_{D \rightarrow A}^{S_1}$) and vertical local acceptor contribution of T_1 ($\Omega_{A \rightarrow A}^{T_1}$) obtained for the 81 dimers, colored based on the acceptor. Evaluated with TheoDORE using results from computations with TDDFT (TDA) at the ω B97X-D/6-31G* level.

in the acceptor (or the donor) may be detrimental to the D-A design strategy for iSF. As a consequence, the dimers involving these acceptors may not undergo efficient iSF, but most likely interchain SF based on local acceptor states. Large singlet-triplet energy splitting has been previously associated with local excitations in organic systems.¹⁴⁵ However, new design principles need to be considered when evaluating the iSF capabilities of D-A copolymers. From our results, it is possible to envision a ‘modular’ design strategy based on the frontier molecular orbital (FMO) energies of the donor and acceptor units to screen the CT or local character of S_1 in the dimer.

3.3.4 Charge transfer prediction

In this section, we correlate the CT character of S_1 in the 81 D-A dimers with the FMOs of the 18 constituent monomers (collected in Table S7). This is represented schematically in Figure 3.6, where it is shown how the CT excitation ($D \rightarrow A$) competes with local excitations in either the donor or the acceptor depending on the relative ordering of the monomer FMOs. Within this approximation, the ratio between the local orbital gaps and the resulting CT energy difference defined as:

$$\frac{D_{LUMO} - D_{HOMO}}{A_{LUMO} - D_{HOMO}} \quad (3.3)$$

and

$$\frac{A_{LUMO} - A_{HOMO}}{A_{LUMO} - D_{HOMO}} \quad (3.4)$$

will estimate favorable (>1) or unfavorable (<1) CT excitations with respect to local excitations. Both ratios above 1 indicate that the FMOs of the monomers will align in such a way that the D-A dimer HOMO originates from the donor monomer and the LUMO from the acceptor monomer. This will favor low-lying CT excitations in the dimer. In contrast, if the first (second) ratio is below 1, the monomer FMOs will be positioned such that both FMOs of the D-A dimer will originate from the acceptor (donor) monomer FMOs. If this occurs, it is expected that the low-lying excited states in the dimer will be dominated by local excitations in the acceptor (donor) core, thus disfavoring CT. Both ratios are therefore necessary to describe the relative positions of the monomer FMOs. The approximation of considering orbital gaps as one-electron transitions is possible because the relationship with the local excited energies is rather linear (see Figures S26-S27). This shows that the exciton binding energy, defined as the difference between the orbital gap and the excitation energies, is relatively constant for all donors and acceptors considered.

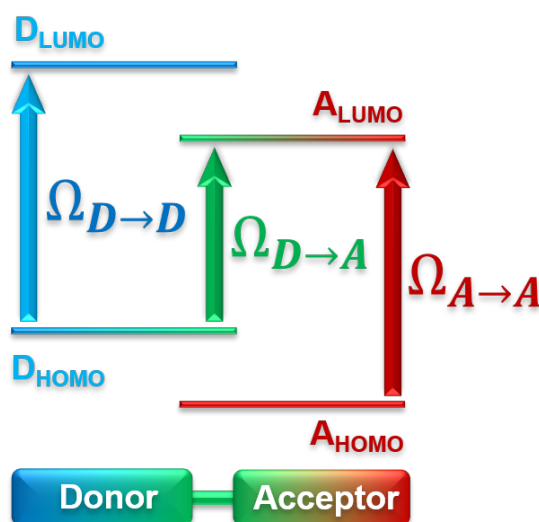


Figure 3.6: Schematic representation of the dependence of $\Omega_{D \rightarrow A}^{S1}$ in the dimer with the FMOs (HOMO, LUMO) of the monomers. The local excitations in the donor (blue) and acceptor (red) compete with the CT excitation (green).

Figure 3.7 associates the computed FMO ratios with the computed $\Omega_{D \rightarrow A}^{S1}$ values. It can be seen that the donor-acceptor monomer pairs with FMOs best suited for CT are located above

1.0 in both axes. In contrast, dimers with FMO ratios below 1 correctly predict minor CT character ($\Omega_{D \rightarrow A}^{S_1} < 0.2$). This numerical comparison using monomer FMO energies is therefore a robust metric for eliminating poor potential iSF candidates.

To illustrate the direct impact of monomer FMO energies on $\Omega_{D \rightarrow A}^{S_1}$, we generated 25 substituted bithiophene-BT donor-acceptor pairs. The monomer energy levels are substantially modulated through functionalization of the conjugated backbone with electron-donating (-OH), electron-withdrawing (-CN) and halide (-F, -Cl) moieties. As a result, the CT character of S_1 in the dimer ($\Omega_{D \rightarrow A}^{S_1} = 0.44$ when unsubstituted) becomes as low as 0.26 when an electron-withdrawing group is placed on the donor unit, and as high as 0.75 when electron-donating (withdrawing) groups are attached to the donor (acceptor) moiety. These variations are correctly captured by the FMO ratio model (Figure 3.7), which reproduces the general increase of $\Omega_{D \rightarrow A}^{S_1}$ as the FMO ratios increase. This example demonstrates that functionalization of monomers can be used to optimize the necessary properties for iSF.

3.4 Screening protocol

The protocol established to evaluate and screen promising iSF candidates among donor-acceptor copolymers consists of the following steps:

Step 1. Compute the ground state FMOs of all donor and acceptor monomer cores, and evaluate the FMO ratios for the donor-acceptor monomer pairs according to the expressions

$$\frac{D_{LUMO} - D_{HOMO}}{A_{LUMO} - D_{HOMO}} \geq 1 \quad (3.5)$$

and

$$\frac{A_{LUMO} - A_{HOMO}}{A_{LUMO} - D_{HOMO}} \geq 1 \quad (3.6)$$

Step 2. For the candidate donor-acceptor combinations resulting from step 1, generate the dimers and compute the vertical S_1 and T_1 excited state energies. Apply the energetic criterion associated with vertical energies:

$$\Delta E_{ST}^{vert} \geq -1 \text{ eV}$$

Step 3. Determine the character of the vertical T_1 state and apply the separation criterion following the Ω value: $\Omega_{A \rightarrow A}^{T_1} \geq 0.4$

Step 4. Optimize the S_1 state and classify the systems according to the coupling criterion $\Omega_{D \rightarrow A}^{S_1}$.

The computations of the different steps consist in ground state (step 1), vertical excitations

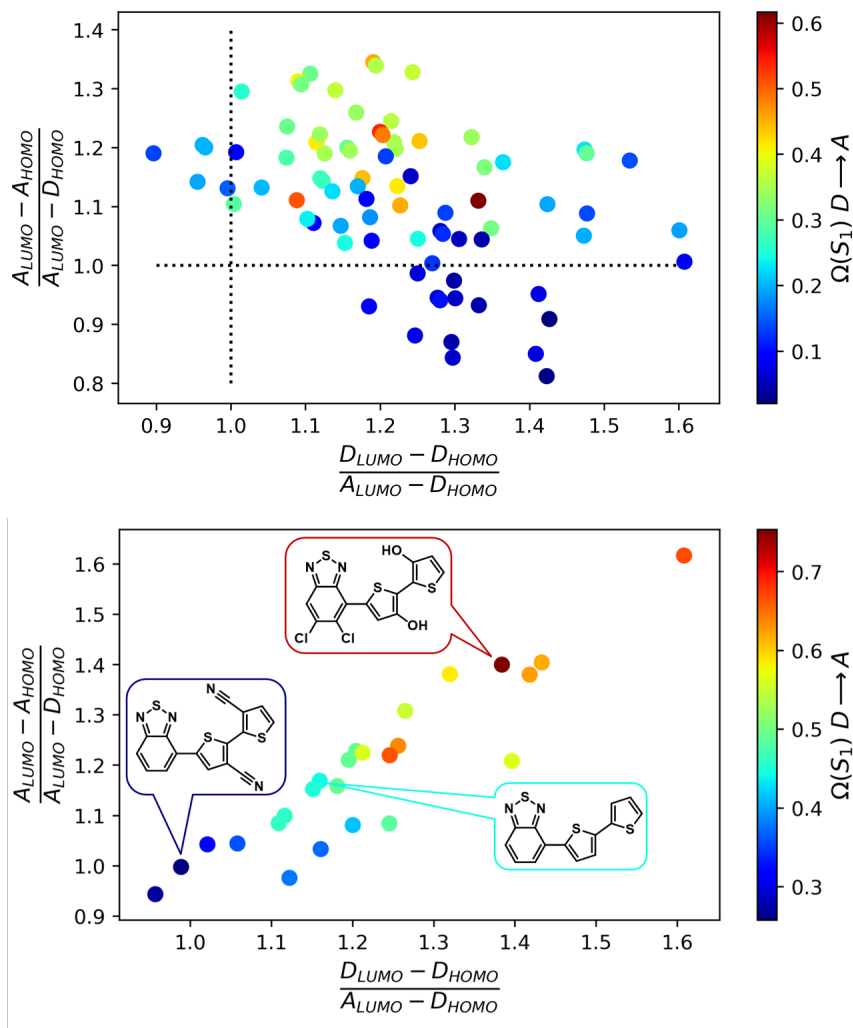


Figure 3.7: FMO ratios of the 81 donor-acceptor monomer pairs included in our dataset (*top*), see section 3.2.2), and of 25 substituted bithiophene-BT monomer pairs (*bottom*). Cutoffs for discarding poor CT dimers are represented by the dotted lines. The structures of the reference (nonsubstituted) dimer and the dimers with the highest and lowest $\Omega_{D \rightarrow A}^{S_1}$ values are shown. In both plots, the $\Omega_{D \rightarrow A}^{S_1}$ of the resulting dimer is given by the color gradient.

(steps 2 and 3), and adiabatic optimizations (step 4), while structures larger than dimers are not required. It is worth emphasizing that step 1 significantly reduces the number of computations from $N_D * N_A$ to $N_D + N_A$ (where N_D is number of donors and N_A is number of acceptors). To illustrate the efficiency of this protocol in filtering candidates, we apply it to the dataset of 81 dimers generated in this work (section 3.2.2). First, 19 possible combinations (representing 23% of the dataset) would be eliminated in step 1 and would not require dimer excited state computations. Then, 42 dimers (52%) would be rejected in step 2. From the remaining 20 systems, 14 fulfill $\Omega_{A \rightarrow A}^{T_1} \geq 0.4$ in step 3 and therefore require further adiabatic optimizations

Chapter 3. Designing singlet fission candidates from donor-acceptor copolymers

in step 4. The $\Omega_{D \rightarrow A}^{S1}$ values of these final 14 systems (17%) are shown in Figure 3.8. The systems reported to undergo iSF (BDT-TDO and CPDT-BT) previously^{6,99} are classified as the most promising ones, and two new promising candidates, thieno[3,2-b]thiophene-BT and 2,2'-bithiophene-BT are predicted. While they exhibit less CT character than these top four candidates, six other TDO-containing dimers (marked in blue) are also flagged for promising iSF character. Interestingly, the reported iSF isoindigo system¹²⁰ (bithiophene-ii) is discarded in our protocol. While it fulfills $\Delta E_{ST}^{vert} \geq -1$ eV and $\Omega_{A \rightarrow A}^{T1} \geq 0.4$, it has a $\Omega_{D \rightarrow A}^{S1}$ value of < 0.1 . To ensure that our predictions for this system are reliable, we re-evaluated $\Omega_{D \rightarrow A}^{S1}$ with alternative methods but similar values are obtained (section S9). In comparison with our reference BDT-TDO system that exhibits iSF in the ultrafast scale (< 1 ps),⁹⁹ bithiophene-ii displays iSF after 60 ps,¹²⁰ which is in the range of timescales observed for other SF materials.¹⁴⁶ Further investigations are therefore needed to determine the iSF mechanism of D-A copolymers characterized by small $\Omega_{D \rightarrow A}^{S1}$ values, particularly those containing the ii acceptor, such as bithiophene-ii and the ii-containing materials marked in green in Figure 3.8.

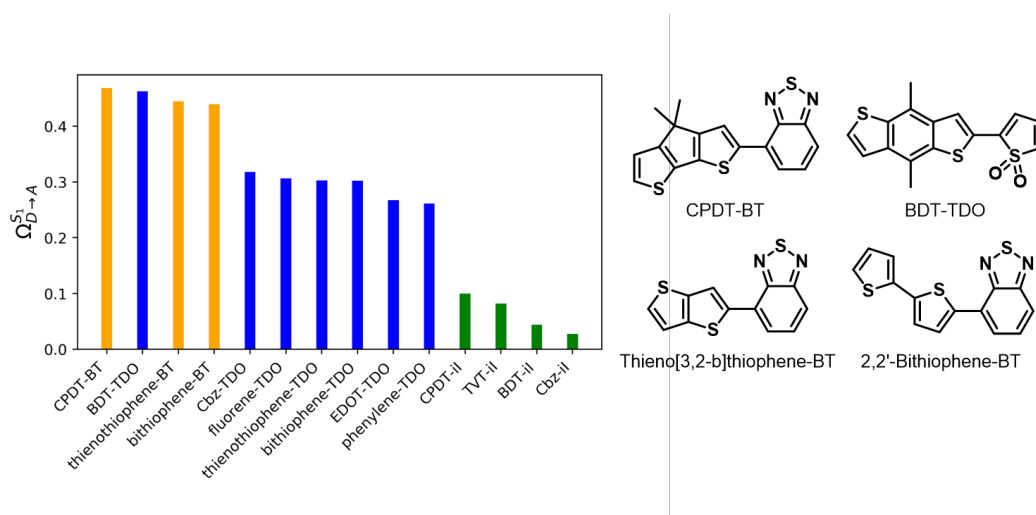


Figure 3.8: (left) Compounds retained following steps 1-3 of the screening protocol, ordered following the ranking criterion of $\Omega_{D \rightarrow A}^{S1}$ as defined in step 4 and colored based on acceptor. (right) The best four potential DA copolymer candidates flagged for iSF.

3.5 Conclusion

We have developed a cost-effective computational protocol to perform large-scale screening of donor-acceptor copolymers with promising features for intramolecular singlet-fission. Using a structurally diverse database of donor and acceptor units, we have established a simplified yet robust computational strategy to evaluate the energy splitting criterion and the charge-transfer requirements of the D-A candidates from conventional vertical excited state computations. In the context of accelerated screening, we have proposed an expression to predict the excited state character of D-A dimers from the FMO energies of their constituent donor and acceptor units. This drastically reduces computational time in initial screening stages, as the number

of computations is reduced from $ND \cdot NA$ to $ND + NA$, ND and NA being the number of donor and acceptors considered.

This protocol is based on the main characteristics of two donor-acceptor pairs that exhibit singlet fission behavior experimentally,^{6,99} and we propose two promising new candidates, thieno[3,2-*b*]thiophene-BT and 2,2'-bithiophene-BT, that have not been studied to date. Benzothiadiazole (BT) and thiophene-1,1-dioxide (TDO) in particular show promise as acceptor units which drive iSF in D-A materials. Altogether, these findings pave the way for high-throughput screening of large, chemically diverse databases of D-A conjugated polymers as a mean to bolster the collective library of SF materials.

4 Identifying the trade-off between intramolecular singlet fission requirements in donor–acceptor copolymers

This chapter is published as:

Blaskovits, J. T.; Fumanal, M.; Vela, S.; Fabregat, R.; Corminboeuf, C. Identifying the trade-off between intramolecular singlet fission requirements in donor–acceptor copolymers. *Chemistry of Materials*, **2021**, 33 (7), 2567–2575. <https://doi.org/10.1021/acs.chemmater.1c00057>

Details of database construction and methods used, supplementary figures and tests for computational methods are made available in the Supporting Information of the original publication. All data discussed in this chapter are available in a Materials Cloud repository (10.24435/materialscloud:xj-9d). Interactive plots of the full dataset of 2944 dimers are freely available on Materials Cloud (<https://www.materialscloud.org/discover/isf>).

4.1 Introduction

Singlet fission (SF) is the process by which a photoexcited singlet state (S_1) couples through a spin-conserving process to a triplet pair (1TT), either directly or via intermediate or virtual states.^{27,64} If the triplet pair does not recombine or decays through other parasitic processes, they may become independent triplets (T_1) and be extracted as two charge-pairs, for instance to generate a photocurrent. In theory, this multiexciton process has the potential to overcome the thermodynamic limit of single junction solar cells.⁵⁸ SF was first described in anthracene^{10,11} and tetracene¹² more than half a century ago, and was first implemented in organic electronic devices using pentacene in the 2000s.^{19,65} And yet, to this day the vast majority of experimental and theoretical studies of both intermolecular (xSF) and intramolecular singlet fission (iSF) still focus on various acene derivatives in their monomeric and dimeric forms, respectively.^{27,45,64,114,115,117,147,148}

Despite the large range of acene-based compounds in the SF materials library, a recent review has highlighted just how few singlet fission-capable materials have been effectively implemented in organic solar cells.⁶⁴ One promising family of materials which may fill this gap

Chapter 4. Identifying the trade-off between intramolecular singlet fission requirements in donor-acceptor copolymers

between concept and implementation is that of donor-acceptor (D–A) intramolecular systems, and in particular conjugated polymers. Their advantages include broad photoabsorption and high stability, and their modular nature enables a rational control of their electronic structure, interchromophore geometries, solubility and molecular packing through the proper selection of DA units, linkers and side-chains. This might help overcome the device-related drawbacks of most SF materials by combining the precise energetic requirements of a small-molecule intramolecular SF material with the structural and chemical advantages of larger conjugated systems.^{6,93,99,118–120,122,149}

The electronic requirements of iSF in D–A polymers can be summarized by three conditions: i) the energy of the lowest excited singlet state ($E(S_1)$) must be no less than twice that of the lowest excited triplet ($E(T_1)$):

$$\Delta E_{ST} = E(S_1) - 2E(T_1) \geq 0 \quad (4.1)$$

ii) the singlet state must be coupled to the triplet pair through low-lying charge transfer states; and iii) the triplet pair state must evolve into two triplet states which are physically separate and energetically independent.^{27,34,36} The first condition is purely thermodynamic, the second ensures efficient fission from the S_1 to the 1TT state, and the third limits the reverse process of triplet-triplet annihilation back to a singlet. These parameters drive iSF in D–A copolymers as follows^{6,7,93,99,118,120,149}: the donor chromophore acts as the site of photon absorption and singlet formation, the coupling between the donor and the acceptor through the conjugated chain leads to the triplet pair being formed on acceptors adjacent to the absorbing donor, and the acceptor has a low triplet energy so as to accommodate the triplets. The spatial separation of the acceptors along the polymer chain is expected to lead to a less bounded 1TT state, thus promoting efficient triplet separation, and to ensure that the triplets, once independent, do not recombine.

Recently, we have proposed a series of straightforward and accurate computational descriptors with which to evaluate these three aforementioned requirements in conjugated polymers, namely the energetic, coupling and separation criteria, using truncated D–A dimers.⁷ On the one hand, we showed that the energetic criterion in the adiabatic regime ($\Delta E_{ST}^{adia} \geq 0$ eV) can be approximated using excitation energies at the Franck-Condon point, such that the energy splitting expression can be evaluated using a much more computationally tractable diagnostic ($\Delta E_{ST}^{vert} \geq -1$ eV) that does not require excited state geometry optimizations. On the other hand, the character of the S_1 and T_1 states can be quantified using charge transfer numbers extracted from the transition density matrix of the partitioned donor and acceptor fragments of the oligomer. In this way, the coupling criterion is measured by considering the donor to acceptor charge transfer character of the S_1 state ($\Omega_{D \rightarrow A}^{S_1}$), and the separation criterion is evaluated from the local acceptor character of the vertical T_1 state ($\Omega_{A \rightarrow A}^{T_1}$). These descriptors enable the quantification of the electronic requirements of the direct iSF mechanism in D–A copolymers, while other secondary routes of splitting are not considered here.¹⁵⁰

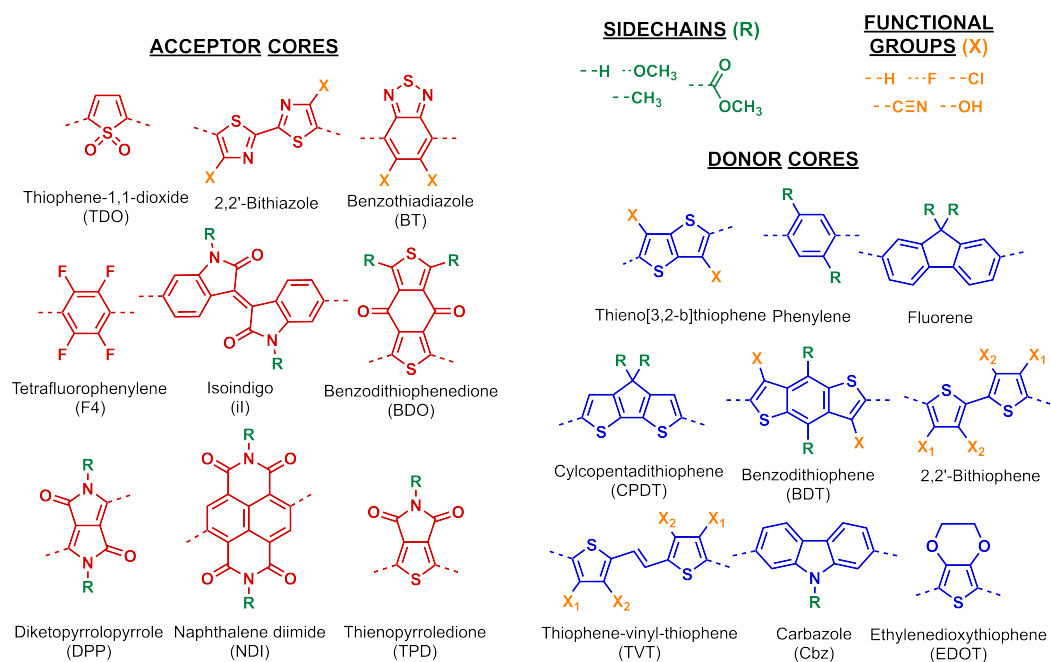


Figure 4.1: Library of acceptor cores, donor cores, side-chains (R) and functional groups (X) used to create the database studied here. Dotted lines denote the sites for linkages to adjacent donor/acceptor cores.

The experimental literature of donor-acceptor conjugated polymers is vast. By contrast, the number of D–A dimers, oligomers and polymers studied for iSF character is insignificant when compared to the acene family. A recent review that collects the D–A systems showing iSF is found in ref⁶⁴. Only a few special cases have shown outstanding iSF efficiencies^{99,118,120}, while other D–A systems which were expected to show iSF have failed.¹⁵¹ This highlights the difficulty to properly balance the three criteria required for iSF in the D–A copolymer strategy, which we now ascribe to the existence of a fundamental trade-off between the key descriptors. Such a trade-off emerges from the computational evaluation of a large database containing 2944 D–A copolymers and is rationalized here using the frontier molecular orbital (FMO) energies of the constituent D and A cores. The dependence of the key descriptors ($\Omega_{D \rightarrow A}^{S1}$, $\Omega_{A \rightarrow A}^{T1}$ and ΔE_{ST}^{vert}) on the FMO energies enables us to establish a set of simple guiding principles that allow for the accelerated screening of appropriate D–A combinations with potential iSF behavior.

4.2 Database

Common, synthetically versatile, and chemically stable building blocks were used to generate the pool of conjugated core structures.^{124–126} Monomers and dimers were generated from libraries of donor, acceptor and substituent fragments, as shown in Figure 4.1. Functionalization plays a key role in the chemistry of conjugated polymers and small molecule

Chapter 4. Identifying the trade-off between intramolecular singlet fission requirements in donor-acceptor copolymers

organic electronics, as it provides opportunities to fine-tune the electronic structure and conformational preferences of the building blocks through electron-donating and -withdrawing groups, and with moieties which form noncovalent inter- and intramolecular interactions, respectively.^{152–154} To include only reasonable functionalization patterns in our database, we considered the substitution sites which have been reported in the experimental literature as amenable to the reactions (e.g., metalation and halogenation) necessary for functionalization, as indicated by the 'X' in Figure 4.1. For instance, the backbone fluorination of thiophene moieties, either alone^{155–159} or as a component of more complex units^{160–163} is a widely-reported approach to tuning the electronic properties of the heterocycle and the resulting extended material.¹⁵² The chlorination of monomers^{164–168} has also been used experimentally to modify the electronic and steric properties of conjugated polymers, as has esterification, cyanation and alkoxylation.^{169–174} N-substituted side-chains on the amide and imide moieties found on isoindigo (iI), diketopyrrolopyrrole (DPP), naphthalene diimide (NDI) and thienopyrroledione (TPD) acceptors are readily accessible through the condensation of anhydrides with amines and substitutions reactions.^{175,176} These sites and similar ones on other cores are tagged for side-chain substitution, as shown by the 'R' in Figure 4.1. The library of donor and acceptor cores was paired with five functional groups (fluoro, chloro, hydroxyl, cyano and hydrogen reference) and four truncated side-chains (methyl, methoxy, methyl ester and hydrogen reference). Each functional group and side-chain was substituted iteratively on each donor and acceptor core which possesses a chemical handle for the relevant substitution, as described above and in section S1. Through the combinatorial addition of these cores with functional groups and side-chains, 92 donors and 32 acceptors are obtained. Dimers were generated by coupling the D and A units through a C_{sp2} - C_{sp2} bond in the positions most commonly used for coupling and polymerization reactions, giving a total number of 2944 D–A compounds. Further details on the fragment-based design of dimers are given in section S1 of the Supporting Information.

4.3 Results

4.3.1 Trade-off

Within the framework of the D–A copolymer strategy, the CT character of the low-lying absorbing singlet modulates the electronic coupling between the donor and the adjacent acceptor cores (coupling criterion). Overstabilization of the CT singlet must however be prevented by ensuring that the singlet energy is larger than twice the triplet energy (energetic criterion). Finally, photoexcitation is followed by the formation of triplets localized in the acceptors, thus preventing recombination and favoring triplet dissociation (separation criterion). These requirements have been quantified using the descriptors of energy splitting (ΔE_{ST}^{vert}), and fragment-based charge transfer numbers ($\Omega_{D \rightarrow A}^{S1}$ and $\Omega_{A \rightarrow A}^{T1}$) for the energetic, coupling and separation criteria, respectively, for the 2944 dimers in our database. The relationship between them is mapped in Figure 4.2a and is also provided in a freely-available interactive representation (see the Supporting Information). It can be seen that the systems with good

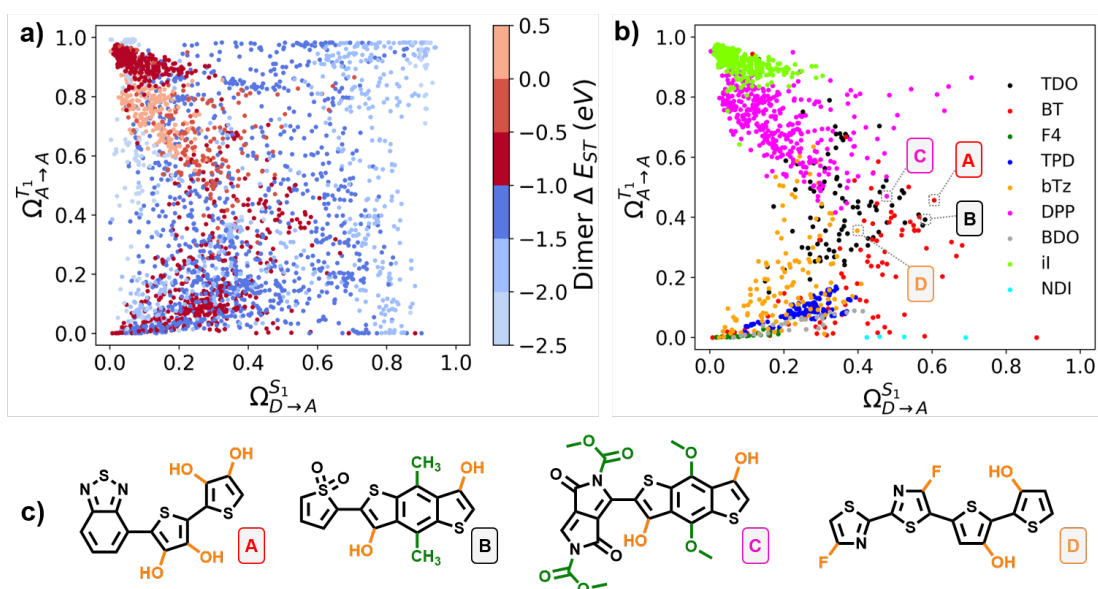


Figure 4.2: Relationship between the donor-to-acceptor charge-transfer character of S_1 ($\Omega_{D \rightarrow A}^{S_1}$, x-axis) and the local acceptor character of T_1 ($\Omega_{A \rightarrow A}^{T_1}$, y-axis) for the 2944 dimers in our database, colored based on (a) the vertical singlet-triplet splitting in the dimer (ΔE_{ST}^{vert}) and (b) the acceptor core, only for those systems with $\Delta E_{ST}^{vert} > -1$. (c) Best dimer candidates with a given acceptor core in the trade-off regime. All structures and their relevant dimer and monomer excited state properties may be visualized interactively at <https://www.materialscloud.org/discover/isf>.

splitting energies ($\Delta E_{ST}^{vert} > -1$ eV, in red) display a chevron-shaped distribution of Ω values, with only a small minority of compounds presenting large (~ 0.5) $\Omega_{D \rightarrow A}^{S_1}$ and $\Omega_{A \rightarrow A}^{T_1}$ values simultaneously. A few exceptions exist to this general trend, which can be found at the top- and bottom-right corners of the plot. In these outliers, the dihedral angle connecting the D and A units (ϕ_{D-A}) becomes significantly large, therefore breaking the copolymer planarity. This is depicted in Figure S3 where the coupling and separation criteria are mapped with respect to ϕ_{D-A} . This shows that the trade-off within the chevron indeed only applies for fully conjugated systems, while its boundaries can be pushed by inducing torsion in the D–A bond. It is, however, unclear at what dihedral angle the conjugation is completely broken, thus making iSF no longer possible.

For coplanar systems fulfilling $\Delta E_{ST}^{vert} > -1$, the most promising for iSF are those with higher $\Omega_{D \rightarrow A}^{S_1}$ and $\Omega_{A \rightarrow A}^{T_1}$ values, which corresponds to the chevron point of Figure 4.2a. Note that the energetic criterion discards systems in which the S_1 state is overstabilized by CT, in which case iSF is thermodynamically not possible. It can be seen in Figure 4.2b that the distribution of Ω values largely depends on the acceptor core. BT- and TDO-containing systems (e.g., compounds A and B in Figure 4.2c) lie in the target chevron-region of coplanar structures, as well as those systems containing DPP as the acceptor, which transition from the top-left corner toward the chevron peak (compound C). In contrast, the systems with the bTz acceptor

Chapter 4. Identifying the trade-off between intramolecular singlet fission requirements in donor-acceptor copolymers

transition from the bottom-left corner toward the chevron peak (compound D). Still within the systems that fulfill $\Delta E_{ST}^{vert} > -1$, those containing F4 display large $\Omega_{A \rightarrow A}^{T1}$ but small $\Omega_{D \rightarrow A}^{S1}$ (top-left), while those containing TPD and BDO remain in the bottom-left corner where both $\Omega_{D \rightarrow A}^{S1}$ and $\Omega_{A \rightarrow A}^{T1}$ approach to zero. Interestingly, the latter systems are only paired with TVT or CPDT donors, while top-left systems do not show a specific dependence on donor core (Figure S4). Clearly, the ability to fulfill the trade-off between ΔE_{ST}^{vert} , $\Omega_{D \rightarrow A}^{S1}$ and $\Omega_{A \rightarrow A}^{T1}$ originates in the electronic properties of the constituent monomers, which opens the question of how to engineer the most appropriate combination. This is addressed in the next section.

4.3.2 FMO model

To understand why it is so difficult to simultaneously optimize $\Omega_{D \rightarrow A}^{S1}$, $\Omega_{A \rightarrow A}^{T1}$ and ΔE_{ST}^{vert} , we resort to the analysis of the FMO expressions A_{crit} and D_{crit} (see Figure 4.3), which we designed to enable a fragment-based analysis of these key descriptors, in a computationally-efficient manner.⁷ These two variables suffice to describe the four FMO energies of the individual D and A monomers, and to predict their behavior once they are coupled in a DA dimer (see Figure 4.3). Systems with both values above 1 constitute the target regime, since then the D-to-A charge transfer (CT, green arrows) excitation will be favored over the local excitation in either the acceptor (red arrows) or the donor (blue arrows), thus fulfilling the coupling criterion. Systems fulfilling only D_{crit} or A_{crit} display a mismatch in the HOMO or LUMO energies, respectively, while systems with both D_{crit} and A_{crit} below 1 lie in the inverted regime, in which the D plays the role of the A, and vice versa, which indicates that the initial designated roles are not correct. In both the mismatched and inverted regimes, local excitations prevail over the desired CT one (see Figure S5).

It can be seen in Figure 4.4 (left) that large values of D_{crit} and A_{crit} correspond to systems with a larger D-to-A CT character of the S_1 excited state ($\Omega_{D \rightarrow A}^{S1}$), which highlights that the FMO model is able to assess the character of the S_1 state for the 2944 dimers based on the constituent monomer FMO energies (see Figure S7). This very same model is indeed able to provide a recipe on how to maximize the local acceptor character of T_1 ($\Omega_{A \rightarrow A}^{T1}$) to fulfill the separation criterion. Unlike the gradual evolution observed for $\Omega_{D \rightarrow A}^{S1}$, Figure 4.4 (right) reveals a stark partitioning of compounds with poor (< 0.3) and large (> 0.6) $\Omega_{A \rightarrow A}^{T1}$ values along the narrow $D_{crit} \approx A_{crit}$ diagonal boundary. This boundary splits the dimers showing $D_{crit} > A_{crit}$, associated with a large $\Omega_{A \rightarrow A}^{T1}$, from the opposite ($D_{crit} < A_{crit}$), in which case the triplet contains significant undesired contributions from local donor transitions ($\Omega_{D \rightarrow D}^{T1}$, Figure S6 and S8). Systems with large $\Omega_{D \rightarrow D}^{T1}$ in combination with significant $\Omega_{A \rightarrow D}^{S1}$ would correspond to the ‘inverted regime’, as discussed above, in which the roles of the ‘donor’ and ‘acceptor’ are reversed. However, no systems display such a combination as the dataset is intentionally built from D and A cores to promote $\Omega_{D \rightarrow A}^{S1}$. Finally, no appreciable CT character in the triplet is found except in a small number of dimers with concurrently very high values of D_{crit} and A_{crit} , because exchange interactions dominate in the high spin states and thus local excitations are energetically favored.

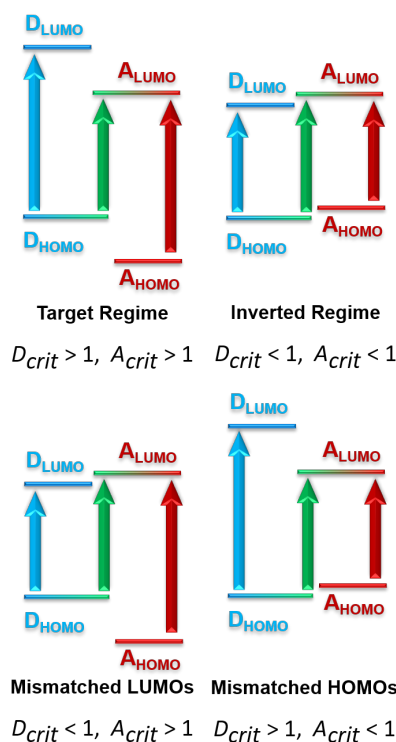


Figure 4.3: The competition between charge transfer (green), local donor (blue) and local acceptor (red) transitions leads to four regimes in the FMO dimer model.

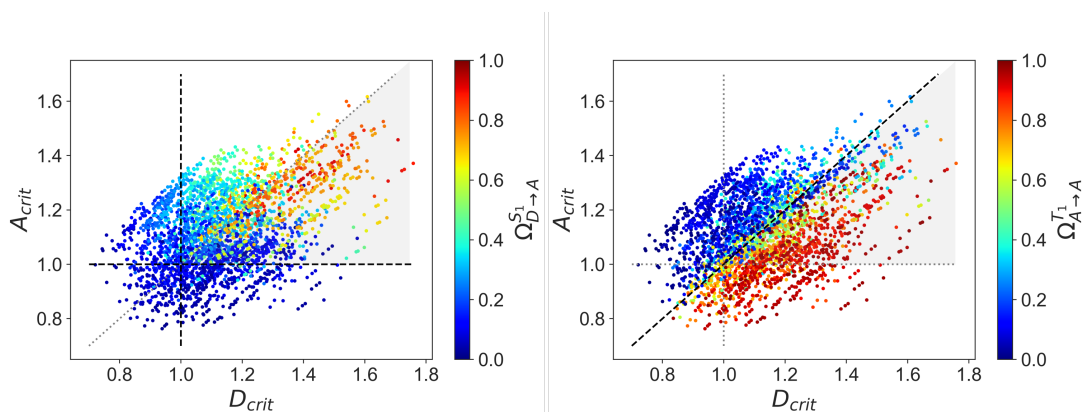


Figure 4.4: Monomer FMO criteria D_{crit} and A_{crit} , colored according to the descriptors: (a) $\Omega_{D \rightarrow A}^{S_1}$, (b), $\Omega_{A \rightarrow A}^{T_1}$. The gray background indicates the region of FMO space where both descriptors show optimal values.

It is already clear at this stage that an appropriate trade-off between $\Omega_{D \rightarrow A}^{S_1}$ and $\Omega_{A \rightarrow A}^{T_1}$ is necessary to build up potential iSF D–A copolymer candidates. A comparison of the plots in Figure 4.4 shows that systems with a too small A_{crit} may result in acceptor-centered transitions in both the T_1 and the S_1 states, such that the separation criterion is satisfied, but the coupling criterion (requiring significant $\Omega_{D \rightarrow A}^{S_1}$) is not. Therefore, only acceptors of ‘intermediate’ gap

Chapter 4. Identifying the trade-off between intramolecular singlet fission requirements in donor-acceptor copolymers

size, where all three FMO-based expressions ($D_{crit} > 1$, $A_{crit} > 1$, and $D_{crit} - A_{crit} > 0$) are fulfilled simultaneously once coupled to a donor, are of interest to iSF materials. This target region is represented by the gray background triangle in Figure 4.4. Only 37% of the database systems are located in this spot, regardless of fulfilling or not the energetic criterion.

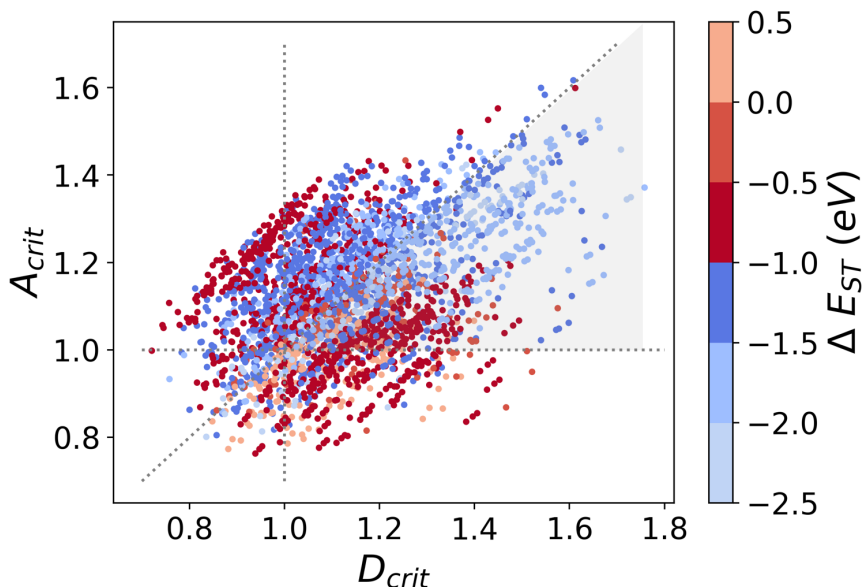


Figure 4.5: Monomer FMO criteria D_{crit} and A_{crit} , colored according to ΔE_{ST} . The gray background indicates the region of FMO space where $\Omega_{D \rightarrow A}^{S1}$ and $\Omega_{A \rightarrow A}^{T1}$ show optimal values (see Figure 4.4).

The relationship between the monomer FMO ratios and the dimer ΔE_{ST} (see Figure 4.5) is less evident than for the $\Omega_{D \rightarrow A}^{S1}$ and $\Omega_{A \rightarrow A}^{T1}$ values discussed above. One reason is that the FMO picture lacks excitonic effects and is thus imperfect at explaining the dimer ΔE_{ST} . A better correlation is found when monomer singlet-triplet state energies are used, instead of FMO energies, to explain ΔE_{ST} (see Figure S9a). It can be seen that ΔE_{ST} is indeed dictated by the highest singlet-triplet gap among the constituent D and A units. In other words, to obtain an adequate ΔE_{ST} , either the D or the A must have an inherently good singlet-triplet gap, which in most cases can be associated with a small local FMO gap (see Figure S9b). This is the case of DPP and iI acceptors, which have small FMO gaps and thus, systematically show $\Delta E_{ST}^{vert} > -1$ eV when paired with a given donor (top-left region in Figure 4.2b). On the other hand, systems containing CPDT and TVT donors show large singlet-triplet splitting for the same reason, while leading to poor $\Omega_{A \rightarrow A}^{T1}$ values when paired with most acceptors. Considering that the separation criterion aims at a large $\Omega_{A \rightarrow A}^{T1}$, achievable by a small-gap acceptor, the logical choice is therefore an acceptor unit with a small FMO gap, yet not too small to penalize $\Omega_{D \rightarrow A}^{S1}$ (mismatched HOMOs regime, see Figure 4.3), revealing once again the difficulty to optimize all descriptors simultaneously. Exceptionally, only the TDO acceptor displays large splitting while having a remarkably large FMO gap (see section S7 for details), which makes it

particularly attractive to build promising D–A candidates.

In summary, the FMO model explains the existing optimization problem as follows: $\Omega_{D \rightarrow A}^{S1}$ is optimal when A_{crit} and D_{crit} are > 1 , which implies that $A_{LUMO} - D_{HOMO}$ is minimized (see Figure 4.4, left); $\Omega_{A \rightarrow A}^{T1}$ is optimal when A_{crit} is smaller than D_{crit} (see Figure 4.4, right); while ΔE_{ST} is optimized when either the donor or the acceptor has a small FMO gap. There is thus a small region in the FMO space that concurrently optimizes the three descriptors. It now remains to be seen which components of our dataset contribute to generate D–A dimers whose properties lie within this hotspot.

4.3.3 Functionalization

The chemical modification of bare D–A pairs using functional groups and side-chains affects their iSF capabilities due to electronic and structural effects. These effects are tracked in the 1D-histograms of the change in $\Omega_{D \rightarrow A}^{S1}$ and $\Omega_{A \rightarrow A}^{T1}$ upon functional group and side-chain substitution, with respect to the H-substituted reference (see Figures 4.6 and S11-S13). In these histograms, narrower peaks indicate consistent changes induced by a given functionalization, while broader distributions indicate that the substituent has a different effect depending on the nature of the core being functionalized. An example of the former is fluorine as the acceptor substituent (see Figure 4.6a), as it leads to a systematic increase of $\Omega_{D \rightarrow A}^{S1}$, which indicates that this substitution reliably promotes D-to-A CT. An example of the latter case is the OH substitution on the donor (acceptor), which systemically increases (decreases) $\Omega_{D \rightarrow A}^{S1}$ due to its electron-donating effect (see Figure 4.6a for acceptor substitution and Figure S11a for donor substitution). The overall increase (decrease) in $\Omega_{D \rightarrow A}^{S1}$ upon addition of an electron-withdrawing (donating) group to the acceptor core can be understood intuitively from the FMO model: a more electron-poor (rich) acceptor core has deeper (higher) FMOs than the unfunctionalized analogue, thus reducing (increasing) the denominator of A_{crit} and D_{crit} and increasing (reducing) the value of these expressions. This explains the trend observed in Figure 4.2a-b, in which the systems showing mostly local excitations on the acceptor (top-left) and the donor (bottom-left) corners can be optimized toward the chevron peak by the appropriate functionalization of the D–A combination.

Contrary to $\Omega_{D \rightarrow A}^{S1}$, functional group substitutions have no consistent effect on $\Omega_{A \rightarrow A}^{T1}$, which in most cases displays nonshifted distributions (see Figures 4.6b and S11b). In general, the mild effect of substitutions on $\Omega_{A \rightarrow A}^{T1}$ emerges from their little-to-no change on the FMO gaps, as most of the electron-withdrawing (donating) groups considered stabilize (destabilize) the HOMO and LUMO simultaneously. In some cases, however, the chlorination or hydroxyl substitution on the acceptor provides larger values of $\Omega_{A \rightarrow A}^{T1}$ as seen in the shoulder in these histograms. This is mainly due to the induced dihedral torsion.

The impact of functionalization on the energetic descriptor (ΔE_{ST}) is shown in Figures 4.6c and S11c. Generally broad and unstructured distributions point to the absence of a systematic effect upon donor or acceptor substitution. This is expected considering the dependence

Chapter 4. Identifying the trade-off between intramolecular singlet fission requirements in donor-acceptor copolymers

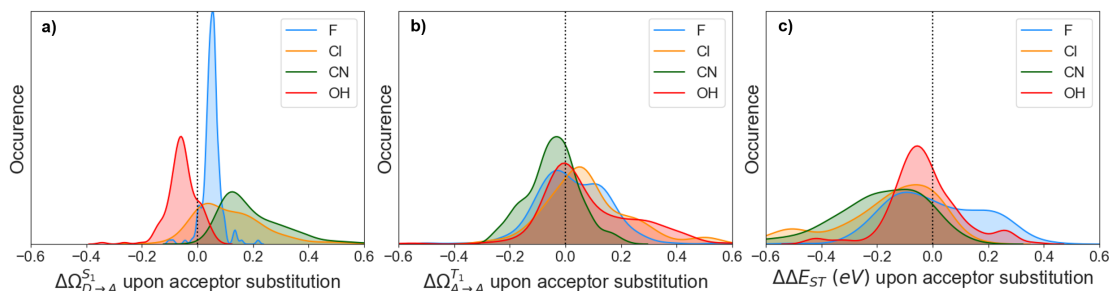


Figure 4.6: Histograms showing the change in the descriptors (a) $\Omega_{D\rightarrow A}^{S1}$ (b) $\Omega_{A\rightarrow A}^{T1}$ (c) ΔE_{ST} upon different acceptor functionalization. ΔX is evaluated as the difference between a substituted dimer with respect to the dimer with H in the substituted position.

of ΔE_{ST} on the local monomer FMO gap (see section 3.2), which in turn remains mostly unchanged upon functionalization as stated above. Certainly, tuning the splitting criterion in DA copolymers requires chemical modifications beyond the functionalization with electron-withdrawing and electron-donating groups. In particular, the acceptor cores need to be chemically modified to intrinsically display large singlet-triplet splitting values without strongly penalizing the D-A CT capabilities ($\Omega_{D\rightarrow A}^{S1}$). This is the case of the TDO acceptor, which in combination with BDT, showed 170% iSF in solution.⁹⁹ According to our computations, the TDO acceptor has the unique combination of a large monomer FMO gap (8.9 eV) and a high monomer ΔE_{ST} (-0.9 eV). Given the small-size and short conjugation length of TDO¹⁷⁷, its relatively-high splitting energy is ascribed to the dioxide functionalization. For this reason, we propose that another avenue to develop iSF materials which overcomes the trade-off between charge transfer on one hand, and ΔE_{ST} on the other, is to explore new acceptor cores combining small triplet energies (as previously reported⁹⁹) with large FMO gaps. This can be achieved through i) moderately extending the conjugation, ii) increasing the quinoidal¹⁷⁸ or iii) biradicaloid¹²³ character of the core, and iv) using moieties which have shown to improve ΔE_{ST} . Examples of the latter are sulfonyl (as in the TDO acceptor) and nitrene/N-oxide groups, as recently reported.¹²¹ Future work will be devoted to quantifying the diradical character y_i of promising candidates.¹⁷⁹

Finally, side-chain functionalization provides attenuated electronic effects, which lead to very mild changes in $\Omega_{D\rightarrow A}^{S1}$ and $\Omega_{A\rightarrow A}^{T1}$ (see Figures S12-S13). This reinforces their use to tune the polymer physical properties while leaving their iSF capabilities mostly unchanged. A relevant exception is the ester side-chain substitution in the DPP acceptor, which leads to significantly higher values of $\Omega_{D\rightarrow A}^{S1}$ than the unsubstituted analog. Remarkably, all the outperforming systems pointing to the top-right corner of Figure 4.2b are built from ester-substituted DPP acceptors, which not only display large $\Omega_{D\rightarrow A}^{S1}$ but also important $\Omega_{A\rightarrow A}^{T1}$ and appropriate splitting. The role of the ester side-chain substitution in favoring $\Omega_{D\rightarrow A}^{S1}$ in those dimers can be understood from the stabilization of the DPP FMO energies, which otherwise displays a HOMO energy as high as that of most of the donors considered (mismatched HOMOs regime

in Figure 4.3; see section S9 for further analysis). This is also the case of the il acceptor, although its smaller FMO gap (Figure S10) prevents it from being as tunable as DPP and as a consequence displays small $\Omega_{D \rightarrow A}^{S1}$ in most cases (Figure 4.2b).

4.4 Conclusion

In this work, we unravel the trade-off between the energetic, coupling, and separation requirements for iSF in D–A copolymers. By mapping these descriptors within a comprehensive database of 2944 systems we show that the singlet-triplet energy splitting compromises the $\Omega_{D \rightarrow A}^{S1}$ and $\Omega_{A \rightarrow A}^{T1}$ values around 0.5 for conjugated planar systems. These values can be further pushed by inducing torsion between the donor and acceptor cores. Breaking (or diminishing) the conjugation between the D and the A may be detrimental to iSF, and therefore further analysis on the capabilities of the nonplanar systems will be addressed in the future. For now, we have only considered the dihedral obtained during the ground-state geometry optimization, although including information about the distribution of energetically accessible dihedrals¹⁸⁰ may be beneficial for a more complete description of the descriptors described here. Still, the electronic character of the excited states is mostly dictated by the FMO energies of the donor and acceptor fragments, thus providing intuitive guidelines to predict $\Omega_{D \rightarrow A}^{S1}$ and $\Omega_{A \rightarrow A}^{T1}$ within a given D–A pair. Ideally, the acceptor core with a small FMO gap provides both a favorable energy splitting and a localized triplet state, while the donor intervenes only to drive charge transfer upon photon absorption. We show that functionalization plays a key role in fine-tuning the FMO relative energies that promote charge transfer, however, it does not modulate the local acceptor character nor the energy splitting, which mostly depend on the local FMO gaps.

From these results, we propose a three-step strategy with which to design appropriate D–A pairs for iSF. The first step is to establish a polymerizable acceptor with $\Delta E_{ST} > -1$ eV, as the energetic criterion is the most stringent requirement with little sensitivity to functionalization or subsequent choice of donor. The second step involves choosing a pairing donor with a larger local FMO gap than the acceptor, such that $D_{crit} - A_{crit} \geq 0$, so that the separation criterion is fulfilled. The third step consists in tuning the D–A combination into the target regime (Figure 4.3), so as to fulfill the coupling criterion. This is achieved through chemical functionalization of the donor (acceptor) with electron-donating (-withdrawing) groups, which in turn, is unlikely to perturb ΔE_{ST} or $\Omega_{A \rightarrow A}^{T1}$.

We expect these conclusions to provide a new avenue by which to generate more donor-acceptor copolymer materials that fit into the currently sparsely populated iSF ‘sweet spot’, which can now easily be mapped using simple and readily accessible ground state properties of the monomer chromophores.

4.5 Computational details

The full method used for dataset construction and computations is detailed in sections S1-2 of the Supporting Information, and all data are made available in the Materials Cloud repository. The functionalized monomers and dimers were encoded as SMILES strings.¹³³ The SMILES strings were converted to Cartesian coordinates using the gen3d operation in OpenBabel¹³⁴, which includes a conformational search and a geometry optimization at the force field level. Tighter convergence criteria were then applied by reoptimizing the geometries using density functional theory (DFT) at the ω B97X-D/6-31G* level¹³⁶ with the Gaussian09 package (Revision D.01).¹⁸¹ Vertical excitations were computed using time-dependent density functional theory (TD-DFT), within the Tamm-Dancoff approximation (TDA) to correct for triplet instabilities.¹³⁸ Full details for the choice of method and benchmarking are given in previous work⁷, which shows that the key excited state descriptors (ΔE_{ST} , $\Omega_{D \rightarrow A}^{S1}$ and $\Omega_{A \rightarrow A}^{T1}$) of extended conjugated chains can be readily approximated using vertical computations on dimers, as used here. This same earlier study also shows that solvation has little effect on the quantification of these descriptors.

The character of the excited states is evaluated using the charge transfer numbers ($\Omega_{i \rightarrow j}^E$) gathered from the transition density matrices of a given excited state E, which express the accumulation of hole and electron density on molecular fragments i and j , respectively.¹⁸² These values are obtained by parsing the Gaussian output files with cclib¹⁴³ and using TheoDORÉ (version 1.7.2)^{102,103} to compute the quantity of hole and electron density accumulated on the donor and acceptor fragments of the dimer.

The interactive plots were constructed with the Python framework Dash for web applications (<https://plotly.com/dash/>).

5 Heteroatom oxidation controls singlet–triplet energy splitting in singlet fission building blocks

This chapter is published as:

Blaskovits, J. T.; Fumanal, M.; Vela, S.; Cho, Y.; Corminboeuf, C. Heteroatom oxidation controls singlet–triplet energy splitting in singlet fission building blocks. *Chem. Commun.*, **2022**, 58 (9), 1338–1341. <https://doi.org/10.1039/d1cc06755a>

Details of database construction and methods used and supplementary figures are made available in the Electronic Supplementary Information (ESI) of the original publication. All data discussed in this chapter are available in a Materials Cloud repository (10.24435/materialscloud:m1-dg).

5.1 Introduction

Singlet fission (SF) has shown potential to improve the power conversion efficiency in photovoltaic devices beyond the detailed balance limit by promoting the splitting of a photon-absorbing singlet exciton into two triplet excitons.³⁶ SF involves the excitation of a ground state (S_0) chromophore to an excited singlet state (S_1) upon absorption of light, followed by energy transfer to a second chromophore. The initial S_1 state is coupled to a triplet pair (1TT) state, a process which may be mediated by low-lying charge transfer (CT) states or may proceed directly, via a resonance mechanism.^{27,104} The triplet pair then evolves into physically separate and energetically independent triplets (T_1), one on each chromophore.

Among the requirements necessary for a system to be capable of SF, the most inflexible is that the process be thermodynamically possible, meaning that the energy of the S_1 state must be no less than twice that of the T_1 state:

$$\Delta E_{ST} = E(S_1) - 2E(T_1) \geq 0 \quad (5.1)$$

This energy splitting term ΔE_{ST} , is therefore the most relevant target property in the discovery

Chapter 5. Heteroatom oxidation controls singlet–triplet energy splitting in singlet fission building blocks

of new SF materials.^{36,121,123} It has been shown that (i) extending the conjugation, and increasing the (ii) biradicaloid¹²³ or (iii) quinoidal¹⁷⁸ character of a chromophore can improve ΔE_{ST} , as summarized in Figure 5.1. These strategies have drawbacks. For instance, compounds with high diradicaloid and quinoidal character tend to suffer from chemical instability.¹⁸³

A particular challenge arises in designing materials which fall into the $\Delta E_{ST} \geq 0$ regime: the S_1 and T_1 energies tend to move in parallel. When the excitation energies are stabilized to the point that ΔE_{ST} is fulfilled, T_1 is often too low to be of value for device applications. A historically relevant example of this is the acene family, in which the excited state energies decrease with an increasing number of fused rings. In early reports of SF in anthracene (3 rings), SF was not favored due to a negative ΔE_{ST} and, therefore, the endothermicity of SF.¹⁰ This was also the case for tetracene (4 rings)¹², while pentacene (5 rings) became the poster child for SF due to it being the first acene in which SF is exergonic ($\Delta E_{ST} > 0$), although its T_1 energy is already somewhat lower (0.9 eV) than desirable.⁶⁵ The next acene, hexacene¹⁸⁴, exhibits much more favorable ΔE_{ST} for SF, but has a far too low T_1 energy (0.4 eV).

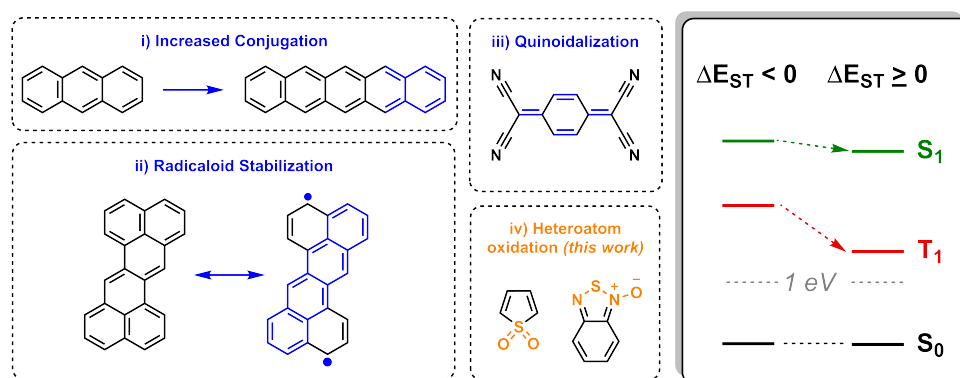


Figure 5.1: Proposed strategies to increase singlet-triplet splitting (ΔE_{ST}) in organic chromophores.

A moiety which stabilizes T_1 incrementally to the point that it can be tuned to remain above 1 eV (for exciton injection into silicon for instance, whose band gap is 1.1 eV) without also lowering S_1 substantially would be greatly beneficial (Figure 5.1, right panel). Here, we identify a chemical functionality, heteroatom oxidation, which modulates the ΔE_{ST} in potential SF chromophores in a foreseeable way (Figure 5.1 (iv)). This approach is motivated by the experimental observation that the oxidized form of thiophene (thiophene-S,S-dioxide) is an effective acceptor in donor-acceptor copolymers capable of intramolecular SF (iSF)^{7,99,185}, and that nitronium/ N -oxide groups were found in large numbers in a recent screening of thousands of crystal structures for compounds with high ΔE_{ST} .¹²¹ The present results show that, indeed, heteroatom oxidation governs the S_1 and T_1 energies and thus can be used to improve the singlet-triplet splitting of potential SF chromophores.

5.2 Methods

To establish if a systematic improvement in ΔE_{ST} can be achieved through heteroatom oxidation, we constructed a dataset consisting of 11 heteroatom-containing building blocks found widely in the organic electronics literature (see Figure S1 for full dataset). These are classified by the number of heteroatoms in the conjugated system, as shown in Figure 5.2a. All oxidized derivatives of these compounds were generated by placing one oxygen atom at the electron pair of all sp^2 -hybridized nitrogen atoms, thereby forming *N*-oxide (nitrene) moieties, and one or two oxygen atoms at the electron pairs of all sulfur atoms, forming *S*-oxide or *S,S*-dioxide moieties, respectively (as shown for bithiophene in Figure 5.2b). This produced a total of 67 oxidized compounds (all structures shown in ESI). The oxidation of sp^3 nitrogens was not considered, as this would lead to charged or radical species. Compound geometries were relaxed using density functional theory (ω B97X-D¹³⁶/6-31G*), and the S_1 and T_1 excited-state energies were computed both vertically and at their minima using time-dependent DFT within the Tamm-Dancoff approximation at the same level of theory (see ESI for details).

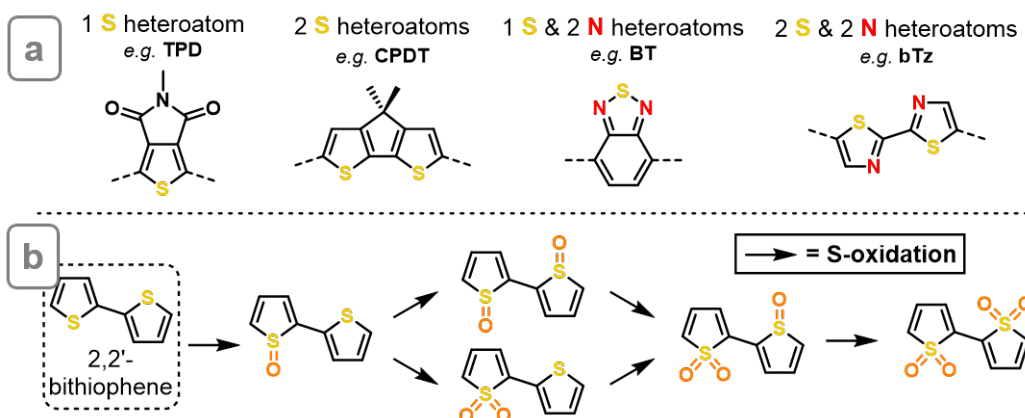


Figure 5.2: (a) Examples of building blocks studied in this work. (b) Five oxidized derivatives of 2,2'-bithiophene.

5.3 Results

5.3.1 Excited state energies

Representative results for the effect of oxidation on the vertical and adiabatic S_1 , T_1 and ΔE_{ST} energies of bithiophene are shown in Figure 5.3a, and results for all other compounds are given in the ESI. We observe a constant difference between the vertical and adiabatic excitation energies. This allows us to extend our previous observation in dimers⁷ - that the adiabatic energy splitting cutoff ($\Delta E_{ST}^{vert} \geq 0$ eV) can be expressed as $\Delta E_{ST}^{vert} \geq -1$ eV in the Franck-Condon regime - to smaller (monomer) building blocks, due to the linear relationship between the two ΔE_{ST} values (Figure S2). Although it is immediately clear that increasing the number of oxygens (regardless of their position) stabilizes T_1 in an additive fashion across all compounds,

Chapter 5. Heteroatom oxidation controls singlet–triplet energy splitting in singlet fission building blocks

the effect on S_1 is less evident. While mono-oxidation of sulfur leads to a sharp reduction in both S_1 and T_1 energies, which has little positive effect on ΔE_{ST} , a second oxidation of the same sulfur increases the S_1 energy while further stabilizing T_1 , leading to a strong improvement in ΔE_{ST} . For example, the dioxide derivatives of bithiophene have $\Delta E_{ST}^{vert} \geq 0$ eV (above the grey line in Figure 5.3a) while bare bithiophene and its mono-oxidized derivatives do not. The same conclusions can be drawn with all other sulfur-containing units (Figures S3–S6): as outlined in Figure 5.3b, single sulfur oxidations have little effect on ΔE_{ST} as they stabilize S_1 more than T_1 , while double oxidations of sulfur are invariably beneficial to ΔE_{ST} due to their similar stabilization of T_1 but smaller impact on S_1 . N -oxidation systematically improves ΔE_{ST} through a robust stabilization of T_1 (Figures S7–S8). These trends are observed regardless of the degree of oxidation of all other heteroatoms, resulting in a remarkably simple cumulative effect across all compounds: the most highly oxidized structures have the highest ΔE_{ST} of all combinations of oxidation products (Figure 5.3 and section S2 of ESI).

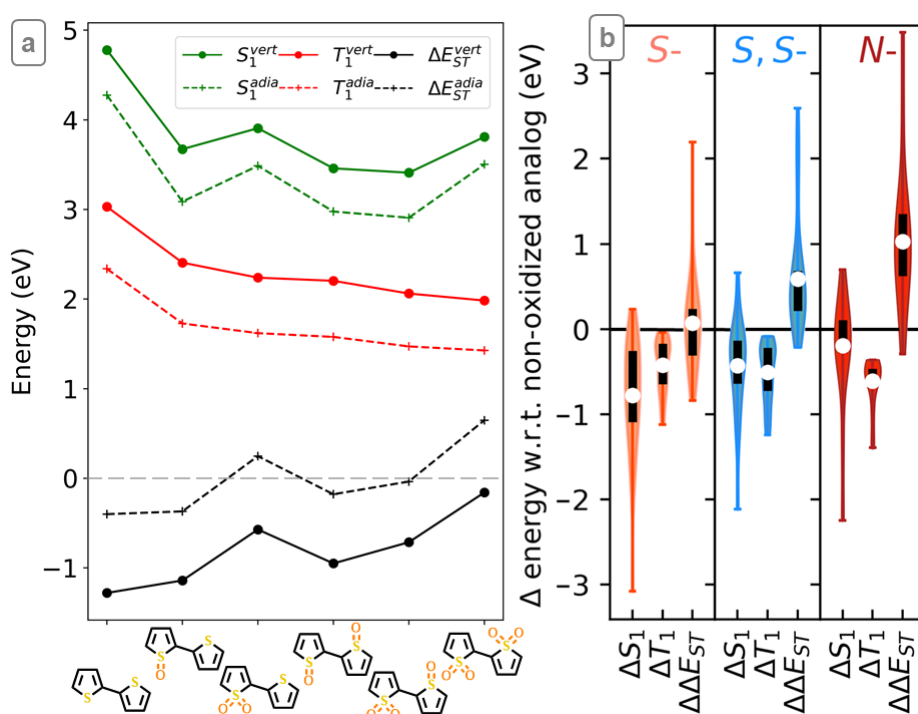


Figure 5.3: (a) Vertical and adiabatic S_1 , T_1 , and ΔE_{ST} energies of bithiophene and its oxidized derivatives. Grey line indicates the ΔE_{ST} cut-off. (b) Summary of the change of adiabatic S_1 , T_1 , and ΔE_{ST} upon S-, S,S- and N-oxidation for all compounds, showing averages (white points), 1st-3rd quartiles (black bars), and maximal/minimal values (whiskers). See ESI for details.

5.3.2 State character

To understand the effect of oxidation on S_1 and T_1 energies, we turned to the nature of the excitations in the simplest sub-unit, thiophene (Figure 5.4). The T_1 state of thiophene

is dominated by a local HOMO \rightarrow LUMO transition in the carbon backbone, while the S_1 state involves predominantly charge transfer (CT) from sulfur (HOMO-1) into the backbone. In thiophene-*S*-oxide, the T_1 excitation is a localized HOMO-1 \rightarrow LUMO transition on the backbone, as the HOMO is located on the oxygen. It is instead the S_1 excitation which corresponds to a HOMO \rightarrow LUMO CT state from oxygen into the backbone π^* orbital, which explains the significant stabilization of S_1 upon mono-oxidation. Finally, in thiophene-*S,S*-dioxide both S_1 and T_1 are characterized by backbone HOMO \rightarrow LUMO ($\pi \rightarrow \pi^*$) transitions, as the O and S orbitals are much lower in energy.

Similarly, in benzodithiophenedione (BDO) and thienopyrroledione (TPD, see Figure S12), S_1 is stabilized by CT states from the oxygen *n* orbitals into the π^* orbital of the backbone. The difference compared to thiophene is that BDO and TPD already contain oxygens in their conjugated systems by virtue of their carbonyls, such that S_1 in non-oxidized TPD and BDO is described by CT from the carbonyls into the heterocycle. A first *S*-oxidation stabilizes S_1 through CT from the S=O moiety, as with thiophene-*S*-oxide, while a second oxidation shifts the source of CT back to the carbonyls. Therefore, the nature of the CT (i.e., the *n* orbitals involved) changes, depending on the structure of the unit, but the stabilizing effect of a single *S*-oxidation on S_1 remains constant across all compounds. And yet, the oscillator strength of S_1 tends to drop significantly for *S*-mono-oxidized compounds (see Fig S14), which may have consequences on the SF decay pathway and overall mechanism.¹⁸⁶ Less impact is expected on the photophysical properties of the S_1 state of *S,S*- and *N*-oxidized compounds.

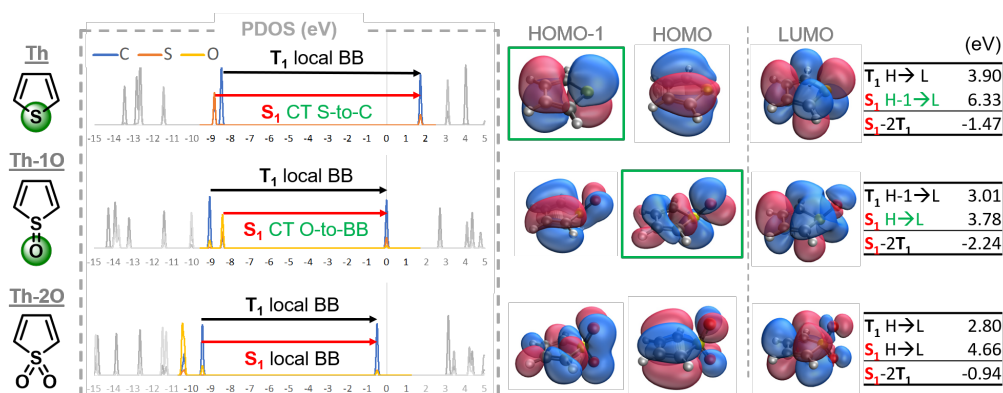


Figure 5.4: Projected density of states (PDOS), key molecular orbitals and vertical excitation energies for thiophene (Th) and its two *S*-oxidized derivatives (Th-1O and Th-2O). Transitions between the states most involved in the T_1 and S_1 excitations are marked with black and red arrows, respectively. The molecular orbitals contributing to the charge transfer (CT) character of certain excitations and the atoms on which they are centered are highlighted in green. All energies are given in eV. BB = carbon backbone.

Recent work has rationalized ΔE_{ST} based on ground- and excited-state aromaticity.^{187,188} To explain the effect of these substitutions on aromaticity, we computed the nucleus independent chemical shifts (NICS) of thiophene, TPD, and thiazole (Figure S15). While thiophene is aromatic in the ground state and anti-aromatic in the first triplet state, thiophene-*S*-oxide

Chapter 5. Heteroatom oxidation controls singlet–triplet energy splitting in singlet fission building blocks

is much less aromatic in the ground state, but still significantly anti-aromatic in the triplet. The absence of lone pairs on the sulfur atom of thiophene-*S,S*-dioxide leads to non-aromatic character of both the ground state singlet and first triplet. This is reflected in the bond order of the backbone which, like butadiene, is reversed in the triplet (.CH-CH=CH-CH.) compared to the singlet (CH=CH-CH=CH). This is not the case for non-oxidized or mono-oxidized thiophene (Figure S16). The TPD ring aromaticity is similarly suppressed upon the double oxidation of sulfur. Put together, these results suggest that the destabilization of S_1 upon *S,S*-dioxidation, and its consequently beneficial effect on ΔE_{ST} , originate from the SO_2 moiety eliminating the aromatic character of the heterocycle and instead inducing a polarized butadiene-like behavior to the backbone.¹⁷⁷ In this way, T_1 is sufficiently stabilized, while the stabilizing effect of CT from S (in thiophene rings) or O (in thiophene-*S*-oxide rings) into the π -system observed in S_1 is eliminated. This is similar to the ‘breaking’ of conjugation in polycyclic hydrocarbons through boron-doping, an approach proposed to build molecules that fulfill ΔE_{ST} .¹⁸⁹

CT, primarily from oxygen into sulfur (HOMO→LUMO+1), also accounts for the stabilization of S_1 in *N*-oxidized benzothiadiazole (BT, see Figure S13), compared to non-oxidized BT, which has a local $\pi\rightarrow\pi^*$ (HOMO→LUMO) character. The T_1 states are also described by a $\pi\rightarrow\pi^*$ transition in both non-oxidized and *N,N'*-dioxidized BT. The inclusion of the N-O moiety in the conjugated system reduces the π/π^* energy gap, leading to an extreme lowering of both the S_1 and T_1 energies by approximately 2 eV. *N*-oxidation has the effect of strongly reducing the antiaromatic character of the triplet (Figure S15), while retaining ground state aromaticity, explaining the significant T_1 stabilization and consequent increase in ΔE_{ST} .

5.3.3 Oxidized units in donor-acceptor systems

iSF has been demonstrated experimentally in donor-acceptor (D-A) polymers^{6,99,120}, in which the triplet pair formation is mediated through low-lying donor-to-acceptor CT states, while the spatial separation of the acceptors by the absorbing donor leads to a weakly-bound 1TT state. We have recently proposed a protocol with which to identify potential polymer candidates for iSF based on the ΔE_{ST} of the constituent monomers and their relative frontier molecular orbital (FMO) energies.^{7,185} To assess the performance of these new oxidized units to form iSF-capable D-A pairs, we treat all those in the dataset that fulfill $\Delta E_{ST}^{vert} \geq 0$ (and $\Delta E_{ST}^{vert} \geq -1$ eV, *vide supra*) as acceptor monomers (34 compounds). The FMOs of each acceptor were compared to all other building blocks (2244 monomer pairs), and only those whose FMO arrangement is conducive to CT (i.e., donor HOMO higher than acceptor HOMO and donor LUMO higher than acceptor LUMO; see earlier work for details¹⁸⁵) were retained. For these 631 D-A combinations, the dimers were generated, their ground state geometries optimized, and their vertical excited states were evaluated at the same level of theory as the monomers. All dimers exhibit energy splitting above the vertical threshold $\Delta E_{ST}^{vert} \geq -1$ eV (Figure S17), which is consistent with our observation¹⁸⁵ that the dimer ΔE_{ST} originates from the monomer with the higher (i.e., more positive) ΔE_{ST} .

We have previously outlined two other requirements beyond ΔE_{ST} for iSF to be possible in D-A systems: S_1 must have significant donor-to-acceptor CT character to drive triplet-pair formation ($S_1 \rightarrow {}^1\text{TT}$), and T_1 must be located on the acceptor to promote dissociation of the triplet states ($({}^1\text{TT} \rightarrow T_1 + T_1)$).^{7,185} Deactivation of S_1 towards higher energy triplet states is neglected but the $S_1 \rightarrow {}^1\text{TT}$ transition required for iSF is expected to be the most efficient decay pathway (see section S6 of the ESI). Quantum chemical descriptors were introduced to quantify these criteria using the character of excited states (see ESI). Figure 5.5 shows the fraction of CT from donor to acceptor in S_1 ($\Omega_{D \rightarrow A}^{S_1}$) and the fraction of local T_1 character on the acceptor ($\Omega_{A \rightarrow A}^{T_1}$). The upper righthand corner corresponds to the ‘ideal’ region in which these two criteria are fulfilled simultaneously. The majority of the present dimers display a highly localized T_1 ($\Omega_{A \rightarrow A}^{T_1} = 0.5 \sim 1.0$) and non-negligible S_1 CT character ($\Omega_{D \rightarrow A}^{S_1} = 0.1 \sim 0.4$), but are nonetheless not in the ideal region.

A striking exception are dimers containing *N,N*-dioxidized benzothiadiazole along the top of Figure 5.5, indicating pure localization of T_1 on the acceptor (Figure S17). In addition to stabilizing T_1 to achieve positive ΔE_{ST} , this acceptor induces dihedral torsion to the D-A linkage ($\varphi_{D-A} \approx 50^\circ$), thereby contributing to very high CT in S_1 (up to 0.8). The best of these dimers is shown in Figure 5.5 (compound **A**), and is revealed to have a donor partner which differs from the acceptor only with regard to the sulfur oxidation. However, the *N*-oxidation of **A** stabilizes T_1 too much for it to be of practical use if extracted (0.41 eV). All other dimers constructed with this acceptor suffer from this problem ($T_1 = 0.3 - 0.9$ eV). Two other dimers (**B** and **C**) have a similar acceptor, albeit without *N*-oxidation, which leads to promising excited state behavior in the dimer and appropriate ΔE_{ST} (as with **A**), but importantly, they retain attractive T_1 energies (1.47 eV and 1.24 eV, respectively; see Table S2). The absence of nitroxides leads to smaller dimer dihedrals (30° and 19°) and therefore slightly lower CT compared to **A**, although **B** and **C** are still located near the ideal region. This analysis demonstrates that through judicious chromophore oxidation, both ΔE_{ST} and T_1 can be fine-tuned without losing the CT character which mediates the SF process in D-A copolymers.

5.4 Conclusion

We have disclosed heteroatom oxidation as a convenient handle through which to modulate singlet-triplet splitting in SF building blocks. Beneficial ΔE_{ST} through double oxidation of sulfur is obtained by suppressing aromaticity while maintaining overall conjugation, thereby stabilizing T_1 compared to non-oxidized analogs, while having a smaller impact on S_1 . A higher number of heteroatom oxidations stabilizes T_1 additively, making it possible to drive the T_1 energy down as far as necessary to achieve exergonic splitting. The utility of this approach is demonstrated using new *S*- and *N*-oxidized compounds to construct D-A materials for iSF, although this method is equally valid in intermolecular SF materials design. D-A systems based on a new benzothiadiazole-*S,S*-dioxide acceptor may be excellent candidates, as sulfur oxidation modulates the excited state energies for SF to be thermodynamically possible while ensuring that the resulting T_1 is appropriate for injection into silicon (1.1 – 1.7 eV).

Chapter 5. Heteroatom oxidation controls singlet–triplet energy splitting in singlet fission building blocks

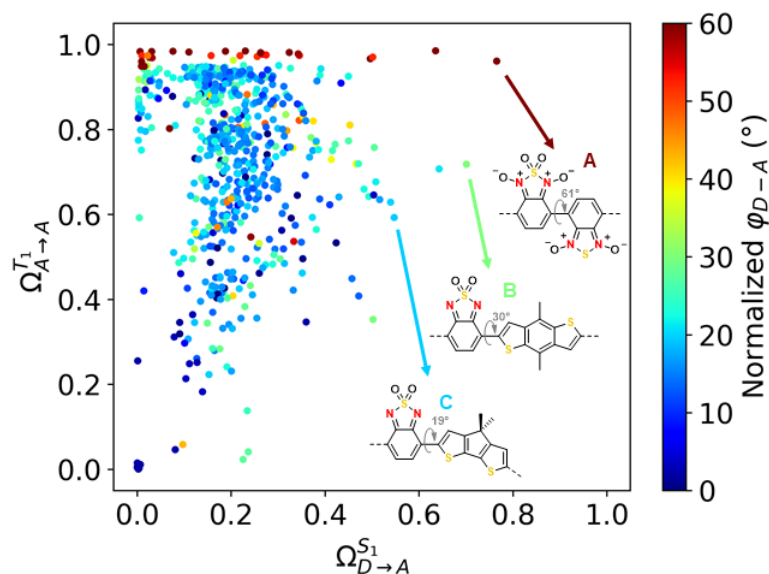


Figure 5.5: Donor-to-acceptor charge-transfer character of S_1 ($\Omega_{D \rightarrow A}^{S_1}$, x-axis) and local acceptor character of T_1 ($\Omega_{A \rightarrow A}^{T_1}$, y-axis) in dimers, colored by the dihedral between the donor and acceptor (ϕ_{D-A}).

N-oxidations, on the other hand, also systematically improve ΔE_{ST} , but at the expense of an attractive T_1 energy. While these specific units have not been described in the literature, previously reported preparation of *S*-oxidized¹⁹⁰ and *S,S*-(di)oxidized^{190,191} analogs of benzothiadiazole, as well as *N*-oxidized thiazoles¹⁹², bithiazoles¹⁹³, and thiadiazoles¹⁹⁴ suggest that they are synthesizable.

6 Data-driven discovery of organic electronic materials enabled by hybrid top-down/bottom-up design

This chapter is based on the following work:

Blaskovits, J. T.; Laplaza, R.; Vela, S.; Corminboeuf, C. Data-driven discovery of organic electronic materials enabled by hybrid top-down/bottom-up design. **2023**, *Under review*. *ChemRxiv preprint*: <https://doi.org/10.26434/chemrxiv-2022-88t32>

The automated cross-coupling tool and scripts for XGBoost models and diverse subset selection are available on GitHub at https://github.com/lcmd-epfl/FORMED_ML. All other details on dataset curation and methods used are made available in the Supporting Information of the original publication. All data discussed in this chapter are available as a Materials Cloud repository (10.24435/materialscloud:nh-gb), and are provided in an interactive format using Chemiscope.¹⁹⁵

6.1 Introduction

The strength of a fragment-based approach to materials design resides in its synthetic flexibility: chemical building blocks are prepared and functionalized separately, and then coupled together in a final reaction step. This methodology has been applied successfully across many fields of experimental organic materials science, and has recently been adapted to high-throughput virtual screening: given a library of molecular fragments and a template for how to combine them, structures can be generated combinatorially and screened, with a high chance of the hit candidates being synthesizable (Figure 6.1a).^{196–198} Moreover, statistical models can be trained on the initial pool of fragments and then used to power further screening efforts at a significantly reduced cost.^{199–203} This *bottom-up* approach has been applied to the construction of organic materials based on predefined fragments inspired by the literature and experimental insight, such as non-fullerene acceptors^{198,204} and organic light-emitting diodes (OLEDs).^{196,205}

The most widely used bottom-up fragment-based strategy in both the experimental and

Chapter 6. Data-driven discovery of organic electronic materials enabled by hybrid top-down/bottom-up design

computational design of organic materials is the donor-acceptor template, where conjugated electron-donating (D) and electron-accepting (A) units are selected in such a way as to manipulate various optical and electronic properties. This is used notably in the virtual screening of thermally-activated delayed fluorescence (TADF) emitters for OLEDs^{206,207}, in which the D and A units are often orthogonal to one another to limit the overlap of the HOMO and LUMO, thus reducing the gap between the lowest singlet (S_1) and triplet (T_1) excited states.^{208,209} Conjugated polymers^{124,126}, used as donor materials in bulk heterojunction solar cells, and non-fullerene acceptors²¹⁰, are also often constructed according to $(-D-A)_n$ and A-D-A arrangements, respectively, to modify electron affinity, minimize energy loss upon electron transfer, maximize the materials' complementary absorption profiles and promote exciton dissociation at the donor-acceptor interface.²¹¹ The facile tunability of donor-acceptor systems has also recently been applied experimentally to materials for intramolecular singlet fission (iSF), a multiexciton-generation process which has the potential of overcoming the detailed balance limit in photovoltaic cells, both in small molecules^{85,93,212} and polymers.^{93,99,118,120}

Bottom-up approaches, however, are limited by the choice of initial fragments and will only generate combinations and variations thereof.^{204,213,214} The notion of a 'good' donor or acceptor for a given application depends on a preconceived set of criteria, primarily related to desirable electronic properties. The search for promising materials is therefore inherently biased towards variations of building blocks which have already been reported for that application and the discovery of new families of molecules exhibiting desired properties is impossible. Furthermore, specific rules must be set to put fragments together.

To mitigate such limitations, the search may be conducted in a *top-down* manner instead (Figure 6.1b): existing repositories are screened for compounds with desirable characteristics for a given application that may differ from their original purpose. Examples of this in organic materials include the extraction and high-throughput screening of crystal structures from the Cambridge Structural Database (CSD) for materials with high charge carrier mobilities based on the evaluation of transfer integrals and reorganization energy²¹⁵, for singlet fission (SF) candidates¹²¹ and TADF materials²¹⁶ based on excitation energies (as discussed above), and for other user-defined targets.²¹⁷ The outcome of such a screening may lead to unexpected results which push research into a new direction of chemical compound space.

A key drawback of such schemes is the difficulty of extracting design principles from the identified molecules. Contrary to bottom-up approaches, in which the influence of a specific sub-unit (e.g., a core, spacer or side-chain) on a particular property can be ascertained from the fragment assembly process, additional investigation is required on the output of a top-down screening to understand what features are responsible for the good performance. Additionally, there are inherent problems related to the initial, pre-existing data, which may be of heterogeneous composition, quality and size. Given the prohibitive computational cost of accurately evaluating every molecule in large datasets (on the order of 10^4 - 10^6), initial screening stages often involve very approximate methods followed by increasingly expensive

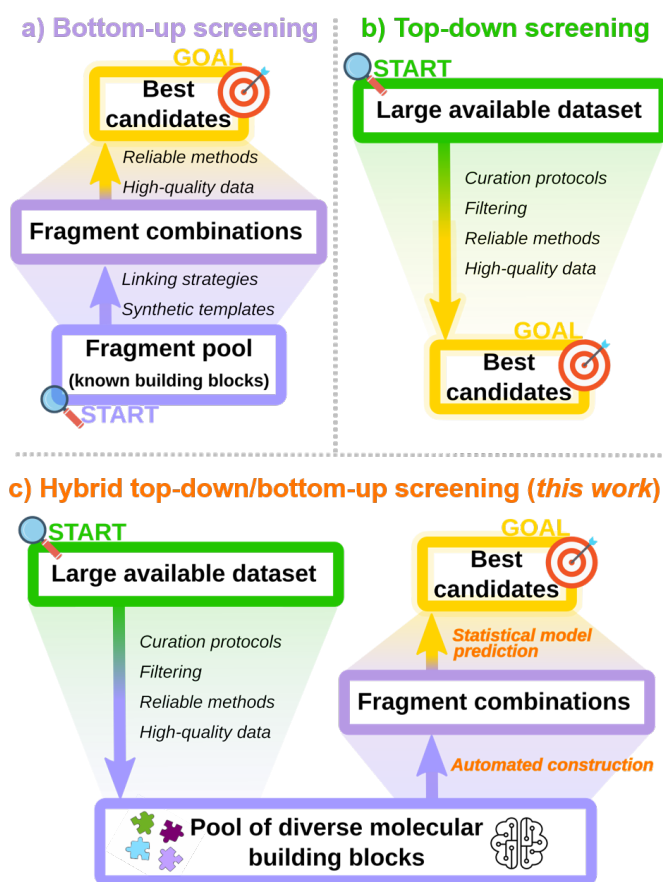


Figure 6.1: General view of the (a) *bottom-up* (purple) and (b) *top-down* (green) philosophies of high-throughput virtual screening, with end-goals in yellow. Requirements for the different stages of a successful screening campaign are indicated in italics and datasets are shown as blocks, whose widths represent the datasets' sizes relative to one another. (c) The *hybrid* screening methodology described in this work, with the union of top-down (green) and bottom-up (purple) elements enabled by statistical models and automated fragment coupling (orange).

methods as the size of the dataset decreases (Figure 6.1b).¹⁹⁶ High-quality data, in addition to chemically correct structures (e.g., which are absent of crystallographic errors, a non-trivial challenge), are therefore crucial for an effective top-down screening protocol.²¹⁸

It must be noted that the philosophy underlying the molecular space to be explored is critical for the training of predictive statistical models.^{219–221} While design campaigns for molecules and materials using statistical models are reported at an increasing rate,^{201,202,222–227} direct applications for materials design face two challenges regarding access to data: on one hand, using available small molecule data to train predictive models may compromise extrapolation towards larger, more complex chemical species of interest. On the other hand, curated top-down data including relevant properties (e.g., excitation energies) is not widely available,

Chapter 6. Data-driven discovery of organic electronic materials enabled by hybrid top-down/bottom-up design

severely limiting the applicability of statistical models.

Here, we provide a computational framework to systematically generate combinations of molecular building blocks in a chemically meaningful way following predetermined design rules, such as a donor-acceptor strategy, and evaluate their electronic properties (Figure 6.1c). To do this, we construct a diverse, experimentally reported database of over 110K crystal structures in a top-down fashion, which we treat as molecular building blocks for the subsequent fragment-based generation of hierarchical structures. We encode these building blocks' topology so as to identify available sites for carbon-carbon bond-forming reactions and automate the generation of chemically relevant cross-coupling products between these units without manual input. We then use these building-block structures, a diverse subset of a few thousand of the billions of possible cross-coupled products, and their associated *ab initio* electronic properties to train statistical models for the prediction of relevant optical properties – excitation energies and orbital gap – to near-TDDFT accuracy across organic chemical compound space. The ability to evaluate these optical properties on-the-fly unlocks the screening of organic electronic materials on a much larger scale than would be possible with conventional virtual screening techniques. We propose this as a platform to construct donor-acceptor structures in a way that is unbiased towards preconceived notions of 'good' building blocks and thus combines the advantages of both top-down and bottom-up materials discovery strategies. We demonstrate the potential of this workflow by constructing and screening over a million donor-acceptor combinations for intramolecular SF using the experimental building blocks as the initial pool of both donor and acceptor units. In this manner, hitherto unexplored singlet fission candidates are identified.

6.2 Results and discussion

The results are organized as follows. section 6.2.1 outlines the construction of the Fragment-Oriented Materials Design (FORMED) database. This involves the curation of building block structures and their associated electronic properties (section 6.2.1.1), and the evaluation of their topological and chemical composition (section 6.2.1.2), as outlined in Figure 6.2. All discussed properties are made available and may be visualized interactively through the Materials Cloud using Chemiscope (<https://doi.org/10.24435/materialscloud:nh-gb>).¹⁹⁵ The electronic properties from the FORMED dataset are then used to train predictive statistical models (section 6.2.2). In the final part (section 6.2.3), we outline the requirements for efficient singlet fission materials (6.2.3.1), identify leading structural motifs in the FORMED dataset that contribute to fulfilling these requirements (6.2.3.2), and finally use the dataset and associated automated cross-coupling tool in concert with statistical models to construct intramolecular donor-acceptor SF candidates in a bottom-up approach (section 6.2.3.3).

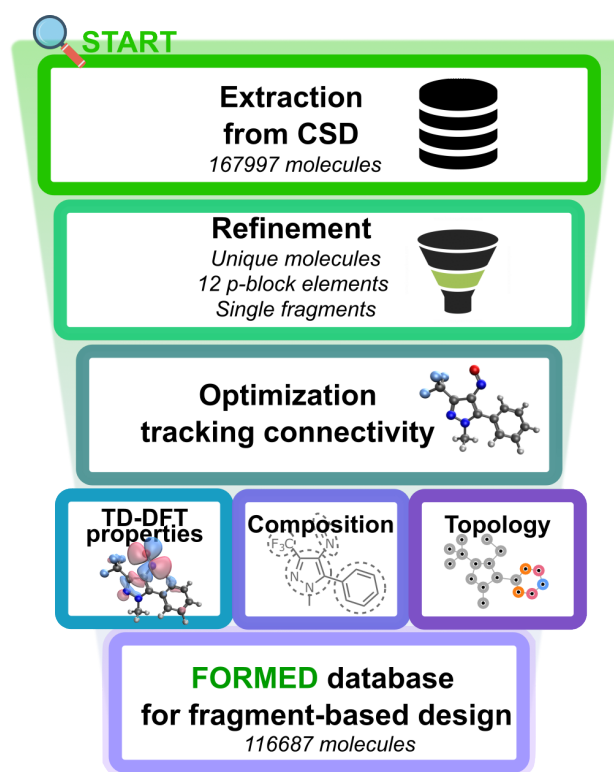


Figure 6.2: Overview of the preparation of the FORMED dataset, consisting of a top-down screening of the CSD, extensive refinement based on structure and composition, and subsequent evaluation of electronic, structural and topological properties.

6.2.1 Dataset

Structure curation

We performed a top-down screening of the Cambridge Structural Database (CSD), the largest repository of experimental crystal structures (Figure 6.2, see Methods section for details). Structures were refined by optimizing the crystal structure geometries with the GFN2-xTB semi-empirical method²²⁸ and ground state energies and vertical excitations were computed with density functional theory and Tamm-Dancoff approximated time-dependent DFT (TDDFT), respectively, at the ω B97X-D/6-31G(d) level (see Methods section).

It was found that the geometry optimization could be used as a screening tool for filtering out compounds with crystallographic errors: compounds which underwent any change in connectivity (i.e., the bond network) over the course of optimization were eliminated, as many of these were found to contain structural errors or inconsistencies, such as omitted hydrogens (see section S2). This resulted in a set of nearly 117K computationally clean organic molecules whose synthesis is experimentally reported, comprised of hydrogen and 12 *p*-block non-metals and metalloids (boron through bromine), for which the frontier molecular orbitals (FMOs), ground- and excited-state energies, exciton character and oscillator strengths of

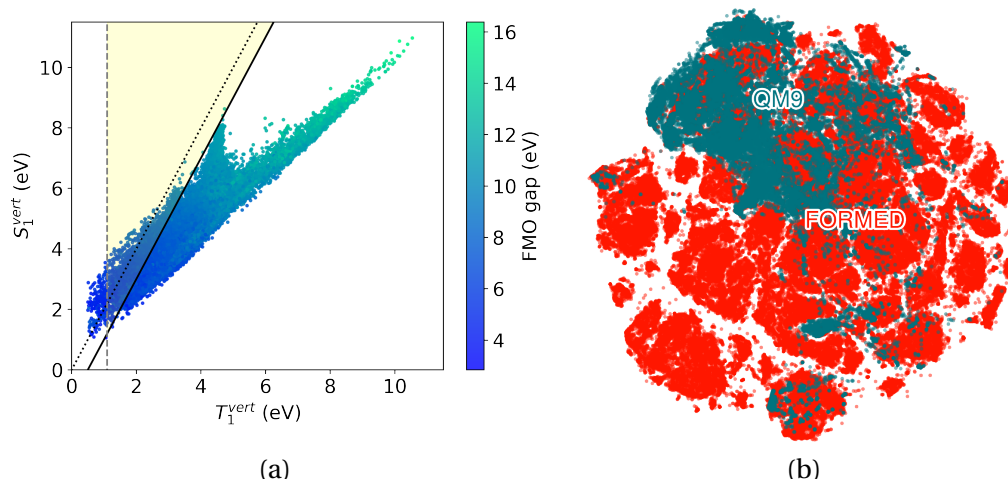


Figure 6.3: (a) S_1 and T_1 excitation energies across the FORMED dataset; points are colored according to the frontier molecular orbital gap. The yellow region defines both the thermodynamically feasible regime for singlet fission and T_1 energies well-matched to the bandgap of conventional semiconductors (to the right of the vertical dashed grey line). The dotted grey line indicates the hard thermodynamic cutoff for singlet fission ($S_1 \geq 2T_1$), while the solid black line is the same cutoff but relaxed to the Franck-Condon regime ($S_1 - 2T_1 > -1$ eV) based on linear trends between vertical and adiabatic excitation energies reported previously^{7,8} (see section S7). (b) Dimensionality reduction plot of the molecules in the FORMED and QM9 datasets using the t-distributed stochastic neighbor embedding algorithm generated from the 3D structures encoded using the spectrum of London and Axilrod-Teller-Muto potentials⁹ representation (see Methods section for details).

the first five singlet and triplet excited states were evaluated (Figure 6.2). The character of the exciton provides insight into the nature of the electronic transition²²⁹ and a physically intuitive description of the excited state wave function (localized versus charge transfer, for instance), while the oscillator strength relates to the probability of a transition to occur. The FMO gap and lowest singlet and triplet excitation energies are shown in Figure 6.3a, and a dimensionality reduction plot highlighting the diversity of the dataset in relation to one of the most widely-used datasets for statistical models (QM9)^{230,231} is given in Figure 6.3b. While QM9 comprises a slightly larger number (134K) of organic molecules with up to 9 heavy atoms and only main organic chemistry elements (C, N, O, F and H), FORMED covers a much broader region of the chemical space by virtue of it not being limited in size, and by adding 8 other elements to the palette (B, Si, P, S, Cl, As, Se, Br). We point out that this diversity is also significantly larger than that of previous datasets, such as those generated via the combination and fusion of a small set of molecular motifs²¹³, or via the execution of a number of predefined morphing operations²¹⁴.

Topology and automated generation of coupling products

The vast majority of π -conjugated organic materials are synthesized via carbon-carbon bond-forming reactions between building blocks.^{232,233} These usually involve the cross-coupling of an aryl halide (or pseudohalide) and another substrate which has been pre-functionalized with an organometallic leaving group. In these reactions, the leaving groups and halogens serve the same purpose of preactivating the particular desired C-H site on the organic building block where the coupling should take place. Under certain reaction conditions, unsaturated substrates may even undergo coupling at $C(sp/sp^2)$ -H sites directly without preactivation.^{129,234–238} The coupling of fragments at these sites, such as the aryl rings highlighted in Figure 6.4, leads to electronic communication between the coupled fragments via π -conjugation, from which a broad range of optical and electronic properties can be accessed.

The first step of an automated approach to fragment coupling is therefore to identify unsaturated C-H sites which may be amenable to cross-coupling, provided the appropriate coupling conditions and necessary site preactivation. For this, we developed a tool to generate molecular graphs characterizing the connectivity between atoms in each structure, identify available sites for cross-coupling using a series of simple connectivity-based rules, and encode the topological environments of these sites using resistance distances^{239,240} between atoms in the molecule, directly from reported 3D structures (Figure 6.4, see Methods section for details). This last part is done to detect symmetry-related coupling sites and thus avoid the construction of identical dimers. This information is indeed crucial since many molecules in the dataset are highly symmetric, and is therefore stored as a molecular property in all FORMED entries (Figure 6.2). While it is not expected that all resulting compounds will have a clear synthetic route, it is reasonable to assume that many are within the realm of synthetic feasibility given that their component parts, which have been prepared in the literature, are combined in a way consistent with well-established coupling procedures. This is supported by the synthetic accessibility²⁴¹ and complexity²⁴² scores, which were evaluated for both FORMED and dimers generated using this protocol (see section S8).

By including the potential sites for the formation of carbon-carbon bonds as a property of each compound in FORMED, these dataset entries can then be used as building blocks for the construction of larger materials in a bottom-up strategy. Chemically reasonable coupling products are generated automatically using the approach described above, in which coupling between fragments is achieved by replacing the hydrogens at the available coupling sites with the partner fragment, and screening the dihedral around the newly formed bond, to limit steric clashes while promoting favourable π -orbital overlap. This workflow is outlined in Figure 6.4, and the full details are given in the Methods section. While we acknowledge that certain functional groups on the existing building blocks may not be compatible with cross-coupling reactions, we reiterate that analysis of the synthetic accessibility and feasibility suggest that the coupling products are generally not more complex synthetic targets than the existing building blocks, as discussed above. The tool for automated cross-coupling is made available at https://github.com/lcmd-epfl/FORMED_ML.

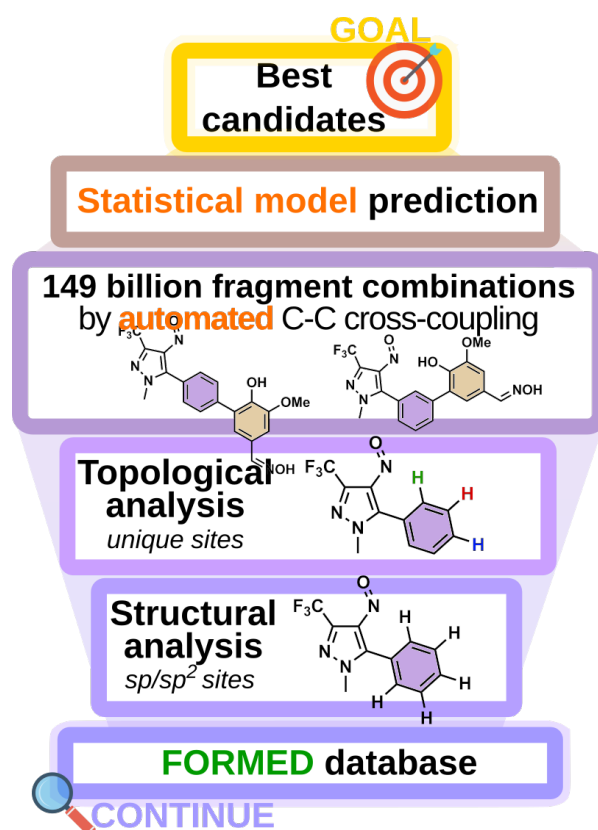


Figure 6.4: Bottom-up application of the FORMED dataset, including the automated unsaturated C-H site identification, topological analysis of coupling sites, and cross-coupling of molecular building blocks, followed by property prediction on the resulting dimer space.

Finally, 160 moieties, mainly representing functional groups made up of one or more of the 13 element types present in the dataset, were defined and encoded as SMARTS strings, a graph-based representation of chemical fragments and molecules (see section S4). These were used in a sub-graph search on each molecule^{243–245}, the output of which constitutes a rudimentary description of the composition of each molecule. A vectorial representation of these molecular compositions (see section S4) will be used in section 6.2.3.2 to build a functional-group-based scoring function that correlates chemical structures to properties.

6.2.2 Prediction of optical properties

The FORMED dataset was used to construct statistical models to predict key optical properties across the full range of organic compounds. We targeted both excited state and ground state properties, focusing in particular on the frontier molecular orbital (FMO) gap, and the S_1 and T_1 state energies and excitonic character, given the importance of these properties across multiple applications in organic electronic materials. Extreme gradient boosting (XGBoost²⁴⁶) models were trained using a 3D geometry-based representation, the spectrum of London

and Axilrod-Teller-Muto potentials⁹, which contains one-, two- and three-body terms (see Methods).

To ensure that the model is able to predict the optical properties of extended structures generated by the automated cross-coupling pipeline, we produced a selected number of dimers and incorporated them into the training data (see section S5). Considering that all possible coupling products derived from the FORMED set would lead to a combinatorial explosion (149 billion unique compounds), far exceeding what is possible to generate and compute, we turned to a sampling workflow to generate the most diverse possible subset of 2,506 coupling products that could be constructed from the building blocks available in the FORMED database (Figure 6.5). This was done by performing a dimensionality reduction on the collection of the optical properties and results of the substructure analysis described above, selecting the 1,000 most unique compounds as building blocks, clustering all possible pairwise combinations of these, evenly sampling each cluster, and generating the coupling products of the sampled pairs via automated cross-coupling (see section S5).

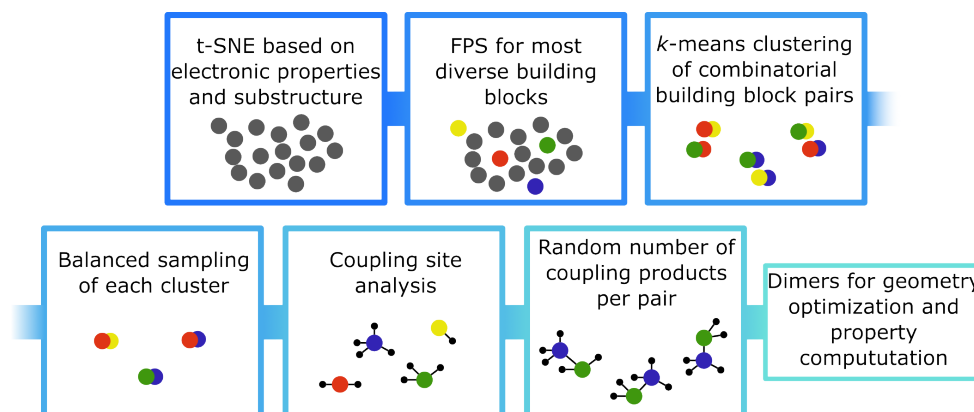


Figure 6.5: Workflow for the generation of diverse dimers from the FORMED dataset. Details are provided in section S5.

Using the FORMED dataset enriched with cross-coupling products, excellent predictions are obtained, with 10-fold cross-validation mean absolute errors of 0.18 eV for T_1 , 0.20 eV for S_1 and 0.26 eV for the FMO gap (see Methods). We note that these errors are comparable to TDA-TDDFT accuracy for excitation energies (see section S6).²⁴⁷ With these models able to predict optical properties with high accuracy, we turned towards high-throughput screening of D-A compounds for singlet fission.

6.2.3 Discovery of materials for singlet fission

Requirements for singlet fission

SE, the downconversion of a high-energy singlet spin state to two lower-energy triplets¹¹, has attracted much attention as a non-conventional avenue to increased photocurrent gener-

Chapter 6. Data-driven discovery of organic electronic materials enabled by hybrid top-down/bottom-up design

ation in solar cells.^{58,66} This process has also been demonstrated in photodetectors¹⁹ and OLEDs²⁴⁸, and proposed for quantum computing applications.²⁴⁹ The primary limitation on development to state-of-the-art SF applications is that too few practical SF-capable materials have been reported (and those that have been implemented in solar cell technologies display very low efficiencies). This is due primarily to the thermodynamic constraint that the energy of the lowest-lying excited singlet state (S_1) must be greater than or (approximately) equal to twice the energy of the first triplet (T_1)³⁶ (quite rare in organic molecules¹²¹, see yellow region in Figure 6.3a), and that SF is very sensitive to relative orientation between the chromophores involved.^{45,81} As a result, most recent developments in SF materials design rely on modifications to existing chemical scaffolds known to exhibit SF, the vast majority of which are acenes and rylenes.^{10,27,64,250,251} Furthermore, the triplet energies of most existing SF-capable molecules are too low for the charge carriers to be injected into conventional solar cell materials, such as silicon ($E_g=1.1$ eV), GaAs ($E_g=1.4$ eV) and CdTe ($E_g=1.5$ eV).⁶⁴ High photostability and chemical stability, and broad absorption profiles are also necessary requirements for potential SF sensitizers for solar cells.²⁵⁰

D-A materials, and conjugated polymers in particular, have emerged as strong candidates for SF implementation in devices, due to their merging of these parameters.^{85,93,99,118,120,122,212} An advantage of covalently-bound D-A templates for intramolecular over intermolecular SF materials is that their SF propensity is not dependent on intermolecular couplings, and they are therefore less sensitive to orientation in the solid state. Instead, the necessary parameters to achieve SF via a photoinduced charge-transfer-mediated mechanism²⁷ and subsequent triplet separation¹⁴⁴ can be tuned simultaneously and in a modular way through a fragment-based approach, as shown in Figure 6.6. Intuitive computational guidelines, based on the electronic properties of the constituent D and A units, have recently been established to do this with conjugated polymers.^{7,99,185}

Exploration of chemical space

The substructure analysis implemented in the FORMED dataset enables us to investigate the relationship between chemical structure and the desirable electronic requirements for singlet fission. We define a score function ξ which evaluates compounds concomitantly by their thermodynamic propensity for SF - the energy splitting criterion adapted to the Franck-Condon regime^{7,8} ($S_1 - 2^*T_1 > -1$ eV) - and the usability of the T_1 energy, as described above (see section S7). The region of excited state space described by these two requirements is highlighted in yellow in Figure 6.3a. A multivariate linear model was fit to the substructure composition of all compounds, from which the coefficients attributed to each substructure were extracted. The most positive (negative) coefficients correspond to substructures whose contribution the score is most beneficial (detrimental). Although this naive technique does not take into account the role of interaction between substructures on the overall molecular property and is therefore not quantitative, it provides a means to identify and classify the most significant substructures based on their overall ability to induce desirable SF energetics. The

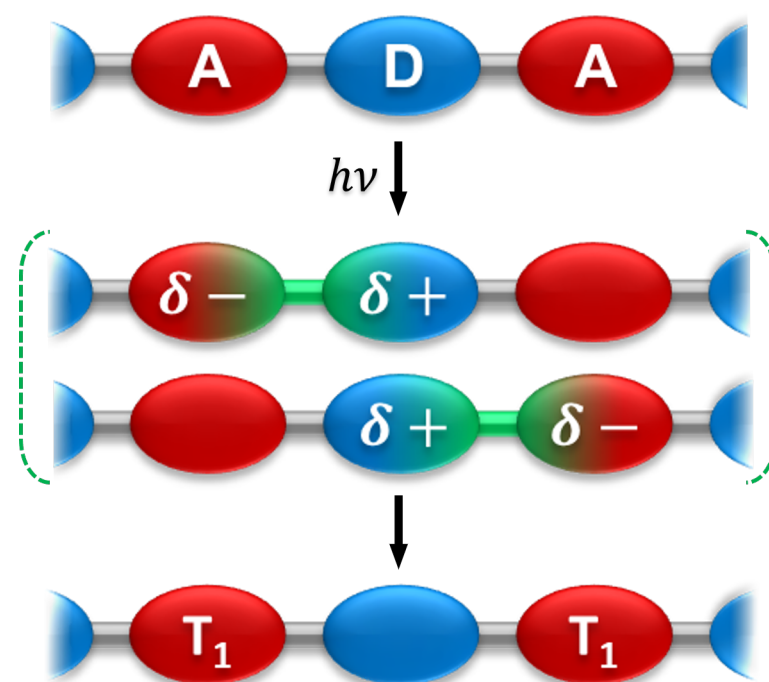


Figure 6.6: Charge-transfer-mediated intramolecular singlet fission in donor-acceptor systems. Upon photoexcitation, charge transfer (green) from the donor (blue) to the acceptors (red) mediates the formation of triplets on neighboring acceptors.

largest and smallest coefficients and representative molecules are shown in Figure 6.7.

While disilenes¹²¹ and boron dipyrromethene (BODIPY) derivatives²⁵² (a boron-containing ring system) have been proposed theoretically for SF, silene-, nitroso-, sulfenate- and dicoordinate ($R_2C = As - R$) arsenic-containing compounds and other substructures identified here are entirely unstudied moieties for this application. Many of these structures are quite rare in the FORMED dataset (occurrences are shown in Figure 6.7); as such, they constitute a potentially fruitful avenue to be incorporated in SF materials. Particularly worth mentioning is that the $C=As$ moiety has recently been successfully incorporated as a building block in a conjugated polymer, which is air-stable in the solid state.²⁵³ We also observe that boron-containing rings are the most widely-occurring structure with a very positive coefficient. Their well-established chemistry and the recent suggested application of boron-doping^{189,254} as a means to control S_1/T_1 splitting by interrupting π -conjugation positions them as an excellent starting structure for the design of SF-capable molecules.

Bottom-up design of donor-acceptor compounds

We leverage the FORMED database (Figure 6.2), the automated cross-coupling tool, and models for excited state energy prediction (Figure 6.4) to apply the reported iSF recipe on a large scale as follows. In the intramolecular D-A strategy, the T_1 state is located on the

Chapter 6. Data-driven discovery of organic electronic materials enabled by hybrid top-down/bottom-up design

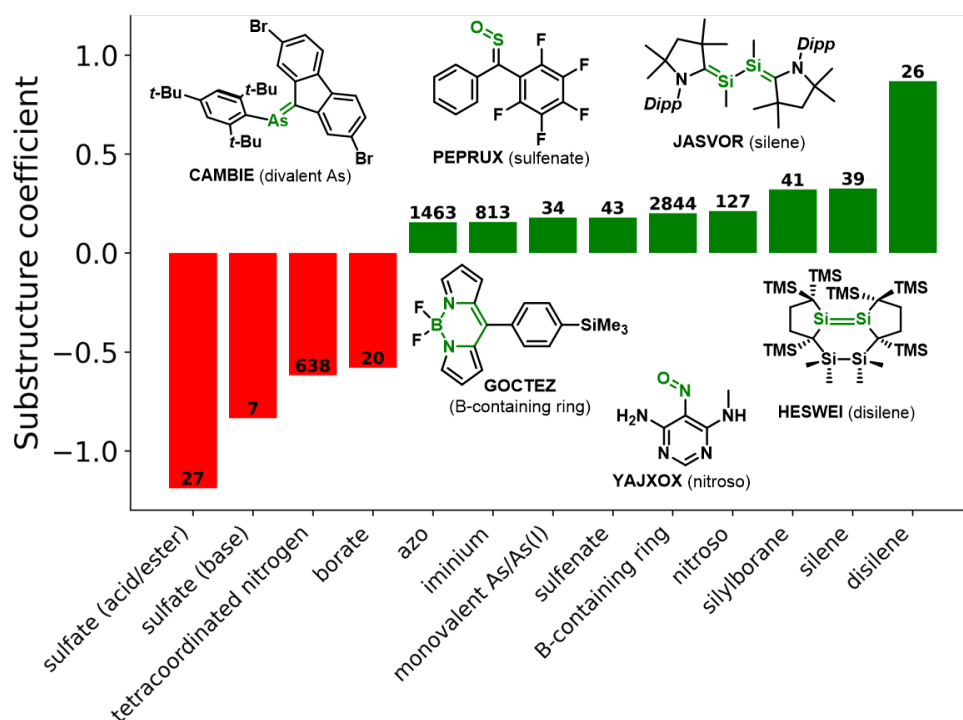


Figure 6.7: Largest (green) and smallest (red) coefficients to the multilinear regression $\xi = c_i n_i + c_j n_j + c_k n_k + \dots$, where each coefficient c_i corresponds to the contribution of functional group i to the score function ξ and n_i is the number of instances of the functional group i in each given molecule. Representative examples of molecules containing some of the most favorable substructures for singlet fission are presented. The number of occurrences of each substructure in FORMED is given in black; substructures with fewer than five occurrences in the dataset are not shown. *Dipp* = 2,6-diisopropylphenyl; *TMS* = trimethylsilyl.

acceptor (A)⁹⁹; A therefore determines the overall T_1 energy of the D-A system and must possess appropriate energy levels to imbue the resulting polymer with appropriate excited state energy levels for exergonic singlet-to-triplet splitting.⁷ We select as A units building blocks from the FORMED dataset with sufficiently high triplet energies to be practically useful in a solar cell ($T_1 > 1.5$ eV)⁷¹, which fulfill the thermodynamic requirement discussed above, and which have a significantly higher T_2 energy ($T_2 > 2 * T_1$) so as to prevent deactivation channels via triplet-triplet annihilation.³⁶ For the resulting A units, appropriate donor (D) partners are selected from the same source of building blocks (FORMED) which satisfy the FMO-based criteria laid out in earlier work: the FMO gap of A must be larger than that of D to ensure that the triplet state is localized on A¹⁸⁵, and the FMOs of the D and A fragments must be ordered in such a way as to promote sufficient charge transfer in the S_1 state upon photoexcitation to induce S_1 to $^1[TT]$ splitting.⁷

We selected building blocks that contain available C-H sites, to form linkages with coupling partners, and that are comprised of no more than 20 heavy (non-hydrogen) atoms. We

privilege small units to preserve the notion of ‘donor’ and ‘acceptor’ within an extended π -conjugated manifold and to promote intrachain triplet transport in an eventual polymer, as it has been shown that shorter distances between acceptors promote efficient separation of the intramolecular triplet-pair state ($^1[TT]$)⁵⁰ into independent triplets ($T_1 + T_1$).²⁵⁵ This pre-screening of acceptors and donors, automated cross-coupling of appropriate D-A combinations and subsequent semi-empirical geometry optimization (GFN2-xTB) results in 1,002,268 unique dimers. The models discussed above are employed to predict their excited state energies, and the score function outlined in Figure S12 is then used to rank the resulting compounds based on potential SF exergonicity and T_1 energy.

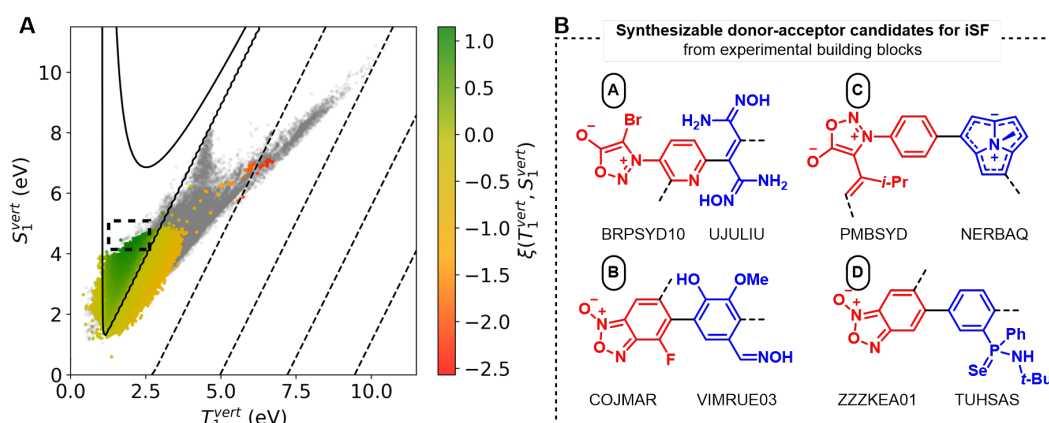


Figure 6.8: (a) Predicted excited state energies of the million donor-acceptor dimers generated by automated fragment coupling, colored according to the ζ score function (see section S7). Compounds with the highest score are located in the dashed box. Contour lines give the shape of the score function, with positive and negative contours shown as solid and dotted lines, respectively. The full FORMED dataset, containing the building blocks from which the dimers were constructed, is shown in grey in the background for comparison. (b) Leading candidates of D-A dimers generated through automated cross-coupling and proposed to have favourable energetics for singlet fission. Donor and acceptor cores are colored blue and red, respectively, and are shown alongside their CSD names; dotted lines indicate possible linkages to adjacent repeating units in a polymer.

The predicted S_1 and T_1 energies are shown in Figure 6.8a, which highlights the effectiveness of the fragment-based screening approach at locating D-A dimers with desirable energies for SF. In fact, by using the most SF-appropriate building blocks from the FORMED dataset to construct conjugated D-A units, the initial pool of 7,474 synthesized and theoretically useful molecules (6% of the original FORMED dataset, found in the very sparsely-populated yellow region of Figure 6.3a), was enriched with 560,394 not synthesized – though equally chemically valid – molecules (56% of the novel dimers, shown in the green region of Figure 6.8a) using the D-A template.

A selection of a few top D-A candidates is shown in Figure 6.8b (all compounds and their predicted properties are made available for interactive visualization on <https://doi.org/10.24435/>

Chapter 6. Data-driven discovery of organic electronic materials enabled by hybrid top-down/bottom-up design

materialscloud:nh-gb). TDA-TDDFT computations confirmed the accuracy of the excited state prediction, with similar errors to those obtained in the cross-validation of the XGBoost models (~ 0.2 eV, see Table S2). All compounds display appropriate energy splitting for SF while retaining T_1 energies higher than those of the vast majority of SF-capable materials⁶⁴: in fact, the triplet energies match very closely the bandgaps of the most widely-used photovoltaic materials when the correction associated with adiabatic relaxation is applied (~ 1.5 eV, see section S7 for details). These compounds tend to be fully conjugated, and comprise polarizing electron-donating and -withdrawing groups, especially on the D and A units, respectively. Many acceptors, including all those shown in Figure 6.8b, display the nitron ($R_2C = N^+(O^-)R$) motif in the form of furoxan (5-membered ring with a $N - O - N^+O^-$), which also emerges as a strong candidate in our substructure analysis of the score function (coefficient = 0.1). This confirms it to be a highly attractive moiety for inducing SF-appropriate S_1/T_1 energy splitting, in line with the conclusions of previous screening efforts^{8,121}, although one which to our knowledge has not been reported in any experimental SF material to date despite its well-studied chemistry.²⁵⁶ Pentacene motifs are notably absent from these promising candidates, due to the low T_1 of this building block (see section S7). Of particular note are two unconventional donor candidates: the highly aromatic, zwitterionic [9]annulene NERBAQ, studied as a synthetic curiosity of aromaticity²⁵⁷ and the phosphoselenoic amide TUHSAS²⁵⁸, a ligand for alkaline earth metals. No compound remotely like either has been reported as a possible donor unit or SF material, although these results demonstrate that they are clearly deserving of experimental attention. The flagging of such unexpected structures as iSF candidates highlights the value of automated materials discovery based on a pool of molecular fragments that is synthetically accessible, but at the same time not limited to the known literature or established conventions for the application in question. Finally, we highlight that the same database and model could be readily adapted to any other materials target application given a set of energy-based requirements, such as the small $S_1 - T_1$ gap required for TADF emitters.

6.3 Methods

6.3.1 Quantum chemistry computations

All density functional theory (DFT) optimizations and vertical excitations (time-dependent DFT using the Tamm-Dancoff approximation) employed the ω B97X-D functional¹³⁶ with the 6-31G(d) basis set. Structures were refined by optimizing the crystal structure geometries using the extended tight-binding (GFN2-xTB) semi-empirical method.²²⁸ Ground state energies were then computed with DFT, followed by vertical excitations using Tamm-Dancoff approximated time-dependent DFT (TDA-TDDFT). Both ground- and excited-state computations were done at the ω B97X-D/6-31G(d) level. We benchmarked GFN2-xTB against DFT as the optimization method on 4,000 structures from the dataset, selected from Farthest-Point Sampling, and found excellent agreement with respect to electronic properties between the two methods (see Figure S2). Further computational details are provided in section S1.

6.3.2 Dataset

An initial filtering of the CSD using the Cambridge Crystallographic Data Centre's Conquest interface²⁵⁹ based on queries regarding composition and lack of crystallographic errors yielded 167,997 crystal structures, which were downloaded as *pdb* and *mol2* files and then converted to the *xyz* format. Compounds containing anything other than *p*-block elements and consisting of more than one fragment were removed. Duplicate structures were identified by the initial six-letter code of their names, and only one entry from each chemical species was retained. The number of electrons in each compound was counted and those with an odd number of electrons, likely due to missing hydrogens, were eliminated.

All 127,002 remaining crystal structures were optimized at the GFN2-xTB semi-empirical level of theory. Changes in bonding over the course of geometry optimization give an indication as to the correctness of the initial crystal structure.²⁶⁰ The Laplacian of the connectivity matrix of each compound was therefore evaluated pre- and post-xTB optimization, and compounds with any difference between the two matrices were eliminated. Although the attribution of bonding is sensitive to the choice of the covalent radius, this screening criterion was nonetheless imposed in order to remove unusual or ill-defined structures. Following this, each compound was submitted for TDA-TDDFT computation and substructure analysis. Structures whose ground states could not be described reliably at the TDA-TDDFT level due to multireference character, based on an analysis of low-lying excited states and LUMO energies, were set aside (see section S2). We note that this subset merits further investigation from a quantum-chemical point of view. In all, 116,687 structures of ground-state singlet electronic configuration successfully completed the full screening and substructure analysis. All structures, computed properties, synthetic complexity²⁴² and accessibility²⁴¹ scores, and results of the substructure search are provided at <https://doi.org/10.24435/materialscloud:nh-gb>. A complete discussion of the refinement protocol, including the number of compounds removed from each curation step, is provided in section S2.

6.3.3 Automated cross-coupling

The topological environment of each molecule's coupling sites is encoded as follows.

For each structure, the adjacency matrix is generated using the atoms' covalent radii and all sites amenable to forming bonds with other fragments through a hypothetical cross-coupling reaction are identified based on simple connectivity rules. A molecular graph is generated from the adjacency matrix for each structure, in which atoms and bonds are described by nodes and vertices, respectively. An element-weighted resistance-distance matrix²⁴⁰ – constructed from the resistance distances²³⁹ between all pairs of atoms – is generated for each graph. The topological environments of the carbon atoms of the identified coupling sites are then compared to one another by evaluating the collection of resistance distances with respect to their n^{th} -order neighbors, where n is increased until either the resistance distances of two nodes diverge, or every pairwise resistance distance in the molecule has been considered.

Chapter 6. Data-driven discovery of organic electronic materials enabled by hybrid top-down/bottom-up design

Coupling sites are thus classified as either topologically unique or equivalent to another site in that molecule. However, we note that this topology-based approach does not distinguish between geminal C-H bonds on terminal (e.g., vinylic) double-bonds. Coupling between fragments is achieved by replacing the hydrogens at the available coupling sites with the coupling C atom of the partner fragment at an appropriate C-C bond distance. A screening of dihedral angles around the newly formed bond is performed to limit steric clash while promoting favourable π -orbital overlap. Dimer generation is then followed by a geometry optimization, such that the ground state geometry is used for subsequent computations and property predictions. Further details are provided in section S3.

6.3.4 Statistical models

All statistical models used in this study are extreme gradient boosting ensembles (XGBoost²⁴⁶) and were trained using the spectrum of London and Axilrod-Teller-Muto potentials⁹ representation, which uses physics-inspired one, two- and three-body potentials bagged over pairs and triads of element types. Given the large elemental diversity of FORMED with respect to QM9, many of the bagged potential terms are empty for the latter (as no molecules contain one or more of the participating elements). Coherently, the chemical space of QM9 is a fraction of the one in FORMED, as captured by the t-distributed stochastic neighbor embedding (Figure 6.3b). Note that the potentials are computed using information from the 3D coordinates and thus capture geometric information. Hyperparameters for all models were optimized using a grid search approach (see section S6). These representations were developed to be used in kernel-based statistical models. However, we found that kernel ridge regression models performed comparatively worse. For a comparison with other statistical methods see Figure S9 and section S6.1. We note that the FORMED database is significantly more diverse in terms of molecule size and elemental composition than typical datasets used to develop and benchmark statistical models in chemistry, and thus pre-existing approaches may require significant adaptation.

The XGBoost models have remarkable 10-fold cross-validation mean absolute errors of 0.18 eV for T_1 , 0.20 eV for S_1 and 0.26 eV for the FMO gap in the FORMED dataset enriched with cross-coupling products. Parity plots are shown in Figure S8, and a detailed error analysis is presented in section S6.2; the highest errors of the model occur in molecules containing infrequent functional groups such as selenoketones or phosphasilenes. Finally, we ascertained that incorporating some cross-coupling products leads to slightly improved performance on dimer prediction (see section S6.3) and thus decided to add the 2,506 dimer subset to FORMED to train the final models. The corresponding ML models without the added dimers, including their respective training and cross-validation, as well as software for the diverse subset selection, fine-tuning scripts and associated data have been made available at https://github.com/lcmd-epfl/FORMED_ML.

6.4 Conclusion

We have proposed a platform for the fragment-based discovery of organic materials based on a hybrid *top-down/bottom-up* approach. This consists of *a*) generating a curated dataset of the structures and TDA-TDDFT-computed properties of over a hundred thousand compounds extracted from an experimental crystallographic database comprising the first three rows of *p*-block non-metals; *b*) automating the identification of available unsaturated C-H coupling sites and subsequent formation of cross-coupling products using chemical topology; and *c*) training statistical models on an enriched version of the dataset in (*a*) which are able to predict optical properties relevant to state-of-the-art optoelectronic applications to high accuracy. The compounds from (*a*) and their associated coupling site information from (*b*) constitute the Fragment-Oriented Materials Design (FORMED) dataset, which is made available at <https://doi.org/10.24435/materialscloud:nh-gb>. The model architectures from (*c*) are then used in the prediction of target electronic properties in larger structures constructed according to predefined fragment-based design principles from the building blocks of the FORMED set.

This platform is used to enrich significantly the palette of intramolecular SF materials by generating a library of over a million donor-acceptor dimers and evaluating their excited state energies on a scale that would be unfeasible with a standard computationally-driven virtual screening approach. This constitutes a crucial step in the discovery of SF-capable molecules that are both outside the range of currently studied compound families and which may be effectively implemented in solar cells, based on favourable $S_1 - 2 * T_1$ splitting and high T_1 energies. These tools, when used in concert, may be applicable to any fragment-based materials design protocol and will enable future large-scale *in silico* molecular design campaigns in organic electronics.

7 Symmetry-Induced Singlet-Triplet Inversions in Non-Alternant Hydrocarbons

This chapter is published as:

Blaskovits, J. T.†; Garner, M. H.†; Corminboeuf, C. Symmetry-induced singlet-triplet inversions in non-alternant hydrocarbons. *Angewandte Chemie International Edition*, **2023**, e202218156. <https://doi.org/10.1002/anie.202218156>

† *These authors contributed equally.*

All computational details and additional figures are made available in the Supporting Information of the original publication. All data discussed in this chapter are supplied with the publication on the journal website.

7.1 Introduction

Hund's rule stipulates that for a given electronic configuration, the one with the highest spin is the lowest in energy.^{261,262} This rule is broadly applicable across organic molecules with closed-shell ground states, where the excited singlet states will have higher energy than the triplets of the same electron configuration (Figure 7.1a). Given the first excited triplet state (T_1) is thermodynamically favored over the first excited singlet state (S_1), Hund's rule constitutes a fundamental limitation for the efficiency of molecular emitters. The energetic inversion of the S_1 and T_1 excited states illustrated in Figure 7.1b is a uniquely desirable property for organic light-emitting diode (OLED) materials, as fluorescence from the S_1 state is no longer impeded by population transfer to the T_1 state. This process has very recently been demonstrated experimentally by Aizawa *et al.*²⁶³ and shows great promise in the design of next-generation thermally-activated delayed fluorescence (TADF) emitters whose fluorescence rates are no longer limited by spin statistics.^{264–266}

Until recently, Hund's rule violations were restricted to unstable diradicals,^{267,268} charge-transfer excited-states of large molecules,^{269,270} and cases where strong light-matter coupling is achieved.^{271,272} This changed when negative S_1 - T_1 gaps ($E(S_1-T_1) < 0$) were theoretically

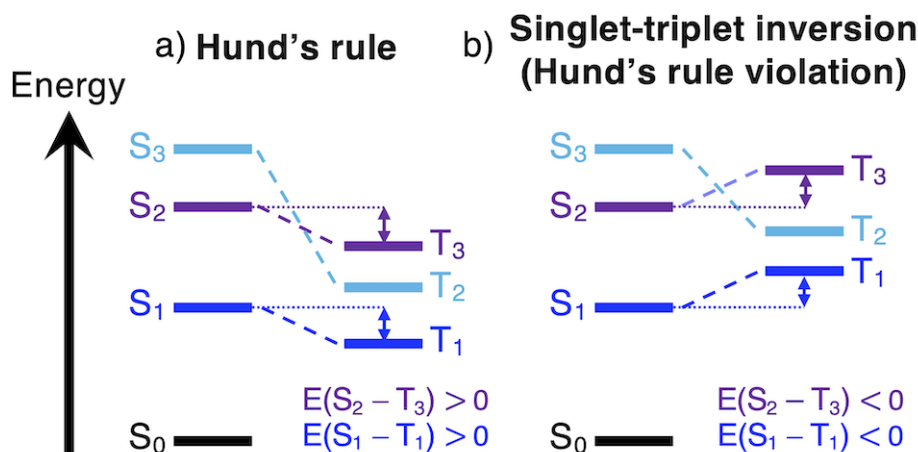


Figure 7.1: Schematic of three excited states, color-coded to indicate state pairs of identical electron configuration. a) Three pairs of excited states that obey Hund's rule, i.e., each triplet is of lower energy than the singlet of the same configuration. b) The S_1 and S_2 states violate Hund's rule by having lower energy than the equivalent triplet states, T_1 and T_3 .

identified in cycl[3.3.3]azine and its aza-substituted analogs by Ehrmaier *et al.*²⁷³ and de Silva.²⁷⁴ While a number of analogous azaphenalenenes had been studied experimentally since the 1980s due to their photophysical properties^{275,276} and later as TADF emitters by Li *et al.*,^{277,278} the possibility of higher-order Hund's rule violations had been overlooked.^{279–281} The 40-year gap between the discovery of azaphenalenenes as inverted gap molecules and their implementation in devices, despite all being in the same molecular family, highlights the scarcity of compounds with singlet-triplet inversions.²⁸²

With the prospect of superior emissive properties, it is imperative to find new classes of molecules with singlet-triplet inversions. Given the historic lack of focus on the possible existence of Hund's rule violations among excited states, and because inverted singlet-triplet gaps can only be modelled using high-level quantum chemical methods,^{274,283–288} we suggest that there may be many cases of excited state singlet-triplet inversions among already synthesized molecules. Such molecules would provide an excellent starting point for future computational and synthetic efforts in the design of molecular emitters.

7.2 Results

7.2.1 Screening protocol

Here, we focus on vertical excitations as an initial molecular screening step, while acknowledging that adiabatic relaxation would be required for a complete picture. For a molecule in the S_1 state, adiabatic relaxation followed by fluorescence is likely to be a more efficient decay pathway than intersystem crossing if the lowest triplet is thermodynamically disfavored. We mine a dataset of existing crystal structures to identify compounds which exhibit

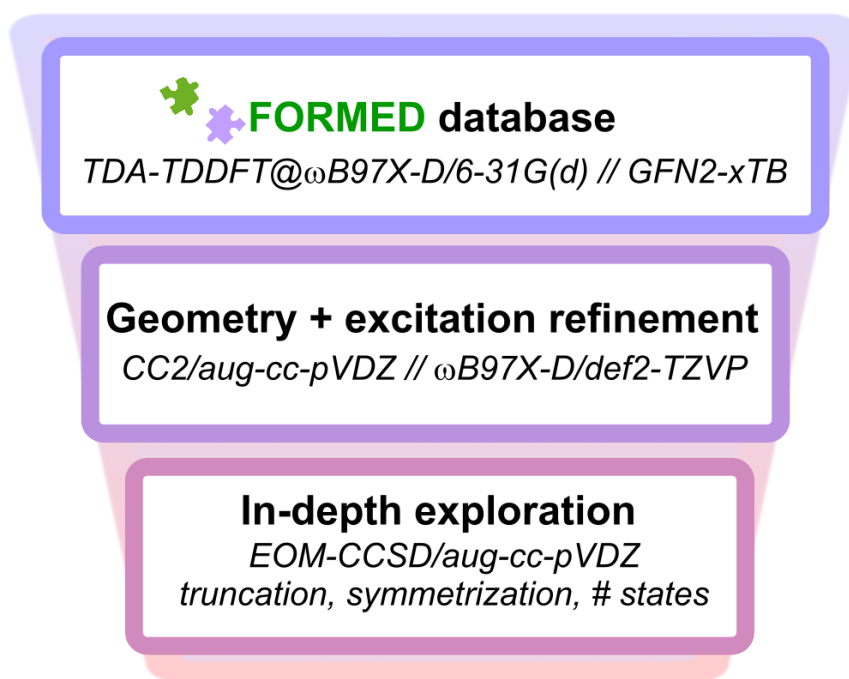


Figure 7.2: Three-step protocol for screening compounds in the FORMED database (top) for excited-state violations of Hund's rule with increasingly complex methods.

violations of Hund's rule in the lowest excited states through sequential refinement of the geometry and excitation energies with increasingly precise computational methods (Figure 7.2). We have recently introduced a curated database tailored to materials design applications, the Fragment-Oriented Materials Design (FORMED) dataset²⁸⁹, consisting of over 117,000 experimentally-reported organic crystal structures and their associated optical properties computed with Tamm-Dancoff-approximated time-dependent density functional theory (TDA-TDDFT) using ω B97X-D¹³⁶/6-31G(d) and geometries with GFN2-xTB²²⁸ (Figure 7.2, top box).

The screening procedure illustrated in Figure 7.2 starts with a pre-selection of the molecules in the FORMED dataset based on $E(S_1 - T_1)$ (TDA-TDDFT level) and to the extent necessary prioritized by smallest number of atoms in the molecule (Figure S1).²⁹⁰ We optimize the select 1514 geometries at a tighter level (ω B97X-D/def2-TZVP) and recompute the excited states at the second-order approximate coupled-cluster level (CC2/aug-cc-pVDZ); Figure 7.2, middle box. The states are then paired according to their electronic configuration in order to identify possible Hund's rule violations between the lowest (S_1 and T_1 in Figure 7.1b), or alternatively between higher-lying excited states (e.g., S_2 and T_3 in Figure 7.1b). The 54 molecules we identify with negative or near-degenerate gaps among the first three singlet excitations are explored at the equations-of-motion coupled-cluster level (EOM-CCSD/aug-cc-pVDZ); Figure 7.2, bottom box (see section S1 for details).²⁹⁰

7.2.2 Azaphenalenenes

From this virtual screening protocol, we identify three potential classes of materials which exhibit Hund's rule violations among the first three excited state singlets, Figure 7.3. The first of these belong to the well-established azaphenalene family.^{263,273–276,291–293} TAZCAZ²⁹⁴ and the methyl-substituted analog COSFIZ²⁹⁵, are penta-azaphenalenes with negative $E(S_1-T_1)$. State diagrams are shown in Figures S9-S10. The utility of the screening protocol is validated by our ability to recover compounds structurally similar to those for which S_1-T_1 inversions are known from both experimental and computational studies.^{285,286}

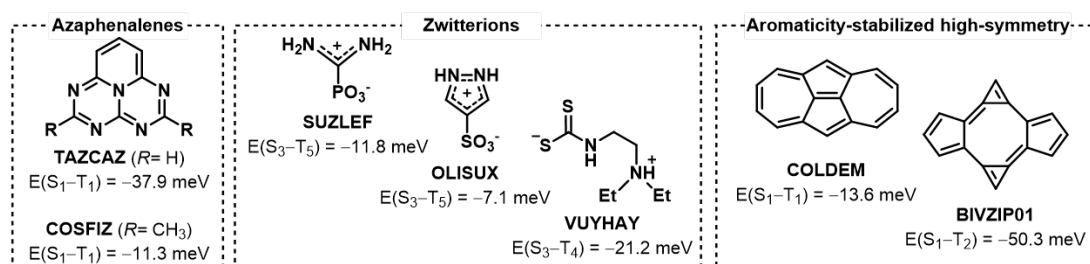


Figure 7.3: Survey of three classes of compounds exhibiting Hund's rule violations identified through screening: azaphenalenes, zwitterions, and polycyclic aromatic hydrocarbons with high symmetry induced by aromaticity. The energy splitting labels correspond to singlet-triplet pairs of the same configuration. Structures are labeled according to their Cambridge Structural Database codes. Excitation energies were obtained with EOM-CCSD/aug-cc-pVDZ using ground state geometries optimized at the ω B97X-D/def2-TZVP level.

7.2.3 Zwitterions

The second class comprises small zwitterionic compounds with Hund's rule violations among the higher-lying excited states. SUZLEF²⁹⁶ and OLISUX²⁹⁷ consist of a positive charge delocalized over protonated aminoiminium and pyrazole rings balanced out by phosphonate and sulfonate, respectively, while VUYHAY is the zwitterion of the fully non-conjugated *N*-(2-diethylaminoethyl)dithiocarbamic acid²⁹⁸. State diagrams are provided in Figures S11-S13. Furthermore, several molecules in this class are almost gapless with state-paired $E(S_1-T_1) < 10$ meV in the form of AMMCHC11, ROFJAY, TIRZAX, and VICGOE as listed in Table S1. We note that many zwitterionic compounds exhibit inverted or degenerate state-paired singlet and triplet excitations at the CC2/aug-cc-pVDZ level. These gaps often become slightly positive when the more precise EOM-CCSD/aug-cc-pVDZ method is employed, Table S1.

7.2.4 Non-alternant hydrocarbons

The third, and most promising class of compounds consists of fused polycyclic hydrocarbons containing odd-membered rings. We identify the dicyclohepta[*cd,gh*]-pentalene COLDEM²⁹⁹, a fused azulene dimer with negative $E(S_1-T_1)$ of -14 meV with D_{2h}

symmetry, the state diagram of which is given in Figure S14. As with the azaphenalenenes,^{273,274} the S_1 and T_1 states are both described predominantly by HOMO→LUMO configurations. The highest occupied (HOMO) and lowest unoccupied (LUMO) molecular orbitals of COLDEM are spatially proximal, though non-overlapping: the HOMO is centered on the pentalene-like core, and the LUMO on the tropylium rings (Figure A.1), thus minimizing the exchange interactions necessary for inverted singlet-triplet splitting. Both the 5- and 7-membered rings of COLDEM are aromatic, as evidenced by the respective nucleus-independent chemical shifts ($NICS(1)_{zz}$) of -36 and -32 ppm, see section S1 for details.³⁰⁰ While the 5-membered rings of COLDEM are slightly less aromatic than the equivalent ring in the parent azulene (Figure S3), the 7-membered rings are more aromatic than that of azulene. Due to the aromatic nature of the rings, COLDEM exhibits D_{2h} symmetry with almost no bond-length alternation.

7.3 Discussion

Given the unique electronic behavior of COLDEM, we examined the pentalene core to understand the origin of this inverted singlet-triplet splitting (Figure A.1).³⁰¹ Pentalene is a textbook Hückel antiaromatic system.³⁰² Its C_{2h} ground-state structure is a frequently-studied antiaromatic molecule ($NICS(1)_{zz} = 58$ ppm) with significant bond-length alternation,³⁰²⁻³⁰⁴ and a strongly positive $E(S_1 - T_1) = 1018$ meV. If the D_{2h} symmetry of COLDEM is imposed on pentalene it achieves an inverted $E(S_1 - T_1) = -125$ meV, but becomes strongly antiaromatic owing to its 8π -electrons distributed in two symmetric rings.³⁰³ We do not assess D_{2h} -pentalene further due to its inherent multireference character, see Figure S5. Pentalene sub-units in larger molecules often cause them to distort into lower symmetry through bond-length alternation to escape antiaromaticity. By virtue of aromatic stabilization due to the presence of the fused 7-membered rings, the pentalene core of COLDEM retains the highest possible symmetry. The similarity between the two is evident from the D_{2h} symmetry, the alternating form of the HOMO and LUMO (Figure 4), and the concomitant singlet-triplet inversion ($E(S_1 - T_1) = -14$ meV). And yet, unlike D_{2h} -pentalene, COLDEM is not a sensitive case for static correlation, as revealed by fractional occupation number weighted electron density analysis (FOD, see Figure S5).³⁰⁵ With the pentalene core embedded within an aromatic ring system, COLDEM is a stable molecule that has been synthesized with³⁰⁶ and without substituents²⁹⁹, and more recently in an annulated form.³⁰⁷

The high symmetry and non-overlapping nature of the orbitals involved in the $S_0 \rightarrow S_1$ excitation of COLDEM results in null oscillator strength ($f_{S_1}^{osc}$). For COLDEM derivatives to work as emitters, such functionalized molecules must achieve appreciable oscillator strengths. As an initial assessment, we carry out a cursory screening with amino ($-NH_2$) and cyano ($-CN$) substituents on the available C–H sites of the COLDEM core. Both excitation energy and $f_{S_1}^{osc}$ can be modulated through substitution effects while retaining the negative $E(S_1 - T_1)$ values (see Figure S6 and S7). These initial results reveal the potential for chemical optimization of the emissive properties of COLDEM. A combined computational and experimental approach was recently successfully applied by Aizawa *et al.*²⁶³ in the design of azaphenaele-based emitters.

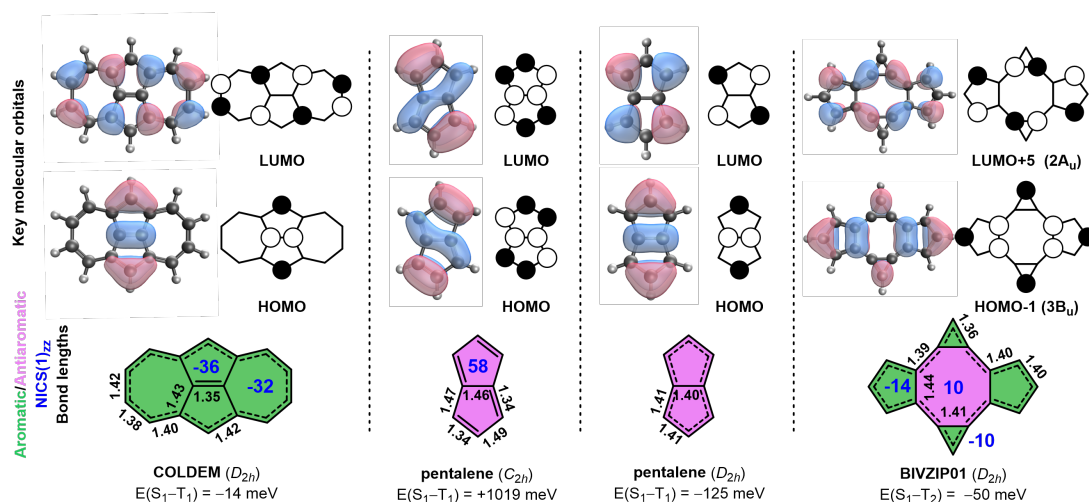


Figure 7.4: Key molecular orbitals, ground-state ring aromaticity (aromatic in green, antiaromatic in magenta) as determined from nucleus-independent chemical shifts (blue), and bond lengths (in Å, black) of ground-state COLDEM, the ground-state (C_{2h}) and high-symmetry (D_{2h}) geometries of pentalene, and ground-state BIVZIP01. Geometries were optimized at the ω B97X-D/def2-TZVP level; SCF orbitals and excitation energies were obtained at the EOM-CCSD/aug-cc-pVDZ level.

To guide future synthetic efforts based on the COLDEM motif, a large-scale screening of more diverse substituents is needed to identify targets with appreciable fluorescence rates.

The excited state singlet-triplet inversion in COLDEM is driven by the D_{2h} symmetry of the central pentalene unit, which is achieved by an aromatic stabilization of the pentalene core by the peripheral tropylium rings. Here, we have identified the singlet-triplet inversion in COLDEM through high-throughput screening of experimental molecules. However, COLDEM and pentalene were among several conjugated hydrocarbons proposed by Toyota and co-workers as possible Hund's rule violations in the 1980s,^{308–310} which have been overlooked in the recent literature. Given that this prior work was based on symmetry analysis and HF/STO-3G level calculations with a simplified configuration interaction scheme, we surveyed all proposed molecules from this earlier work at the EOM-CCSD/aug-cc-pVDZ level (Figure S16). Out of those suggested by Toyota and co-workers, the only other Hund's rule violation is bicalicene (see Figure A.1). This structure also exists in our database in bare^{311,312} and functionalized³¹² forms (Cambridge Structural Database codes BIVZIP01 and DUWXIC, respectively). These were beyond the cutoff of molecule sizes yet considered in our screening protocol.

The D_{2h} -symmetry bicalicene BIVZIP01 has a positive gap between the lowest excited singlet and triplet states, but the configuration-paired $E(S_1 - T_2) = -50$ meV constitutes a Hund's rule violation, as shown by the state diagram in Figure S15. BIVZIP01 consists of a calicene dimer forming a central 8-membered ring structurally reminiscent of cyclooctatetraene (COT) that is stabilized by the aromaticity of the peripheral cyclopentadienyl and cyclopropenium rings through a push-pull mechanism.^{313–315} The NICS-values and bond lengths of the 5- and 3-

membered rings in the dimer are almost equivalent to those of the corresponding rings in the parent calicene (see Figure S3). The central COT-ring of BIVZIP01 is only weakly anti-aromatic ($NICS(1)_{zz} = 10$ ppm, Figure 4). As with COLDEM discussed above, the non-overlapping orbitals describing the S_1/T_2 states coincide with the HOMO and LUMO of D_{2h} -pentalene, albeit separated from one another by the central COT-like ring and with additional features on the latter. The presence of the high-symmetry pentalene-like core of COLDEM and BIVZIP01 is the necessary requirement for the existence of the negative singlet-triplet gap in this class of molecules. We further assess the gaps of simplified analogs of the substituted bicalicenes, which all have inversion of the S_1-T_2 gap similar to BIVZIP01 (Figure S8). As with the COLDEM core, the Hund's rule violation in bicalicene is persistent under structural modification, and it is therefore a parent unit within the same D_{2h} -pentalenic class as COLDEM. Finally, we note that OLISUX, in the zwitterionic class discussed above, is also highly symmetric as a result of its aromatic ring structure (see Figure S3).

COLDEM and BIVZIP01 are Hückel aromatic molecules in the ground state. Future work must address their fluorescent properties and excited state dynamics, which are potentially governed by antiaromaticity in the excited state.^{316,317} Using excited-state aromaticity as a strategy to tune the energies has recently been applied successfully, for instance in the context of singlet fission.^{304,318} We briefly assess the aromaticity of the T_1 excited-state structures (Figure S4). As expected for a planar hydrocarbon with a Hückel aromatic ground state, COLDEM is Baird antiaromatic in the T_1 excited state.^{319,320} BIVZIP01 distorts into C_{2v} symmetry and only one of the five-membered rings becomes Baird antiaromatic in the T_1 state (Figure S4). A strategy based on excited-state aromaticity which lowers the state inversion to being between S_1 and T_1 may enable rational chemical design. In future screening efforts, it is also clear that the initial step (Figure 7.2, top) must consider higher-order Hund's rule violations than simply the $S_1 - T_1$ gap, which is the subject of ongoing work.

7.4 Conclusion

In conclusion, we have reported two classes of molecules that exhibit a violation of Hund's rule in the lowest excited singlet state. The first class consists of zwitterions that exhibit violations in the higher excited states, and are therefore unlikely to be of practical use for OLED emitters. The second class of D_{2h} -pentalenic molecules is comprised of high-symmetry non-alternant polycyclic hydrocarbons. These consist of the fused azulene dimer COLDEM and bicalicene BIVZIP01 and their derivatives, which demonstrate significant potential for materials applications. Both these molecules have D_{2h} -symmetry ground-state structures due to aromatic stabilization, which enables the higher symmetry pentalene moieties that are key to achieving singlet-triplet inversion. The S_1-T_1 states are inverted in COLDEM, and we show that the energies and oscillator strength of this compound are tunable via functionalization while retaining the inverted gap. We highlight that all of the parent compounds discussed here have been synthesized, and therefore constitute an excellent starting point for the synthetic design of new OLED emitters beyond azaphenalenenes. We are currently applying our screening

Chapter 7. Symmetry-Induced Singlet-Triplet Inversions in Non-Alternant Hydrocarbons

protocol to a broader range of compounds, and applying these symmetry-based design rules to new core motifs exhibiting excited-state singlet-triplet inversions.

8 Conclusions and Outlook

8.1 Conclusions

This thesis concerned the manipulation of excited states and the elaboration of data-driven computational workflows for the discovery of singlet fission chromophores and inverted gap emitters for applications in high-efficiency photovoltaics and organic light-emitting diodes. In particular, it involved identifying and rationalizing correlations between the ground state (energies and locations of orbitals; symmetry) and excited state properties that may be exploited for molecular design and screening purposes.

The SF design process required establishing quantum chemical descriptors based on the energy and character of the excited states invoked in the SF mechanism using time-dependent density functional theory (TDDFT) techniques, and identifying extant or synthetically attainable compounds located in the desirable region of this descriptor space. Rather than evaluating the triplet-pair state directly, at great computational cost due to its complexity, we have identified a proxy criterion: the fragment-based charge transfer numbers extracted from the transition density matrix computed with TDDFT.^{102,103} These were used to quantify the propensity of (*a*) the S_1 state to exhibit charge transfer character, and (*b*) the T_1 states to be localized on geometrically separate sites, thus favouring triplet-pair separation.⁷

By building on the rich chemistry of conjugated donor-acceptor (D-A) materials and well-established techniques for polymer synthesis, we used computational approaches to identify new, albeit synthetically feasible, D + A fragment combinations which, when coupled together in a D-A conjugated polymer, achieve the required excited state behaviour to enable intramolecular SF.⁷ The validity of the proposed descriptors was confirmed by the rediscovery of certain compounds in which SF has been reported experimentally.^{6,99} It was found that these descriptors in D-A compounds could be mapped to ground-state electronic properties of the constituent D and A monomers, which affords a significant computational speedup to compound screening.¹⁸⁵ Structure-property relationships were then identified in rings with oxidized heteroatoms, through which the S_1 and T_1 energies could be manipulated.⁸ To

summarize, we have established intuitive computational guidelines, based on the electronic properties of the constituent D and A units, that allow the parameters for intramolecular singlet fission to be tuned simultaneously in a modular, fragment-based approach.

We then mined and curated a massive database of reported organic crystal structures, developed a Python-based tool to combine molecules together in an automated yet chemically feasible way, and trained machine learning models for the prediction of vertical excitation energies from molecular structure with excellent accuracy. We used our screening parameters and models in tandem to locate new organic molecular candidates for SF beyond the well-trodden realm of pentacene-based materials.²⁸⁹ The collection of structural, optical and graph-topological properties is termed the *Fragment-Oriented Materials Design* (FORMED) dataset, and it may be repurposed to any other fragment-based materials design campaign, provided the design rules are known.

This molecular dataset, which is the largest of its kind, was then extended for use in the discovery of molecules with inversions of the S_1 and T_1 states, a highly attractive property for the design of OLED emitters.³²¹ To do this, we employed a filtering procedure to screen candidates using increasingly accurate (and expensive) methods, from TDDFT to approximate second-order coupled-cluster to equations-of-motion coupled-cluster. A new class of molecules displaying an inversion of the lowest singlet and triplet excited states was identified. This observed behavior is attributed to a high-symmetry non-alternant hydrocarbon core motif, which is stabilized via captodative aromaticity. The link between high symmetry and negative $E(S_1 - T_1)$ gaps enables the rational design of a new class of molecules beyond previously-synthesized structures.

8.2 Outlook

The next stage of the design process for both SF and inverted singlet-triplet materials will require the embedding of the best candidates identified thus far in the solid state to account for effects induced by the local environment.

Any future design of SF chromophores must consider the issue of the diffusion of triplet excitons from the site of SF to the chromophore/acceptor or chromophore/semiconductor interface, and subsequent charge separation at that interface.³²² This would require the parametrization of force fields and the subsequent simulation of bulk morphologies. The simulation of an amorphous polymer environment is challenging due to the conformational diversity of extended π -conjugated chains and the possibility of both amorphous and crystalline domains existing in a polymer film. As a result, it may be necessary to construct simpler trimer and tetramer models, and use coarse-graining techniques. Once the morphology for a chromophore-acceptor combination is available, charge injection rates from a SF chromophore into an acceptor material can be modelled using expressions such as those discussed in Chapter 2; charge dynamics can in turn be simulated using kinetic Monte Carlo methods.³²³ Electrostatic effects are significant at donor-acceptor interfaces, and the ionization energy

of the chromophore plays a role in promoting efficient charge separation of the T_1 states at the SF-chromophore/acceptor interface. Such parameters may be included in future design requirements for SF chromophores for photovoltaic applications. With ‘bulk’ information in hand, it may be possible to map charge injection ability back to chromophore properties, thus bridging the gap between *molecular* design (which has been the sole focus of this thesis) and measurable, experimental *device* characteristics.

Beyond conjugated polymers, other D-A-type arrangements have also shown promise for SF, and the design rules established here are likely applicable to these templates as well. In particular, long-lived T_1 states have been observed in liquid-crystalline motifs formed from hexabenzocoronene flanked with acceptors.⁸⁵ The columnar structure formed by the π -stacked hexabenzocoronene core may also allow triplets to be channeled between acceptor chromophores aligned along the periphery of the self-assembled column. Including T_1 transport as a parameter to optimize, either between self-assembled acceptors or along a polymer chain in an intramolecular fashion²⁵⁵, will lead to compounds and design templates with improved triplet diffusion pathways, and therefore less triplet recombination and higher rates of charge injection.

As with the SF candidates, the identification of molecules with singlet-triplet inversions constitutes only the first step towards high-performance OLEDs, and the work presented here does not consider any aspect of their practical implementation. To bridge this gap between molecule and device, it will be necessary to study the excited state dynamics, ideally in a simulated environment, such as in a ‘pure’ emitter layer or embedded in a host material. Competing relaxation pathways would need to be considered to tailor the molecular candidates to limit parasitic non-radiative decay pathways from the S_1 state. With appropriate core structures available, the logical next step is to modify them through functionalization to tune their emission wavelengths (and therefore colour) and to maximize emission probability. The transition probability is proportional to the oscillator strength f^{osc} , which is expressed by the following:

$$f_{i \rightarrow f}^{osc} \approx \frac{2}{3} \frac{m_e}{\hbar} (E_j - E_i) |\langle \Psi_i | R | \Psi_j \rangle|^2 \quad (8.1)$$

where m_e is the mass of the electron, Ψ_i and Ψ_j are the ground and excited state wavefunctions, R is the operator for the sum over the coordinates of the electrons in the system, and \hbar is the reduced Planck’s constant. If we assume that the $S_0 \rightarrow S_1$ transition is dominated by HOMO \rightarrow LUMO character, this means that in order for there to be a non-negligible $f_{S_0 \rightarrow S_1}^{osc}$, there must be some overlap between the HOMO and LUMO.

Given the direct relation between the HOMO-LUMO overlap and both the $E(S_1 - T_1)$ energy gap (Equation 2.18) and the oscillator strength (above), the highest-symmetry inverted-gap structures discussed in this thesis (i.e., those with perfectly non-overlapping orbital features) have a transition probability of zero. By the same token, perturbation of the electronic struc-

Chapter 8. Conclusions and Outlook

ture of the core responsible for the inversion through substituent effects increases oscillator strength but may easily destroy the $S_1 - T_1$ inversion.^{263,285} It is therefore expected that a trade-off between transition probability and robustly inverted S-T gaps exists, which can be impacted by the degree of symmetry in the orbitals involved. This will need to be elucidated and then optimized through systematic substitution effects on a series of cores exhibiting singlet-triplet inversions.

A Appendix A: Three-minute thesis

In the third year of my PhD, I participated in the "Three-minute thesis" competition for scientific popularization. The goal was to summarize one's PhD thesis topic for a general (non-scientific) audience in a concise and engaging way. The activity also involved a course workshop to train presenters to develop effective ways of presenting research effectively to both non-specialist and specialist audiences. I prepared the following text (with accompanying slide) at the workshop, and presented it at both the qualifications stage and at the university-wide finals.



Figure A.1: Slide serving as a visual aid for my three-minute thesis presentation.

Text:

You probably think what I've written up here is a mistake.

Well, I'm going to tell you that sometimes, 1 is equal to 2. At least, that is something that can happen in solar panels, those black blocks you can sometimes see on rooftops.

You may remember from school that all matter is made of molecules. Every molecule is an assembly of atoms, which are held together by electrons.

Appendix A. Appendix A: Three-minute thesis

A solar panel contains a molecule that can absorb a particle of light, called a photon, and then transfer the energy from that light particle to one of the molecule's electrons. This electron, which has much more energy than all the other electrons, is now able to jump into a nearby wire. This generates an electrical current. So, through this molecule, the energy from light becomes electricity.

There is a special type of molecule that, through a complex process, can transfer this energy from a photon into not one, but two electrons. This process is called singlet fission. I'm not going to explain exactly how it works - just remember this term.

Now, imagine we put this kind of molecule in a solar panel. Getting one photon to make two electrons jump out generates twice the electrical current, and gives us more renewable energy. We will have made solar panels more efficient than they are now.

Great! So where is the problem?

Well, there are millions of different molecules out there, and only a handful have the ability to generate singlet fission. And we need to find more of them.

This is where the science gets more complicated. We need to understand how a molecule behaves when it has a lot of energy. This is called the excited state, and it looks like someone dancing in a nightclub. *[dancing motions]*

Without extra energy, a molecule will be in the ground state. It's more like standing in the queue outside the nightclub. The ground state is much easier to measure and to model.

What we're doing is equivalent to finding out if people will be good dancers before they step inside the nightclub. To do that, we need get as much information as we can from the ground state and use it to predict which molecules have the ideal excited states to undergo this unique process.

This is based on the molecules we already know. It's like looking at experienced dancers, seeing what qualities they have, and then looking at inexperienced ones, to see if they, too, can dance in just the right way. With molecules it's more complicated, so we need computers for that.

Some of these molecules already exist in nature, but I also design new molecules that are likely to display these properties.

Why is this process important?

It takes too much time and money to find the right molecule through trial and error in the lab. My work makes discovering efficient solar energy materials cheaper and easier. In this way, we cycle through millions of possible molecules to find the ones that will be capable of making two electrons jump, producing more renewable energy.

Then, one will be equal to two a bit more often. Thank you.

Bibliography

1. Blaskovits, J. T.; Lin, K.-H.; Fabregat, R.; Swiderska, I.; Wu, H.; Corminboeuf, C. Is a Single Conformer Sufficient to Describe the Reorganization Energy of Amorphous Organic Transport Materials? *J. Phys. Chem. C* **2021**, *125*, 17355–17362.
2. Dong, Z.; Blaskovits, J. T.; Fadaei-Tirani, F.; Scopelliti, R.; Sienkiewicz, A.; Corminboeuf, C.; Severin, K. Tuning the π -Accepting Properties of Mesoionic Carbenes: A Combined Computational and Experimental Study. *Chem. Eur. J.* **2021**, *27*, 11983–11988.
3. Das, S.; Laplaza, R.; Blaskovits, J. T.; Corminboeuf, C. Mapping Active Site Geometry to Activity in Immobilized Frustrated Lewis Pair Catalysts. *Angew. Chem. Int. Ed.* **2022**, *61*, e202202727.
4. Das, S.; Laplaza, R.; Blaskovits, J. T.; Corminboeuf, C. Engineering Frustrated Lewis Pair Active Sites in Porous Organic Scaffolds for Catalytic CO₂ Hydrogenation. *ChemRxiv preprint*; DOI: <https://doi.org/10.26434/chemrxiv-2023-09mdd>
5. Garner, M. H.; Blaskovits, J. T.; Corminboeuf, C. Double-bond delocalization in non-alternant hydrocarbons induces inverted singlet-triplet gaps. *ChemRxiv preprint*; DOI: <https://doi.org/10.26434/chemrxiv-2023-568ks>
6. Grancini, G.; Maiuri, M.; Fazzi, D.; Petrozza, A.; Egelhaaf, H.-J.; Brida, D.; Cerullo, G.; Lanzani, G. Hot exciton dissociation in polymer solar cells. *Nat. Mater.* **2013**, *12*, 29–33.
7. Blaskovits, J. T.; Fumanal, M.; Vela, S.; Corminboeuf, C. Designing Singlet Fission Candidates from Donor–Acceptor Copolymers. *Chem. Mater.* **2020**, *32*, 6515–6524.
8. Blaskovits, J. T.; Fumanal, M.; Vela, S.; Cho, Y.; Corminboeuf, C. Heteroatom oxidation controls singlet–triplet energy splitting in singlet fission building blocks. *Chem. Commun.* **2022**, *58*, 1338–1341.
9. Huang, B.; von Lilienfeld, O. A. Quantum machine learning using atom-in-molecule-based fragments selected on the fly. *Nat. Chem.* **2020**, *12*, 945–951.
10. Singh, S.; Stoicheff, B. P. Double-Photon Excitation of Fluorescence in Anthracene Single Crystals. *J. Chem. Phys.* **1963**, *38*, 2032–2033.

Bibliography

11. Singh, S.; Jones, W. J.; Siebrand, W.; Stoicheff, B. P.; Schneider, W. G. Laser Generation of Excitons and Fluorescence in Anthracene Crystals. *J. Chem. Phys.* **1965**, *42*, 330–342.
12. Swenberg, C.; Stacy, W. Bimolecular radiationless transitions in crystalline tetracene. *Chem. Phys. Lett.* **1968**, *2*, 327–328.
13. Geacintov, N.; Pope, M.; Vogel, F. Effect of magnetic field on the fluorescence of tetracene crystals: exciton fission. *Phys. Rev. Lett.* **1969**, *22*, 593.
14. Merrifield, R.; Avakian, P.; Groff, R. Fission of singlet excitons into pairs of triplet excitons in tetracene crystals. *Chem. Phys. Lett.* **1969**, *3*, 386–388.
15. Ern, V.; Saint-Clair, J.; Schott, M.; Delacote, G. Effects of exciton interactions on the fluorescence yield of crystalline tetracene. *Chem. Phys. Lett.* **1971**, *10*, 287–290.
16. Berera, R.; van Grondelle, R.; Kennis, J. T. Ultrafast transient absorption spectroscopy: principles and application to photosynthetic systems. *Photosynth. Res.* **2009**, *101*, 105–118.
17. Burdett, J. J.; Müller, A. M.; Gosztola, D.; Bardeen, C. J. Excited state dynamics in solid and monomeric tetracene: The roles of superradiance and exciton fission. *J. Chem. Phys.* **2010**, *133*, 144506.
18. Burdett, J. J.; Bardeen, C. J. The dynamics of singlet fission in crystalline tetracene and covalent analogs. *Acc. Chem. Res.* **2013**, *46*, 1312–1320.
19. Lee, J.; Jadhav, P.; Baldo, M. A. High efficiency organic multilayer photodetectors based on singlet exciton fission. *Appl. Phys. Lett.* **2009**, *95*, 033301.
20. Casanova, D. Electronic structure study of singlet fission in tetracene derivatives. *J. Chem. Theory Comput.* **2014**, *10*, 324–334.
21. Kasha, M. Characterization of electronic transitions in complex molecules. *Discuss. Faraday Soc.* **1950**, *9*, 14–19.
22. Korovina, N. V.; Das, S.; Nett, Z.; Feng, X.; Joy, J.; Haiges, R.; Krylov, A. I.; Bradforth, S. E.; Thompson, M. E. Singlet fission in a covalently linked cofacial alkynyltetracene dimer. *J. Am. Chem. Soc.* **2016**, *138*, 617–627.
23. Tayebjee, M. J.; Sanders, S. N.; Kumarasamy, E.; Campos, L. M.; Sfeir, M. Y.; McCamey, D. R. Quintet multiexciton dynamics in singlet fission. *Nat. Phys.* **2017**, *13*, 182–188.
24. Basel, B. S.; Zirzmeier, J.; Hetzer, C.; Phelan, B. T.; Krzyaniak, M. D.; Reddy, S. R.; Coto, P. B.; Horwitz, N. E.; Young, R. M.; White, F. J., et al. Unified model for singlet fission within a non-conjugated covalent pentacene dimer. *Nat. Commun.* **2017**, *8*, 15171.
25. Kolomeisky, A. B.; Feng, X.; Krylov, A. I. A simple kinetic model for singlet fission: A role of electronic and entropic contributions to macroscopic rates. *J. Phys. Chem. C* **2014**, *118*, 5188–5195.

26. Lin, S. On the theory of non-radiative transfer of electronic excitation. *Proc. R. Soc. London, Ser. A* **1973**, 335, 51–66.
27. Casanova, D. Theoretical Modeling of Singlet Fission. *Chem. Rev.* **2018**, 118, 7164–7207.
28. Landau, L. D. Zur theorie der energieubertragung ii. *Z. Sowjetunion* **1932**, 2, 46–51.
29. Wittig, C. The landau- zener formula. *J. Phys. Chem. B* **2005**, 109, 8428–8430.
30. Vineyard, G. H. Frequency factors and isotope effects in solid state rate processes. *J. Phys. Chem. Solids* **1957**, 3, 121–127.
31. Chan, W.-L.; Ligges, M.; Zhu, X. The energy barrier in singlet fission can be overcome through coherent coupling and entropic gain. *Nat. Chem.* **2012**, 4, 840–845.
32. Streidl, N.; Denegri, B.; Kronja, O.; Mayr, H. A practical guide for estimating rates of heterolysis reactions. *Acc. Chem. Res.* **2010**, 43, 1537–1549.
33. Tamura, H.; Huix-Rotllant, M.; Burghardt, I.; Olivier, Y.; Beljonne, D. First-principles quantum dynamics of singlet fission: coherent versus thermally activated mechanisms governed by molecular π stacking. *Phys. Rev. Lett.* **2015**, 115, 107401.
34. Johnson, J. C.; Nozik, A. J.; Michl, J. The role of chromophore coupling in singlet fission. *Acc. Chem. Res.* **2013**, 46, 1290–1299.
35. Smith, M. B.; Michl, J. Recent Advances in Singlet Fission. *Annu. Rev. Phys. Chem.* **2013**, 64, 361–386.
36. Smith, M. B.; Michl, J. Singlet Fission. *Chem. Rev.* **2010**, 110, 6891–6936.
37. Johnson, J. C.; Akdag, A.; Zamadar, M.; Chen, X.; Schwerin, A. E.; Paci, I.; Smith, M. B.; Havlas, Z.; Miller, J. R.; Ratner, M. A., et al. Toward designed singlet fission: solution photophysics of two indirectly coupled covalent dimers of 1, 3-diphenylisobenzofuran. *J. Phys. Chem. B* **2013**, 117, 4680–4695.
38. Berkelbach, T. C.; Hybertsen, M. S.; Reichman, D. R. Microscopic theory of singlet exciton fission. II. Application to pentacene dimers and the role of superexchange. *J. Chem. Phys.* **2013**, 138, 114103.
39. Zheng, J.; Xie, Y.; Jiang, S.; Lan, Z. Ultrafast nonadiabatic dynamics of singlet fission: quantum dynamics with the multilayer multiconfigurational time-dependent Hartree (ML-MCTDH) method. *J. Phys. Chem. C* **2016**, 120, 1375–1389.
40. Giaimo, J. M.; Lockard, J. V.; Sinks, L. E.; Scott, A. M.; Wilson, T. M.; Wasielewski, M. R. Excited singlet states of covalently bound, cofacial dimers and trimers of perylene-3, 4: 9, 10-bis (dicarboximide) s. *J. Phys. Chem. A* **2008**, 112, 2322–2330.

Bibliography

41. Margulies, E. A.; Shoer, L. E.; Eaton, S. W.; Wasielewski, M. R. Excimer formation in cofacial and slip-stacked perylene-3, 4: 9, 10-bis (dicarboximide) dimers on a redox-inactive triptycene scaffold. *Phys. Chem. Chem. Phys.* **2014**, *16*, 23735–23742.
42. Lindquist, R. J.; Lefler, K. M.; Brown, K. E.; Dyar, S. M.; Margulies, E. A.; Young, R. M.; Wasielewski, M. R. Energy flow dynamics within cofacial and slip-stacked perylene-3, 4-dicarboximide dimer models of π -aggregates. *J. Am. Chem. Soc.* **2014**, *136*, 14912–14923.
43. Liu, H.; Nichols, V. M.; Shen, L.; Jahansouz, S.; Chen, Y.; Hanson, K. M.; Bardeen, C. J.; Li, X. Synthesis and photophysical properties of a “face-to-face” stacked tetracene dimer. *Phys. Chem. Chem. Phys.* **2015**, *17*, 6523–6531.
44. Feng, X.; Krylov, A. I. On couplings and excimers: lessons from studies of singlet fission in covalently linked tetracene dimers. *Phys. Chem. Chem. Phys.* **2016**, *18*, 7751–7761.
45. Bhattacharyya, K.; Datta, A. Polymorphism Controlled Singlet Fission in TIPS-Anthracene: Role of Stacking Orientation. *J. Phys. Chem. C* **2017**, *121*, 1412–1420.
46. Klessinger, M. Conical intersections and the mechanism of singlet photoreactions. *Angew. Chem. Int. Ed.* **1995**, *34*, 549–551.
47. Yarkony, D. R. Conical intersections: Diabolical and often misunderstood. *Acc. Chem. Res.* **1998**, *31*, 511–518.
48. Szabo, A.; Ostlund, N. S. *Modern quantum chemistry: introduction to advanced electronic structure theory*; Courier Corporation, 2012.
49. Cudazzo, P.; Sottile, F.; Rubio, A.; Gatti, M. Exciton dispersion in molecular solids. *J. Phys. Condens. Matter* **2015**, *27*, 113204.
50. Miyata, K.; Conrad-Burton, F. S.; Geyer, F. L.; Zhu, X.-Y. Triplet Pair States in Singlet Fission. *Chem. Rev.* **2019**, *119*, 4261–4292.
51. Daiber, B.; van den Hoven, K.; Futscher, M. H.; Ehrler, B. Realistic Efficiency Limits for Singlet-Fission Silicon Solar Cells. *ACS Energy Lett.* **2021**, *6*, 2800–2808.
52. Korovina, N. V.; Chang, C. H.; Johnson, J. C. Spatial separation of triplet excitons drives endothermic singlet fission. *Nat. Chem.* **2020**, *12*, 391–398.
53. De Vos, A. Detailed balance limit of the efficiency of tandem solar cells. *J. Phys. D: Appl. Phys.* **1980**, *13*, 839.
54. Martinho, F. Challenges for the future of tandem photovoltaics on the path to terawatt levels: a technology review. *Energy Environ. Sci.* **2021**, *14*, 3840–3871.
55. Schaller, R. D.; Klimov, V. I. High Efficiency Carrier Multiplication in PbSe Nanocrystals: Implications for Solar Energy Conversion. *Phys. Rev. Lett.* **2004**, *92*, 186601.

56. Beard, M. C.; Knutsen, K. P.; Yu, P.; Luther, J. M.; Song, Q.; Metzger, W. K.; Ellingson, R. J.; Nozik, A. J. Multiple exciton generation in colloidal silicon nanocrystals. *Nano Lett.* **2007**, *7*, 2506–2512.
57. Semonin, O. E.; Luther, J. M.; Choi, S.; Chen, H.-Y.; Gao, J.; Nozik, A. J.; Beard, M. C. Peak external photocurrent quantum efficiency exceeding 100% via MEG in a quantum dot solar cell. *Science* **2011**, *334*, 1530–1533.
58. Hanna, M. C.; Nozik, A. J. Solar conversion efficiency of photovoltaic and photoelectrolysis cells with carrier multiplication absorbers. *J. Appl. Phys.* **2006**, *100*, 074510.
59. Beard, M. C.; Luther, J. M.; Semonin, O. E.; Nozik, A. J. Third generation photovoltaics based on multiple exciton generation in quantum confined semiconductors. *Acc. Chem. Res.* **2013**, *46*, 1252–1260.
60. Beard, M. C.; Johnson, J. C.; Luther, J. M.; Nozik, A. J. Multiple exciton generation in quantum dots versus singlet fission in molecular chromophores for solar photon conversion. *Phil. Trans. R. Soc. A* **2015**, *373*, 20140412.
61. Klimov, V. I. Mechanisms for photogeneration and recombination of multiexcitons in semiconductor nanocrystals: Implications for lasing and solar energy conversion. *J. Phys. Chem. B* **2006**, *110*, 16827–16845.
62. Marcus, R. A. On the theory of oxidation-reduction reactions involving electron transfer. I. *J. Chem. Phys.* **1956**, *24*, 966–978.
63. Levich, V.; Dogonadze, R. Theory of non-radiation electron transitions from ion to ion in solutions. *Dokl. Akad. Nauk* **1959**, *124*, 123–126.
64. Casillas, R.; Papadopoulos, I.; Ullrich, T.; Thiel, D.; Kunzmann, A.; Guldi, D. M. Molecular insights and concepts to engineer singlet fission energy conversion devices. *Energy Environ. Sci.* **2020**, *13*, 2741–2804.
65. Yoo, S.; Domercq, B.; Kippelen, B. Efficient thin-film organic solar cells based on pentacene/C 60 heterojunctions. *Appl. Phys. Lett.* **2004**, *85*, 5427–5429.
66. Congreve, D. N.; Lee, J.; Thompson, N. J.; Hontz, E.; Yost, S. R.; Reuswig, P. D.; Bahlke, M. E.; Reineke, S.; Van Voorhis, T.; Baldo, M. A. External Quantum Efficiency Above 100% in a Singlet-Exciton-Fission-Based Organic Photovoltaic Cell. *Science* **2013**, *340*, 334–337.
67. Thompson, N. J.; Hontz, E.; Congreve, D. N.; Bahlke, M. E.; Reineke, S.; Van Voorhis, T.; Baldo, M. A. Nanostructured Singlet Fission Photovoltaics Subject to Triplet-Charge Annihilation. *Adv. Mater.* **2014**, *26*, 1366–1371.
68. Thompson, N. J.; Wilson, M. W.; Congreve, D. N.; Brown, P. R.; Scherer, J. M.; Bischof, T. S.; Wu, M.; Geva, N.; Welborn, M.; Voorhis, T. V., et al. Energy harvesting of non-emissive

Bibliography

- triplet excitons in tetracene by emissive PbS nanocrystals. *Nat. Mater.* **2014**, *13*, 1039–1043.
69. Kunzmann, A.; Gruber, M.; Casillas, R.; Zirzmeier, J.; Stanzel, M.; Peukert, W.; Tykwinski, R. R.; Guldi, D. M. Singlet fission for photovoltaics with 130% injection efficiency. *Angew. Chem. Int. Ed.* **2018**, *57*, 10742–10747.
70. Jadhav, P. J.; Mohanty, A.; Sussman, J.; Lee, J.; Baldo, M. A. Singlet Exciton Fission in Nanostructured Organic Solar Cells. *Nano Lett.* **2011**, *11*, 1495–1498.
71. Pun, A. B.; Sanders, S. N.; Kumarasamy, E.; Sfeir, M. Y.; Congreve, D. N.; Campos, L. M. Triplet Harvesting from Intramolecular Singlet Fission in Polytetracene. *Adv. Mater.* **2017**, *29*, 1701416.
72. Einzinger, M.; Wu, T.; Kompalla, J. F.; Smith, H. L.; Perkinson, C. F.; Nienhaus, L.; Wieghold, S.; Congreve, D. N.; Kahn, A.; Bawendi, M. G., et al. Sensitization of silicon by singlet exciton fission in tetracene. *Nature* **2019**, *571*, 90–94.
73. Reuswig, P. D.; Congreve, D. N.; Thompson, N. J.; Baldo, M. A. Enhanced external quantum efficiency in an organic photovoltaic cell via singlet fission exciton sensitizer. *Appl. Phys. Lett.* **2012**, *101*, 113304.
74. Pandey, A. K. Highly efficient spin-conversion effect leading to energy up-converted electroluminescence in singlet fission photovoltaics. *Sci. Rep.* **2015**, *5*, 7787.
75. Lin, Y. L.; Fusella, M. A.; Kozlov, O. V.; Lin, X.; Kahn, A.; Pshenichnikov, M. S.; Rand, B. P. Morphological tuning of the energetics in singlet fission organic solar cells. *Adv. Funct. Mater.* **2016**, *26*, 6489–6494.
76. Kawata, S.; Pu, Y.-J.; Saito, A.; Kurashige, Y.; Beppu, T.; Katagiri, H.; Hada, M.; Kido, J. Singlet fission of non-polycyclic aromatic molecules in organic photovoltaics. *Adv. Mater.* **2016**, *28*, 1585–1590.
77. Kawata, S.; Furudate, J.; Kimura, T.; Minaki, H.; Saito, A.; Katagiri, H.; Pu, Y.-J. Controlling the excited-state energy levels of 9, 9'-bifluorenylidene derivatives by twisting their structure to attaining singlet fission character in organic photovoltaics. *J. Mater. Chem. C* **2017**, *5*, 4909–4914.
78. Schrauben, J. N.; Zhao, Y.; Mercado, C.; Dron, P. I.; Ryerson, J. L.; Michl, J.; Zhu, K.; Johnson, J. C. Photocurrent enhanced by singlet fission in a dye-sensitized solar cell. *ACS Appl. Mater. Interfaces* **2015**, *7*, 2286–2293.
79. Nagarajan, K.; Mallia, A. R.; Reddy, V. S.; Hariharan, M. Access to triplet excited state in core-twisted perylenediimide. *J. Phys. Chem. C* **2016**, *120*, 8443–8450.
80. Eaton, S. W.; Shoer, L. E.; Karlen, S. D.; Dyar, S. M.; Margulies, E. A.; Veldkamp, B. S.; Ramanan, C.; Hartzler, D. A.; Savikhin, S.; Marks, T. J., et al. Singlet exciton fission in

- polycrystalline thin films of a slip-stacked perylene-3,4,9,10-tetracarboxylic diimide. *J. Am. Chem. Soc.* **2013**, *135*, 14701–14712.
81. Margulies, E. A.; Miller, C. E.; Wu, Y.; Ma, L.; Schatz, G. C.; Young, R. M.; Wasielewski, M. R. Enabling singlet fission by controlling intramolecular charge transfer in π -stacked covalent terrylenediimide dimers. *Nat. Chem.* **2016**, *8*, 1120–1125.
 82. Hartnett, P. E.; Margulies, E. A.; Mauck, C. M.; Miller, S. A.; Wu, Y.; Wu, Y.-L.; Marks, T. J.; Wasielewski, M. R. Effects of crystal morphology on singlet exciton fission in diketopyrrolopyrrole thin films. *J. Phys. Chem. B* **2016**, *120*, 1357–1366.
 83. Mauck, C. M.; Hartnett, P. E.; Wu, Y.-L.; Miller, C. E.; Marks, T. J.; Wasielewski, M. R. Singlet fission within diketopyrrolopyrrole nanoparticles in water. *Chem. Mater.* **2017**, *29*, 6810–6817.
 84. Levine, A. M.; Schierl, C.; Basel, B. S.; Ahmed, M.; Camargo, B. A.; Guldi, D. M.; Braunschweig, A. B. Singlet fission in combinatorial diketopyrrolopyrrole–rylene supramolecular films. *J. Phys. Chem. C* **2019**, *123*, 1587–1595.
 85. Masoomi-Godarzi, S.; Liu, M.; Tachibana, Y.; Mitchell, V. D.; Goerigk, L.; Ghiggino, K. P.; Smith, T. A.; Jones, D. J. Liquid Crystallinity as a Self-Assembly Motif for High-Efficiency, Solution-Processed, Solid-State Singlet Fission Materials. *Adv. Energy Mater.* **2019**, *9*, 1901069.
 86. Minami, T.; Nakano, M. Diradical character view of singlet fission. *J. Phys. Chem. Lett.* **2012**, *3*, 145–150.
 87. Minami, T.; Ito, S.; Nakano, M. Fundamental of diradical-character-based molecular design for singlet fission. *J. Phys. Chem. Lett.* **2013**, *4*, 2133–2137.
 88. Wang, C.; Tauber, M. J. High-yield singlet fission in a zeaxanthin aggregate observed by picosecond resonance Raman spectroscopy. *J. Am. Chem. Soc.* **2010**, *132*, 13988–13991.
 89. Musser, A. J.; Maiuri, M.; Brida, D.; Cerullo, G.; Friend, R. H.; Clark, J. The nature of singlet exciton fission in carotenoid aggregates. *J. Am. Chem. Soc.* **2015**, *137*, 5130–5139.
 90. Trinh, M. T.; Zhong, Y.; Chen, Q.; Schiros, T.; Jockusch, S.; Sfeir, M. Y.; Steigerwald, M.; Nuckolls, C.; Zhu, X. Intra- to intermolecular singlet fission. *J. Phys. Chem. C* **2015**, *119*, 1312–1319.
 91. Rademaker, H.; Hoff, A. J.; Van Grondelle, R.; Duysens, L. N. Carotenoid triplet yields in normal and deuterated *Rhodospirillum rubrum*. *Biochim. Biophys. Acta, Bioenerg.* **1980**, *592*, 240–257.
 92. Wang, C.; Schlamadinger, D. E.; Desai, V.; Tauber, M. J. Triplet excitons of carotenoids formed by singlet fission in a membrane. *ChemPhysChem* **2011**, *12*, 2891–2894.

Bibliography

93. Masoomi-Godarzi, S.; Liu, M.; Tachibana, Y.; Goerigk, L.; Ghiggino, K. P.; Smith, T. A.; Jones, D. J. Solution-Processable, Solid State Donor-Acceptor Materials for Singlet Fission. *Adv. Energy Mater.* **2018**, *8*, 1801720.
94. Dellepiane, G.; Comoretto, D.; Cuniberti, C. Chemical modulation of the electronic properties of polydiacetylenes. *J. Mol. Struct.* **2000**, *521*, 157–166.
95. Wohlgenannt, M.; Graupner, W.; Leising, G.; Vardeny, Z. Photogeneration action spectroscopy of neutral and charged excitations in films of a ladder-type poly (para-phenylene). *Phys. Rev. Lett.* **1999**, *82*, 3344.
96. Guo, J.; Ohkita, H.; Bente, H.; Ito, S. Near-IR femtosecond transient absorption spectroscopy of ultrafast polaron and triplet exciton formation in polythiophene films with different regioregularities. *J. Am. Chem. Soc.* **2009**, *131*, 16869–16880.
97. Tamai, Y.; Ohkita, H.; Bente, H.; Ito, S. Singlet Fission in Poly (9,9'-di-n-octylfluorene) Films. *J. Phys. Chem. C* **2013**, *117*, 10277–10284.
98. Österbacka, R.; Wohlgenannt, M.; Shkunov, M.; Chinn, D.; Vardeny, Z. Excitons, polarons, and laser action in poly (p-phenylene vinylene) films. *J. Chem. Phys.* **2003**, *118*, 8905–8916.
99. Busby, E.; Xia, J.; Wu, Q.; Low, J. Z.; Song, R.; Miller, J. R.; Zhu, X.; Campos, L. M.; Sfeir, M. Y. A design strategy for intramolecular singlet fission mediated by charge-transfer states in donor-acceptor organic materials. *Nat. Mater.* **2015**, *14*, 426–433.
100. Tilley, A. J.; Pensack, R. D.; Kynaston, E. L.; Scholes, G. D.; Seferos, D. S. Singlet Fission in Core-Shell Micelles of End-Functionalized Polymers. *Chem. Mater.* **2018**, *30*, 4409–4421.
101. Yablon, L. M.; Sanders, S. N.; Li, H.; Parenti, K. R.; Kumarasamy, E.; Fallon, K. J.; Hore, M. J.; Cacciuto, A.; Sfeir, M. Y.; Campos, L. M. Persistent multiexcitons from polymers with pendent pentacenes. *J. Am. Chem. Soc.* **2019**, *141*, 9564–9569.
102. Plasser, F.; Lischka, H. Analysis of Excitonic and Charge Transfer Interactions from Quantum Chemical Calculations. *J. Chem. Theory Comput.* **2012**, *8*, 2777–2789.
103. Plasser, F. TheoDORE: A package for theoretical density, orbital relaxation, and exciton analysis. URL: <http://theodore-qc.sourceforge.net> **2017**,
104. Fuemmeler, E. G.; Sanders, S. N.; Pun, A. B.; Kumarasamy, E.; Zeng, T.; Miyata, K.; Steigerwald, M. L.; Zhu, X.-Y.; Sfeir, M. Y.; Campos, L. M., et al. A direct mechanism of ultrafast intramolecular singlet fission in pentacene dimers. *ACS Cent. Sci.* **2016**, *2*, 316–324.
105. Zimmerman, P. M.; Musgrave, C. B.; Head-Gordon, M. A correlated electron view of singlet fission. *Acc. Chem. Res.* **2013**, *46*, 1339–1347.

106. Beljonne, D.; Yamagata, H.; Brédas, J.; Spano, F.; Olivier, Y. Charge-transfer excitations steer the Davydov splitting and mediate singlet exciton fission in pentacene. *Phys. Rev. Lett.* **2013**, *110*, 226402.
107. Berkelbach, T. C.; Hybertsen, M. S.; Reichman, D. R. Microscopic theory of singlet exciton fission. I. General formulation. *J. Chem. Phys.* **2013**, *138*, 114102.
108. Chan, W.-L.; Berkelbach, T. C.; Provorse, M. R.; Monahan, N. R.; Tritsch, J. R.; Hybertsen, M. S.; Reichman, D. R.; Gao, J.; Zhu, X.-Y. The quantum coherent mechanism for singlet fission: Experiment and theory. *Acc. Chem. Res.* **2013**, *46*, 1321–1329.
109. Swenberg, C.; Ratner, M.; Geacintov, N. Energy dependence of optically induced exciton fission. *J. Chem. Phys.* **1974**, *60*, 2152–2157.
110. Jundt, C.; Klein, G.; Sipp, B.; Le Moigne, J.; Joucla, M.; Villaeys, A. Exciton dynamics in pentacene thin films studied by pump-probe spectroscopy. *Chem. Phys. Lett.* **1995**, *241*, 84–88.
111. Chan, W.-L.; Ligges, M.; Jailaubekov, A.; Kaake, L.; Miaja-Avila, L.; Zhu, X.-Y. Observing the multiexciton state in singlet fission and ensuing ultrafast multielectron transfer. *Science* **2011**, *334*, 1541–1545.
112. Dillon, R. J.; Piland, G. B.; Bardeen, C. J. Different rates of singlet fission in monoclinic versus orthorhombic crystal forms of diphenylhexatriene. *J. Am. Chem. Soc.* **2013**, *135*, 17278–17281.
113. Schwerin, A. F.; Johnson, J. C.; Smith, M. B.; Sreearunothai, P.; Popovic, D.; Cerny, J.; Havlas, Z.; Paci, I.; Akdag, A.; MacLeod, M. K., et al. Toward designed singlet fission: electronic states and photophysics of 1, 3-diphenylisobenzofuran. *J. Phys. Chem. A* **2010**, *114*, 1457–1473.
114. Müller, A. M.; Avlasevich, Y. S.; Müllen, K.; Bardeen, C. J. Evidence for exciton fission and fusion in a covalently linked tetracene dimer. *Chem. Phys. Lett.* **2006**, *421*, 518–522.
115. Müller, A. M.; Avlasevich, Y. S.; Schoeller, W. W.; Müllen, K.; Bardeen, C. J. Exciton fission and fusion in bis (tetracene) molecules with different covalent linker structures. *J. Am. Chem. Soc.* **2007**, *129*, 14240–14250.
116. Sanders, S. N.; Kumarasamy, E.; Pun, A. B.; Steigerwald, M. L.; Sfeir, M. Y.; Campos, L. M. Intramolecular Singlet Fission in Oligoacene Heterodimers. *Angew. Chem. Int. Ed.* **2016**, *55*, 3373–3377.
117. Zirzmeier, J.; Lehnerr, D.; Coto, P. B.; Chernick, E. T.; Casillas, R.; Basel, B. S.; Thoss, M.; Tykwinski, R. R.; Guldi, D. M. Singlet fission in pentacene dimers. *Proc. Natl. Acad. Sci. U.S.A.* **2015**, *112*, 5325–5330.
118. Kasai, Y.; Tamai, Y.; Ohkita, H.; Bente, H.; Ito, S. Ultrafast Singlet Fission in a Push–Pull Low-Bandgap Polymer Film. *J. Am. Chem. Soc.* **2015**, *137*, 15980–15983.

Bibliography

119. Zhai, Y.; Sheng, C.; Vardeny, Z. V. Singlet fission of hot excitons in π -conjugated polymers. *Phil. Trans. R. Soc. A* **2015**, *373*, 20140327.
120. Hu, J.; Xu, K.; Shen, L.; Wu, Q.; He, G.; Wang, J.-Y.; Pei, J.; Xia, J.; Sfeir, M. Y. New insights into the design of conjugated polymers for intramolecular singlet fission. *Nat. Commun.* **2018**, *9*, 1–9.
121. Padula, D.; Omar, O. H.; Nematiram, T.; Troisi, A. Singlet fission molecules among known compounds: Finding a few needles in a haystack. *Energy Environ. Sci.* **2019**, *12*, 2412–2416.
122. Aryanpour, K.; Dutta, T.; Huynh, U. N. V.; Vardeny, Z. V.; Mazumdar, S. Theory of Primary Photoexcitations in Donor-Acceptor Copolymers. *Phys. Rev. Lett.* **2015**, *115*, 267401.
123. Paci, I.; Johnson, J. C.; Chen, X.; Rana, G.; Popović, D.; David, D. E.; Nozik, A. J.; Ratner, M. A.; Michl, J. Singlet fission for dye-sensitized solar cells: Can a suitable sensitizer be found? *J. Am. Chem. Soc.* **2006**, *128*, 16546–16553.
124. Zhou, H.; Yang, L.; You, W. Rational design of high performance conjugated polymers for organic solar cells. *Macromolecules* **2012**, *45*, 607–632.
125. Guo, X.; Baumgarten, M.; Müllen, K. Designing π -conjugated polymers for organic electronics. *Prog. Polym. Sci.* **2013**, *38*, 1832–1908.
126. Cheng, Y.-J.; Yang, S.-H.; Hsu, C.-S. Synthesis of conjugated polymers for organic solar cell applications. *Chem. Rev.* **2009**, *109*, 5868–5923.
127. Szarko, J. M.; Guo, J.; Liang, Y.; Lee, B.; Rolczynski, B. S.; Strzalka, J.; Xu, T.; Loser, S.; Marks, T. J.; Yu, L., et al. When function follows form: effects of donor copolymer side chains on film morphology and BHJ solar cell performance. *Adv. Mater.* **2010**, *22*, 5468–5472.
128. Szarko, J. M.; Rolczynski, B. S.; Lou, S. J.; Xu, T.; Strzalka, J.; Marks, T. J.; Yu, L.; Chen, L. X. Photovoltaic function and exciton/charge transfer dynamics in a highly efficient semi-conducting copolymer. *Adv. Funct. Mater.* **2014**, *24*, 10–26.
129. Pouliot, J.-R.; Grenier, F.; Blaskovits, J. T.; Beaupré, S.; Leclerc, M. Direct (Hetero)arylation Polymerization: Simplicity for Conjugated Polymer Synthesis. *Chem. Rev.* **2016**, *116*, 14225–14274.
130. Blaskovits, J. T.; Leclerc, M. C-H Activation as a Shortcut to Conjugated Polymer Synthesis. *Macromol. Rapid Comm.* **2019**, *40*, 1800512.
131. Bura, T.; Blaskovits, J. T.; Leclerc, M. Direct (Hetero)arylation Polymerization: Trends and Perspectives. *J. Am. Chem. Soc.* **2016**, *138*, 10056–10071.

132. Po, R.; Bernardi, A.; Calabrese, A.; Carbonera, C.; Corso, G.; Pellegrino, A. From lab to fab: how must the polymer solar cell materials design change?—an industrial perspective. *Energy Environ. Sci.* **2014**, *7*, 925–943.
133. Weininger, D. SMILES, a chemical language and information system. 1. Introduction to methodology and encoding rules. *J. Chem. Inf. Model.* **1988**, *28*, 31–36.
134. O’Boyle, N. M.; Banck, M.; James, C. A.; Morley, C.; Vandermeersch, T.; Hutchison, G. R. Open Babel: An open chemical toolbox. *J. Cheminf.* **2011**, *3*, 1–14.
135. Frisch, M. J. et al. Gaussian 16, Revision A.03. 2016; Gaussian Inc.: Wallingford, CT.
136. Chai, J.-D.; Head-Gordon, M. Long-range corrected hybrid density functionals with damped atom–atom dispersion corrections. *Phys. Chem. Chem. Phys.* **2008**, *10*, 6615–6620.
137. Weigend, F.; Ahlrichs, R. Balanced basis sets of split valence, triple zeta valence and quadruple zeta valence quality for H to Rn: Design and assessment of accuracy. *Phys. Chem. Chem. Phys.* **2005**, *7*, 3297.
138. Peach, M. J.; Tozer, D. J. Overcoming low orbital overlap and triplet instability problems in TDDFT. *J. Phys. Chem. A* **2012**, *116*, 9783–9789.
139. Laurent, A. D.; Jacquemin, D. TD-DFT benchmarks: a review. *Int. J. Quantum Chem.* **2013**, *113*, 2019–2039.
140. Adamo, C.; Jacquemin, D. The calculations of excited-state properties with Time-Dependent Density Functional Theory. *Chem. Soc. Rev.* **2013**, *42*, 845–856.
141. Pandey, L.; Doiron, C.; Sears, J. S.; Brédas, J.-L. Lowest excited states and optical absorption spectra of donor–acceptor copolymers for organic photovoltaics: a new picture emerging from tuned long-range corrected density functionals. *Phys. Chem. Chem. Phys.* **2012**, *14*, 14243–14248.
142. Sun, H.; Autschbach, J. Electronic energy gaps for π -conjugated oligomers and polymers calculated with density functional theory. *J. Chem. Theory Comput.* **2014**, *10*, 1035–1047.
143. O’boyle, N. M.; Tenderholt, A. L.; Langner, K. M. Cclib: a library for package-independent computational chemistry algorithms. *J. Comput. Chem.* **2008**, *29*, 839–845.
144. Ren, J.; Peng, Q.; Zhang, X.; Yi, Y.; Shuai, Z. Role of the Dark $2A_g$ State in Donor–Acceptor Copolymers as a Pathway for Singlet Fission: A DMRG Study. *J. Phys. Chem. Lett.* **2017**, *8*, 2175–2181.
145. Chen, T.; Zheng, L.; Yuan, J.; An, Z.; Chen, R.; Tao, Y.; Li, H.; Xie, X.; Huang, W. Understanding the control of singlet-triplet splitting for organic exciton manipulating: a combined theoretical and experimental approach. *Sci. Rep.* **2015**, *5*, 10923.

Bibliography

146. Arias, D. H.; Ryerson, J. L.; Cook, J. D.; Damrauer, N. H.; Johnson, J. C. Polymorphism influences singlet fission rates in tetracene thin films. *Chem. Sci.* **2016**, *7*, 1185–1191.
147. Bhattacharyya, K.; Datta, A. Computationally driven design principles for singlet fission in organic chromophores. *J. Phys. Chem. C* **2019**, *123*, 19257–19268.
148. Pal, A. K.; Bhattacharyya, K.; Datta, A. Remote functionalization through symmetric or asymmetric substitutions control the pathway of intermolecular singlet fission. *J. Chem. Theory Comput.* **2019**, *15*, 5014–5023.
149. Pace, N. A.; Zhang, W.; Arias, D. H.; McCulloch, I.; Rumbles, G.; Johnson, J. C. Controlling Long-Lived Triplet Generation from Intramolecular Singlet Fission in the Solid State. *J. Phys. Chem. Lett.* **2017**, *8*, 6086–6091.
150. Fumanal, M.; Corminboeuf, C. Direct, Mediated, and Delayed Intramolecular Singlet Fission Mechanism in Donor-Acceptor Copolymers. *J. Phys. Chem. Lett.* **2020**, *11*, 9788–9794.
151. Mukhopadhyay, T.; Musser, A. J.; Puttaraju, B.; Dhar, J.; Friend, R. H.; Patil, S. Is the chemical strategy for imbuing “polyene” character in diketopyrrolopyrrole-based chromophores sufficient for singlet fission? *J. Phys. Chem. Lett.* **2017**, *8*, 984–991.
152. Leclerc, N.; Chávez, P.; Ibraikulov, O. A.; Heiser, T.; Lévêque, P. Impact of backbone fluorination on π -conjugated polymers in organic photovoltaic devices: A review. *Polymers* **2016**, *8*, 11.
153. Nguyen, T. L.; Choi, H.; Ko, S.-J.; Uddin, M. A.; Walker, B.; Yum, S.; Jeong, J.-E.; Yun, M.; Shin, T. J.; Hwang, S., et al. Semi-crystalline photovoltaic polymers with efficiency exceeding 9% in a 300 nm thick conventional single-cell device. *Energy Environ. Sci.* **2014**, *7*, 3040–3051.
154. Yum, S.; An, T. K.; Wang, X.; Lee, W.; Uddin, M. A.; Kim, Y. J.; Nguyen, T. L.; Xu, S.; Hwang, S.; Park, C. E., et al. Benzotriazole-containing planar conjugated polymers with noncovalent conformational locks for thermally stable and efficient polymer field-effect transistors. *Chem. Mater.* **2014**, *26*, 2147–2154.
155. El Kassmi, A.; Fache, F.; Lemaire, M. Poly (3-fluorothiophene). *Journal of Electroanal. Chem.* **1994**, *373*, 241–244.
156. Sakamoto, Y.; Komatsu, S.; Suzuki, T. Tetradecafluorosexithiophene: The first perfluorinated oligothiophene. *J. Am. Chem. Soc.* **2001**, *123*, 4643–4644.
157. Heeney, M.; Farrant, L.; Giles, M.; Thompson, M.; Tierney, S.; Shkunov, M.; Sparrowe, D.; McCulloch, I. Mono-, oligo- and poly-4-fluorothiophenes and their use as charge transport materials. 2004; US Patent 6,676,857.

158. Blaskovits, J. T.; Bura, T.; Beaupré, S.; Lopez, S. A.; Roy, C.; de Goes Soares, J.; Oh, A.; Quinn, J.; Li, Y.; Aspuru-Guzik, A.; Leclerc, M. A Study of the Degree of Fluorination in Regioregular Poly(3-hexylthiophene). *Macromolecules* **2016**, *50*, 162–174.
159. Sun, J.-P.; Blaskovits, J. T.; Bura, T.; Beaupré, S.; Leclerc, M.; Hill, I. G. Photovoltaic device performance of highly regioregular fluorinated poly(3-hexylthiophene). *Org. Electron.* **2017**, *50*, 115–120.
160. Yao, H.; Ye, L.; Zhang, H.; Li, S.; Zhang, S.; Hou, J. Molecular design of benzodithiophene-based organic photovoltaic materials. *Chem. Rev.* **2016**, *116*, 7397–7457.
161. Roy, C.; Bura, T.; Beaupré, S.; Lgar, M.-A.; Sun, J.-P.; Hill, I. G.; Leclerc, M. Fluorinated thiophene-based synthons: Polymerization of 1, 4-dialkoxybenzene and fluorinated dithieno-2, 1, 3-benzothiadiazole by direct heteroarylation. *Macromolecules* **2017**, *50*, 4658–4667.
162. Mamone, M.; Bura, T.; Brassard, S.; Soligo, E.; He, K.; Li, Y.; Leclerc, M. Optimized synthesis of fluorinated dithienyl-diketopyrrolopyrroles and new copolymers obtained via direct heteroarylation polymerization. *Mater. Chem. Front.* **2020**, *4*, 2040–2046.
163. Zhao, W.; Li, S.; Yao, H.; Zhang, S.; Zhang, Y.; Yang, B.; Hou, J. Molecular optimization enables over 13% efficiency in organic solar cells. *J. Am. Chem. Soc.* **2017**, *139*, 7148–7151.
164. Wu, Y.; An, C.; Shi, L.; Yang, L.; Qin, Y.; Liang, N.; He, C.; Wang, Z.; Hou, J. The crucial role of chlorinated thiophene orientation in conjugated polymers for photovoltaic devices. *Angew. Chem. Int. Ed.* **2018**, *57*, 12911–12915.
165. Lei, T.; Dou, J.-H.; Ma, Z.-J.; Liu, C.-J.; Wang, J.-Y.; Pei, J. Chlorination as a useful method to modulate conjugated polymers: balanced and ambient-stable ambipolar high-performance field-effect transistors and inverters based on chlorinated isoindigo polymers. *Chem. Sci.* **2013**, *4*, 2447–2452.
166. Chen, H.; Hu, Z.; Wang, H.; Liu, L.; Chao, P.; Qu, J.; Chen, W.; Liu, A.; He, F. A chlorinated π -conjugated polymer donor for efficient organic solar cells. *Joule* **2018**, *2*, 1623–1634.
167. Qiu, B.; Chen, S.; Li, H.; Luo, Z.; Yao, J.; Sun, C.; Li, X.; Xue, L.; Zhang, Z.-G.; Yang, C., et al. A simple approach to prepare chlorinated polymer donors with low-lying HOMO level for high performance polymer solar cells. *Chem. Mater.* **2019**, *31*, 6558–6567.
168. Olla, T.; Ibraikulov, O. A.; Ferry, S.; Boyron, O.; Méry, S.; Heinrich, B.; Heiser, T.; Lévêque, P.; Leclerc, N. Benzothiadiazole halogenation impact in conjugated polymers, a comprehensive study. *Macromolecules* **2019**, *52*, 8006–8016.
169. Seri, M.; Bolognesi, M.; Chen, Z.; Lu, S.; Koopman, W.; Facchetti, A.; Muccini, M. Fine structural tuning of cyanated dithieno [3, 2-*b*: 2', 3'-*d*] silole-oligothiophene copolymers: synthesis, characterization, and photovoltaic response. *Macromolecules* **2013**, *46*, 6419–6430.

Bibliography

170. Casey, A.; Dimitrov, S. D.; Shakya-Tuladhar, P.; Fei, Z.; Nguyen, M.; Han, Y.; Anthopoulos, T. D.; Durrant, J. R.; Heeney, M. Effect of systematically tuning conjugated donor polymer lowest unoccupied molecular orbital levels via cyano substitution on organic photovoltaic device performance. *Chem. Mater.* **2016**, *28*, 5110–5120.
171. Kim, H. G.; Kim, M.; Clement, J. A.; Lee, J.; Shin, J.; Hwang, H.; Sin, D. H.; Cho, K. Energy level engineering of donor polymers via inductive and resonance effects for polymer solar cells: effects of cyano and alkoxy substituents. *Chem. Mater.* **2015**, *27*, 6858–6868.
172. Liu, M. S.; Jiang, X.; Liu, S.; Herguth, P.; Jen, A. K.-Y. Effect of cyano substituents on electron affinity and electron-transporting properties of conjugated polymers. *Macromolecules* **2002**, *35*, 3532–3538.
173. Huo, L.; Zhang, S.; Guo, X.; Xu, F.; Li, Y.; Hou, J. Replacing alkoxy groups with alkylthienyl groups: a feasible approach to improve the properties of photovoltaic polymers. *Angew. Chem. Int. Ed.* **2011**, *50*, 9697–9702.
174. Pomerantz, M.; Yang, H.; Cheng, Y. Poly (alkyl thiophene-3-carboxylates). Synthesis and characterization of polythiophenes with a carbonyl group directly attached to the ring. *Macromolecules* **1995**, *28*, 5706–5708.
175. Guo, X.; Facchetti, A.; Marks, T. J. Imide- and amide-functionalized polymer semiconductors. *Chem. Rev.* **2014**, *114*, 8943–9021.
176. Zindy, N.; Blaskovits, J. T.; Beaumont, C.; Michaud-Valcourt, J.; Saneifar, H.; Johnson, P. A.; Bélanger, D.; Leclerc, M. Pyromellitic Diimide-Based Copolymers and Their Application as Stable Cathode Active Materials in Lithium and Sodium-Ion Batteries. *Chem. Mater.* **2018**, *30*, 6821–6830.
177. Oliva, M. M.; Casado, J.; Navarrete, J. T. L.; Patchkovskii, S.; Goodson, T.; Harpham, M. R.; de Melo, J. S. S.; Amir, E.; Rozen, S. Do [all]-S,S'-Dioxide Oligothiophenes Show Electronic and Optical Properties of Oligoenes and/or of Oligothiophenes? *J. Am. Chem. Soc.* **2010**, *132*, 6231–6242.
178. Streifel, B. C.; Zafra, J. L.; Espejo, G. L.; Gómez-García, C. J.; Casado, J.; Tovar, J. D. An Unusually Small Singlet-Triplet Gap in a Quinoidal 1, 6-Methano[10]annulene Resulting from Baird's $4n\pi$ -Electron Triplet Stabilization. *Angew. Chem. Int. Ed.* **2015**, *54*, 5888–5893.
179. Ito, S.; Nagami, T.; Nakano, M. Molecular design for efficient singlet fission. *J. Photochem. Photobiol. C: Photochem. Rev.* **2018**, *34*, 85–120.
180. Che, Y.; Perepichka, D. F. Quantifying planarity in the design of organic electronic materials. *Angew. Chem. Int. Ed.* **2021**, *60*, 1364–1373.
181. Frisch, M. J. et al. Gaussian 09, Revision D. 01. 2009.

182. Mai, S.; Plasser, F.; Dorn, J.; Fumanal, M.; Daniel, C.; González, L. Quantitative wave function analysis for excited states of transition metal complexes. *Coord. Chem. Rev.* **2018**, *361*, 74–97.
183. Zeng, Z.; Shi, X.; Chi, C.; Navarrete, J. T. L.; Casado, J.; Wu, J. Pro-aromatic and anti-aromatic π -conjugated molecules: an irresistible wish to be diradicals. *Chem. Soc. Rev.* **2015**, *44*, 6578–6596.
184. Monahan, N. R.; Sun, D.; Tamura, H.; Williams, K. W.; Xu, B.; Zhong, Y.; Kumar, B.; Nuckolls, C.; Harutyunyan, A. R.; Chen, G.; Dai, H.-L.; Beljonne, D.; Rao, Y.; Zhu, X.-Y. Dynamics of the triplet-pair state reveals the likely coexistence of coherent and incoherent singlet fission in crystalline hexacene. *Nat. Chem.* **2016**, *9*, 341–346.
185. Blaskovits, J. T.; Fumanal, M.; Vela, S.; Fabregat, R.; Corminboeuf, C. Identifying the Trade-off between Intramolecular Singlet Fission Requirements in Donor–Acceptor Copolymers. *Chem. Mater.* **2021**, *33*, 2567–2575.
186. Fumanal, M.; Corminboeuf, C. Pushing the Limits of the Donor–Acceptor Copolymer Strategy for Intramolecular Singlet Fission. *J. Phys. Chem. Lett.* **2021**, *12*, 7270–7277.
187. El Bakouri, O.; Smith, J. R.; Ottosson, H. Strategies for design of potential singlet fission chromophores utilizing a combination of ground-state and excited-state aromaticity rules. *J. Am. Chem. Soc.* **2020**, *142*, 5602–5617.
188. Fallon, K. J.; Budden, P.; Salvadori, E.; Ganose, A. M.; Savory, C. N.; Eyre, L.; Dowland, S.; Ai, Q.; Goodlett, S.; Risko, C., et al. Exploiting excited-state aromaticity to design highly stable singlet fission materials. *J. Am. Chem. Soc.* **2019**, *141*, 13867–13876.
189. Stoycheva, J.; Tadjer, A.; Garavelli, M.; Spassova, M.; Nenov, A.; Romanova, J. Boron-doped polycyclic aromatic hydrocarbons: A molecular set revealing the interplay between topology and singlet fission propensity. *J. Phys. Chem. Lett.* **2020**, *11*, 1390–1396.
190. Linder, T.; Badiola, E.; Baumgartner, T.; Sutherland, T. C. Synthesis of π -extended thiadiazole (oxides) and their electronic properties. *Org. Lett.* **2010**, *12*, 4520–4523.
191. Pinkowicz, D.; Li, Z.; Pietrzyk, P.; Rams, M. New thiadiazole dioxide bridging ligand with a stable radical form for the construction of magnetic coordination Chains. *Cryst. Growth Des.* **2014**, *14*, 4878–4881.
192. Amir, E.; Rozen, S. Easy access to the family of thiazole N-oxides using HOF· CH₃CN. *Chem. Commun.* **2006**, 2262–2264.
193. Mirabal, R. A.; Vanderzwet, L.; Abuadas, S.; Emmett, M. R.; Schipper, D. Dehydration Polymerization for Poly (hetero) arene Conjugated Polymers. *Chem. Eur. J.* **2018**, *24*, 12231–12235.

Bibliography

194. Konstantinova, L. S.; Knyazeva, E. A.; Obruchnikova, N. V.; Gatilov, Y. V.; Zibarev, A. V.; Rakitin, O. A. Reactions of vicinal nitroamines with sulfur monochloride—a short and convenient route to fused 1, 2, 5-thiadiazoles and their N-oxides. *Tetrahedron Letters* **2013**, *54*, 3075–3078.
195. Fraux, G.; Cersonsky, R.; Ceriotti, M. Chemiscope: Interactive structure-property explorer for materials and molecules. *J. Open Source Softw.* **2020**, *5*, 2117.
196. Gómez-Bombarelli, R. et al. Design of efficient molecular organic light-emitting diodes by a high-throughput virtual screening and experimental approach. *Nat. Mater.* **2016**, *15*, 1120–1127.
197. Forero-Martinez, N. C.; Lin, K.-H.; Kremer, K.; Andrienko, D. Virtual Screening for Organic Solar Cells and Light Emitting Diodes. *Adv. Sci.* **2022**, *9*, 2200825.
198. Markina, A. et al. Chemical Design Rules for Non-Fullerene Acceptors in Organic Solar Cells. *Adv. Energy Mater.* **2021**, *11*, 2102363.
199. Ramprasad, R.; Batra, R.; Pilia, G.; Mannodi-Kanakkithodi, A.; Kim, C. Machine learning in materials informatics: Recent applications and prospects. *npj Comput. Mater.* **2017**, *3*.
200. Janet, J. P.; Chan, L.; Kulik, H. J. Accelerating Chemical Discovery with Machine Learning: Simulated Evolution of Spin Crossover Complexes with an Artificial Neural Network. *J. Phys. Chem. Lett.* **2018**, *9*, 1064–1071.
201. Janet, J. P.; Ramesh, S.; Duan, C.; Kulik, H. J. Accurate Multiobjective Design in a Space of Millions of Transition Metal Complexes with Neural-Network-Driven Efficient Global Optimization. *ACS Cent. Sci.* **2020**, *6*, 513–524.
202. Kulik, H. J.; Sigman, M. S. Advancing Discovery in Chemistry with Artificial Intelligence: From Reaction Outcomes to New Materials and Catalysts. *Accounts Chem. Res.* **2021**, *54*, 2335–2336.
203. Pollice, R.; dos Passos Gomes, G.; Aldeghi, M.; Hickman, R. J.; Krenn, M.; Lavigne, C.; Lindner-D'Addario, M.; Nigam, A.; Ser, C. T.; Yao, Z.; Aspuru-Guzik, A. Data-Driven Strategies for Accelerated Materials Design. *Accounts Chem. Res.* **2021**, *54*, 849–860.
204. Lopez, S. A.; Sanchez-Lengeling, B.; de Goes Soares, J.; Aspuru-Guzik, A. Design Principles and Top Non-Fullerene Acceptor Candidates for Organic Photovoltaics. *Joule* **2017**, *1*, 857–870.
205. Lin, K.-H.; Wetzelaer, G.-J. A. H.; Blom, P. W. M.; Andrienko, D. Virtual Screening of TADF Emitters for Single-Layer OLEDs. *Front. Chem.* **2021**, *9*.
206. Endo, A.; Ogasawara, M.; Takahashi, A.; Yokoyama, D.; Kato, Y.; Adachi, C. Thermally Activated Delayed Fluorescence from Sn⁴⁺-Porphyrin Complexes and Their Application

- to Organic Light Emitting Diodes - A Novel Mechanism for Electroluminescence. *Adv. Mater.* **2009**, *21*, 4802–4806.
207. Uoyama, H.; Goushi, K.; Shizu, K.; Nomura, H.; Adachi, C. Highly efficient organic light-emitting diodes from delayed fluorescence. *Nature* **2012**, *492*, 234–238.
208. Wong, M. Y.; Zysman-Colman, E. Purely Organic Thermally Activated Delayed Fluorescence Materials for Organic Light-Emitting Diodes. *Adv. Mater.* **2017**, *29*, 1605444.
209. Penfold, T. J.; Dias, F. B.; Monkman, A. P. The theory of thermally activated delayed fluorescence for organic light emitting diodes. *Chem. Commun.* **2018**, *54*, 3926–3935.
210. Zhang, G.; Zhao, J.; Chow, P. C. Y.; Jiang, K.; Zhang, J.; Zhu, Z.; Zhang, J.; Huang, F.; Yan, H. Nonfullerene Acceptor Molecules for Bulk Heterojunction Organic Solar Cells. *Chem. Rev.* **2018**, *118*, 3447–3507.
211. Zhang, G.; Lin, F. R.; Qi, F.; Heumüller, T.; Distler, A.; Egelhaaf, H.-J.; Li, N.; Chow, P. C. Y.; Brabec, C. J.; Jen, A. K.-Y.; Yip, H.-L. Renewed Prospects for Organic Photovoltaics. *Chem. Rev.* **2022**, *122*, 14180–14274.
212. Bansal, D.; Kundu, A.; Singh, V. P.; Pal, A. K.; Datta, A.; Dasgupta, J.; Mukhopadhyay, P. A highly contorted push–pull naphthalenediimide dimer and evidence of intramolecular singlet exciton fission. *Chem. Sci.* **2022**, *13*, 11506–11512.
213. Hachmann, J.; Olivares-Amaya, R.; Jinich, A.; Appleton, A. L.; Blood-Forsythe, M. A.; Seress, L. R.; Román-Salgado, C.; Trepte, K.; Atahan-Evrenk, S.; Er, S.; Shrestha, S.; Mondal, R.; Sokolov, A.; Bao, Z.; Aspuru-Guzik, A. Lead candidates for high-performance organic photovoltaics from high-throughput quantum chemistry – the Harvard Clean Energy Project. *Energy Environ. Sci.* **2014**, *7*, 698–704.
214. Kunkel, C.; Margraf, J. T.; Chen, K.; Oberhofer, H.; Reuter, K. Active discovery of organic semiconductors. *Nat. Commun.* **2021**, *12*, 2422.
215. Schober, C.; Reuter, K.; Oberhofer, H. Virtual Screening for High Carrier Mobility in Organic Semiconductors. *J. Phys. Chem. Lett.* **2016**, *7*, 3973–3977.
216. Zhao, K.; Omar, O. H.; Nematiram, T.; Padula, D.; Troisi, A. Novel thermally activated delayed fluorescence materials by high-throughput virtual screening: Going beyond donor–acceptor design. *J. Mater. Chem. C* **2021**, *9*, 3324–3333.
217. Ai, Q.; Bhat, V.; Ryno, S. M.; Jarolimek, K.; Sornberger, P.; Smith, A.; Haley, M. M.; Anthony, J. E.; Risko, C. OCELOT: An infrastructure for data-driven research to discover and design crystalline organic semiconductors. *J. Chem. Phys.* **2021**, *154*, 174705.
218. Vela, S.; Laplaza, R.; Cho, Y.; Corminboeuf, C. cell2mol: Encoding chemistry to interpret crystallographic data. *npj Comput. Mater.* **2022**, *8*, 1–8.

Bibliography

219. Zahrt, A. F.; Henle, J. J.; Denmark, S. E. Cautionary Guidelines for Machine Learning Studies with Combinatorial Datasets. *ACS Comb. Sci.* **2020**, *22*, 586–591.
220. Rinehart, N. I.; Zahrt, A. F.; Henle, J. J.; Denmark, S. E. Dreams, False Starts, Dead Ends, and Redemption: A Chronicle of the Evolution of a Chemoinformatic Workflow for the Optimization of Enantioselective Catalysts. *Accounts Chem. Res.* **2021**, *54*, 2041–2054.
221. Coley, C. W. Defining and Exploring Chemical Spaces. *Trends Chem.* **2021**, *3*, 133–145.
222. Schmidt, J.; Marques, M. R. G.; Botti, S.; Marques, M. A. L. Recent advances and applications of machine learning in solid-state materials science. *npj Comput. Mater.* **2019**, *5*.
223. Tang, H.; Xu, Q.; Wang, M.; Jiang, J. Rapid Screening of Metal–Organic Frameworks for Propane/Propylene Separation by Synergizing Molecular Simulation and Machine Learning. *ACS Appl. Mater. Interfaces* **2021**, *13*, 53454–53467.
224. Zanca, F.; Glasby, L. T.; Chong, S.; Chen, S.; Kim, J.; Fairen-Jimenez, D.; Monserrat, B.; Moghadam, P. Z. Computational techniques for characterisation of electrically conductive MOFs: Quantum calculations and machine learning approaches. *J. Mater. Chem. C* **2021**, *9*, 13584–13599.
225. Mayr, F.; Harth, M.; Kouroudis, I.; Rinderle, M.; Gagliardi, A. Machine Learning and Optoelectronic Materials Discovery: A Growing Synergy. *J. Phys. Chem. Lett.* **2022**, *13*, 1940–1951.
226. Miyake, Y.; Kranthiraja, K.; Ishiwari, E.; Saeki, A. Improved Predictions of Organic Photovoltaic Performance through Machine Learning Models Empowered by Artificially Generated Failure Data. *Chem. Mater.* **2022**, *34*, 6912–6920.
227. Cao, Y.; Ser, C. T.; Skreta, M.; Jorner, K.; Kusanda, N.; Aspuru-Guzik, A. Reinforcement learning supercharges redox flow batteries. *Nat. Mach. Intell.* **2022**, *4*, 667–668.
228. Bannwarth, C.; Ehlert, S.; Grimme, S. GFN2-xTB—An Accurate and Broadly Parametrized Self-Consistent Tight-Binding Quantum Chemical Method with Multipole Electrostatics and Density-Dependent Dispersion Contributions. *J. Chem. Theory Comput.* **2019**, *15*, 1652–1671.
229. Mewes, S. A.; Dreuw, A. Density-based descriptors and exciton analyses for visualizing and understanding the electronic structure of excited states. *Phys. Chem. Chem. Phys.* **2019**, *21*, 2843–2856.
230. Montavon, G.; Rupp, M.; Gobre, V.; Vazquez-Mayagoitia, A.; Hansen, K.; Tkatchenko, A.; Müller, K.-R.; Anatole von Lilienfeld, O. Machine learning of molecular electronic properties in chemical compound space. *New J. Phys.* **2013**, *15*, 095003.
231. Ramakrishnan, R.; Dral, P. O.; Rupp, M.; von Lilienfeld, O. A. Quantum chemistry structures and properties of 134 kilo molecules. *Sci. Data* **2014**, *1*, 1–7.

232. Xu, S.; Kim, E. H.; Wei, A.; Negishi, E.-i. Pd- and Ni-catalyzed cross-coupling reactions in the synthesis of organic electronic materials. *Sci. Technol. Adv. Mat.* **2014**, *15*, 044201.
233. Zani, L.; Dessì, A.; Franchi, D.; Calamante, M.; Reginato, G.; Mordini, A. Transition metal-catalyzed cross-coupling methodologies for the engineering of small molecules with applications in organic electronics and photovoltaics. *Coord. Chem. Rev.* **2019**, *392*, 177–236.
234. Yang, Y.; Lan, J.; You, J. Oxidative C–H/C–H Coupling Reactions between Two (Hetero)arenes. *Chem. Rev.* **2017**, *117*, 8787–8863.
235. Segawa, Y.; Maekawa, T.; Itami, K. Synthesis of Extended π -Systems through C–H Activation. *Angew. Chem. Int. Ed.* **2015**, *54*, 66–81.
236. Bura, T.; Beaupré, S.; Légaré, M.-A.; Quinn, J.; Rochette, E.; Blaskovits, J. T.; Fontaine, F.-G.; Pron, A.; Li, Y.; Leclerc, M. Direct heteroarylation polymerization: guidelines for defect-free conjugated polymers. *Chem. Sci.* **2017**, *8*, 3913–3925.
237. Blaskovits, J. T.; Leclerc, M. Direct (Hetero)arylation Polymerization for the Preparation of Conjugated Polymers. *The Handbook of Conducting Polymers, 4th Edition* **2019**, 195–238.
238. Stepek, I. A.; Itami, K. Recent Advances in C–H Activation for the Synthesis of π -Extended Materials. *ACS Mater. Lett.* **2020**, *2*, 951–974.
239. Klein, D. J.; Randić, M. Resistance distance. *J. Math. Chem.* **1993**, *12*, 81–95.
240. Babić, D.; Klein, D. J.; Lukovits, I.; Nikolić, S.; Trinajstić, N. Resistance-distance matrix: A computational algorithm and its application. *Int. J. Quantum Chem.* **2002**, *90*, 166–176.
241. Ertl, P.; Schuffenhauer, A. Estimation of synthetic accessibility score of drug-like molecules based on molecular complexity and fragment contributions. *J. Cheminform.* **2009**, *1*, 1–11.
242. Coley, C. W.; Rogers, L.; Green, W. H.; Jensen, K. F. SCScore: Synthetic Complexity Learned from a Reaction Corpus. *J. Chem. Inf. Model.* **2018**, *58*, 252–261.
243. Kim, Y.; Kim, W. Y. Universal Structure Conversion Method for Organic Molecules: From Atomic Connectivity to Three-Dimensional Geometry. *Bull. Korean Chem. Soc.* **2015**, *36*, 1769–1777.
244. Jensen, J. H. xyz2mol. *GitHub repository* **2020**,
245. Landrum, G., et al. RDKit: A software suite for cheminformatics, computational chemistry, and predictive modeling. **2013**,
246. Chen, T.; Guestrin, C. XGBoost. Proceedings of the 22nd ACM SIGKDD International Conference on Knowledge Discovery and Data Mining. New York, NY, USA, 2016; pp 785–794.

Bibliography

247. Liang, J.; Feng, X.; Hait, D.; Head-Gordon, M. Revisiting the Performance of Time-Dependent Density Functional Theory for Electronic Excitations: Assessment of 43 Popular and Recently Developed Functionals from Rungs One to Four. *J. Chem. Theory Comput.* **2022**, *18*, 3460–3473.
248. Nagata, R.; Nakanotani, H.; Potscavage, W. J.; Adachi, C. Exploiting Singlet Fission in Organic Light-Emitting Diodes. *Adv. Mater.* **2018**, *30*, 1801484.
249. Smyser, K. E.; Eaves, J. D. Singlet fission for quantum information and quantum computing: The parallel JDE model. *Sci. Rep.* **2020**, *10*, 1–10.
250. Krishnapriya, K. C.; Musser, A. J.; Patil, S. Molecular Design Strategies for Efficient Intramolecular Singlet Exciton Fission. *ACS Energy Lett.* **2018**, *4*, 192–202.
251. Young, R. M.; Wasielewski, M. R. Mixed Electronic States in Molecular Dimers: Connecting Singlet Fission, Excimer Formation, and Symmetry-Breaking Charge Transfer. *Accounts Chem. Res.* **2020**, *53*, 1957–1968.
252. Karlsson, J. K. G.; Harriman, A. Origin of the Red-Shifted Optical Spectra Recorded for Aza-BODIPY Dyes. *J. Phys. Chem. A* **2016**, *120*, 2537–2546.
253. Morales Salazar, D.; Mijangos, E.; Pullen, S.; Gao, M.; Orthaber, A. Functional small-molecules & polymers containing P=C and As=C bonds as hybrid π -conjugated materials. *Chem. Commun.* **2017**, *53*, 1120–1123.
254. Pradhan, E.; Lee, S.; Choi, C. H.; Zeng, T. Diboron- and diaza-doped anthracenes and phenanthrenes: their electronic structures for being singlet fission chromophores. *J. Phys. Chem. A* **2020**, *124*, 8159–8172.
255. Fumanal, M.; Corminboeuf, C. Optimizing the Thermodynamics and Kinetics of the Triplet-Pair Dissociation in Donor–Acceptor Copolymers for Intramolecular Singlet Fission. *Chem. Mater.* **2022**, *34*, 4115–4121.
256. Cerecetto, H.; González, M. Benzofuroxan and furoxan. Chemistry and biology. *Bioactive Heterocycles IV* **2007**, 265–308.
257. Hafezi, N.; Shewa, W. T.; Fettingner, J. C.; Mascal, M. A Zwitterionic, 10 π Aromatic Hemisphere. *Angew. Chem. Int. Ed.* **2017**, *56*, 14141–14144.
258. Bhattacharjee, J.; Kottalanka, R. K.; Adimulam, H.; Panda, T. K. Synthesis of monomeric and polymeric alkali and alkaline earth metal complexes using a phosphinoselenoic amide ligand in metal coordination sphere. *J. Chem. Sci.* **2014**, *126*, 1463–1475.
259. Bruno, I. J.; Cole, J. C.; Edgington, P. R.; Kessler, M.; Macrae, C. F.; McCabe, P.; Pearson, J.; Taylor, R. New software for searching the Cambridge Structural Database and visualizing crystal structures. *Acta Crystallogr., Sect. B: Struct. Sci.* **2002**, *58*, 389–397.

260. Senthil, S.; Chakraborty, S.; Ramakrishnan, R. Troubleshooting unstable molecules in chemical space. *Chem. Sci.* **2021**, *12*, 5566–5573.
261. Hund, F. Zur deutung verwickelter spektren, insbesondere der elemente scandium bis nickel. *Z. Phys.* **1925**, *33*, 345–371.
262. Kutzelnigg, W. Friedrich Hund and chemistry. *Angew. Chem. Int. Ed.* **1996**, *35*, 572–586.
263. Aizawa, N.; Pu, Y.-J.; Harabuchi, Y.; Nihonyanagi, A.; Ibuka, R.; Inuzuka, H.; Dhara, B.; Koyama, Y.; Nakayama, K.-i.; Maeda, S., et al. Delayed fluorescence from inverted singlet and triplet excited states. *Nature* **2022**, *609*, 502–506.
264. Eng, J.; Penfold, T. J. Open questions on the photophysics of thermally activated delayed fluorescence. *Commun. Chem.* **2021**, *4*, 91.
265. Wagner, J.; Zimmermann Crocomo, P.; Kochman, M. A.; Kubas, A.; Data, P.; Lindner, M. Modular Nitrogen-Doped Concave Polycyclic Aromatic Hydrocarbons for High-Performance Organic Light-Emitting Diodes with Tunable Emission Mechanisms. *Angew. Chem. Int. Ed.* **2022**, *61*, e202202232.
266. Sancho-García, J.-C. Fluorescence limitations overcome by engineering light–matter interactions. *Nature* **2022**, *609*, 473–475.
267. Dougherty, D. A. Spin control in organic molecules. *Acc. Chem. Res.* **1991**, *24*, 88–94.
268. Borden, W. T.; Iwamura, H.; Berson, J. A. Violations of Hund’s rule in non-Kekule hydrocarbons: theoretical prediction and experimental verification. *Acc. Chem. Res.* **1994**, *27*, 109–116.
269. Segal, M.; Singh, M.; Rivoire, K.; Difley, S.; Van Voorhis, T.; Baldo, M. A. Extrafluorescent electroluminescence in organic light-emitting devices. *Nat. Mater.* **2007**, *6*, 374–378.
270. Difley, S.; Beljonne, D.; Van Voorhis, T. On the singlet- triplet splitting of geminate electron- hole pairs in organic semiconductors. *J. Am. Chem. Soc.* **2008**, *130*, 3420–3427.
271. Eizner, E.; Martínez-Martínez, L. A.; Yuen-Zhou, J.; Kña-Cohen, S. Inverting singlet and triplet excited states using strong light-matter coupling. *Sci. Adv.* **2019**, *5*, eaax4482.
272. Yu, Y.; Mallick, S.; Wang, M.; Börjesson, K. Barrier-free reverse-intersystem crossing in organic molecules by strong light-matter coupling. *Nat. Commun.* **2021**, *12*, 3255.
273. Ehrmaier, J.; Rabe, E. J.; Pristash, S. R.; Corp, K. L.; Schlenker, C. W.; Sobolewski, A. L.; Domcke, W. Singlet–triplet inversion in heptazine and in polymeric carbon nitrides. *J. Phys. Chem. A* **2019**, *123*, 8099–8108.
274. de Silva, P. Inverted singlet–triplet gaps and their relevance to thermally activated delayed fluorescence. *J. Phys. Chem. Lett.* **2019**, *10*, 5674–5679.

Bibliography

275. Leupin, W.; Wirz, J. Low-lying electronically excited states of cycl [3.3.3] azine, a bridged 12π -perimeter. *J. Am. Chem. Soc.* **1980**, *102*, 6068–6075.
276. Leupin, W.; Magde, D.; Persy, G.; Wirz, J. 1,4,7-Triazacycl [3.3.3] azine: basicity, photoelectron spectrum, photophysical properties. *J. Am. Chem. Soc.* **1986**, *108*, 17–22.
277. Li, J.; Nakagawa, T.; MacDonald, J.; Zhang, Q.; Nomura, H.; Miyazaki, H.; Adachi, C. Highly Efficient Organic Light-Emitting Diodes Based on a Hidden TADF Channel in a Heptazine Derivative. *Adv. Mater.* **2013**, *25*, 3319–3323.
278. Li, J.; Zhang, Q.; Nomura, H.; Miyazaki, H.; Adachi, C. Thermally activated delayed fluorescence from $3n\pi^*$ to $1n\pi^*$ up-conversion and its application to organic light-emitting diodes. *Appl. Phys. Lett.* **2014**, *105*, 98_1.
279. Hwang, D.; Schlenker, C. W. Photochemistry of carbon nitrides and heptazine derivatives. *Chem. Commun.* **2021**, *57*, 9330–9353.
280. Sobolewski, A. L.; Domcke, W. Are heptazine-based organic light-emitting diode chromophores thermally activated delayed fluorescence or inverted singlet–triplet systems? *J. Phys. Chem. Lett.* **2021**, *12*, 6852–6860.
281. Li, J.; Li, Z.; Liu, H.; Gong, H.; Zhang, J.; Li, X.; Wang, Y.; Guo, Q. Down-conversion-induced delayed fluorescence via an inverted singlet-triplet channel. *Dyes Pigm.* **2022**, *203*, 110366.
282. Audebert, P.; Kroke, E.; Posern, C.; Lee, S.-H. State of the Art in the Preparation and Properties of Molecular Monomeric s-Heptazines: Syntheses, Characteristics, and Functional Applications. *Chem. Rev.* **2021**, *121*, 2515–2544.
283. Olivier, Y.; Sancho-Garcia, J.-C.; Muccioli, L.; D’Avino, G.; Beljonne, D. Computational design of thermally activated delayed fluorescence materials: The challenges ahead. *J. Phys. Chem. Lett.* **2018**, *9*, 6149–6163.
284. Ricci, G.; San-Fabián, E.; Olivier, Y.; Sancho-García, J. C. Singlet-Triplet Excited-State Inversion in Heptazine and Related Molecules: Assessment of TD-DFT and ab initio Methods. *ChemPhysChem* **2021**, *22*, 553–560.
285. Pollice, R.; Friederich, P.; Lavigne, C.; dos Passos Gomes, G.; Aspuru-Guzik, A. Organic molecules with inverted gaps between first excited singlet and triplet states and appreciable fluorescence rates. *Matter* **2021**, *4*, 1654–1682.
286. Sancho-García, J. C.; Brímond, E.; Ricci, G.; Pérez-Jiménez, A. J.; Olivier, Y.; Adamo, C. Violation of Hund’s rule in molecules: Predicting the excited-state energy inversion by TD-DFT with double-hybrid methods. *J. Chem. Phys.* **2022**, *156*, 034105.
287. Ghosh, S.; Bhattacharyya, K. Origin of the Failure of Density Functional Theories in Predicting Inverted Singlet–Triplet Gaps. *J. Phys. Chem. A* **2022**, *126*, 1378–1385.

288. Tučková, L.; Straka, M.; Valiev, R. R.; Sundholm, D. On the origin of the inverted singlet–triplet gap of the 5th generation light-emitting molecules. *Phys. Chem. Chem. Phys.* **2022**, *24*, 18713–18721.
289. Blaskovits, J. T.; Laplaza, R.; Vela, S.; Corminboeuf, C. Data-driven discovery of organic electronic materials enabled by hybrid top-down/bottom-up design. *ChemRxiv preprint*; DOI: <https://doi.org/10.26434/chemrxiv-2022-88t32>
290. Structures and data for all compounds in the FORMED dataset²⁸⁹ are provided in a Materials Cloud repository at <https://doi.org/10.24435/materialscloud:nh-gb>. Optimized structures from the final stage of screening and sample input files are available online as Supporting Information.
291. Pios, S.; Huang, X.; Sobolewski, A. L.; Domcke, W. Triangular boron carbon nitrides: An unexplored family of chromophores with unique properties for photocatalysis and optoelectronics. *Phys. Chem. Chem. Phys.* **2021**, *23*, 12968–12975.
292. Sanz-Rodrigo, J.; Ricci, G.; Olivier, Y.; Sancho-García, J. C. Negative singlet–triplet excitation energy gap in triangle-shaped molecular emitters for efficient triplet harvesting. *J. Phys. Chem. A* **2021**, *125*, 513–522.
293. Ricci, G.; Sancho-García, J.-C.; Olivier, Y. Establishing design strategies for emissive materials with an inverted singlet–triplet energy gap (INVEST): a computational perspective on how symmetry rules the interplay between triplet harvesting and light emission. *J. Mater. Chem. C* **2022**, *10*, 12680–12698.
294. Lindqvist, O.; Ljungström, E.; Andréasson, E.; Ceder, O. 1, 3, 4, 6-Tetraazacycl [3.3.3] azine: crystal and molecular structure. *Acta Crystallogr. B Struct. Cryst. Chem.* **1978**, *34*, 1667–1670.
295. Laurent, G.; Boutique, J.-P.; Evrard, G.; Verbist, J.; Durant, F.; Ashwell, G. Structure of 2, 5-dimethyl-1, 3, 4, 6-tetraazacycl [3.3. 3] azine, C₁₀H₉N₅. *Acta Crystallogr., Sect. C: Cryst. Struct. Commun.* **1984**, *40*, 2108–2109.
296. Yang, T.-H.; Zhuang, W.; Wei, W.; Yang, Y.-B.; Chen, Q. [Amino (iminio) methyl] phosphonate. *Acta Crystallogr., Sect. E: Struct. Rep. Online* **2010**, *66*, o2326–o2326.
297. Mezei, G.; Raptis, R. G. Pyrazole-4-sulfonate networks of alkali and alkaline-earth metals. Effect of cation size, charge, H-bonding and aromatic interactions on the three-dimensional supramolecular architecture. *New J. Chem.* **2003**, *27*, 1399–1407.
298. Kokkou, S.; Cheer, C.; Rentzeperis, P.; Karagiannidis, P. Structures of N-(3-diethylaminopropyl) dithiocarbamic acid and N-(2-diethylaminoethyl) dithiocarbamic acid. *Acta Crystallogr., Sect. C: Cryst. Struct. Commun.* **1988**, *44*, 1984–1987.
299. Vogel, E.; Wieland, H.; Schmalstieg, L.; Lex, J. Novel Synthesis and Molecular Structure of the Pyrene Isomer Dicyclohepta[cd,gh]pentalene (Azuleno[2,1,8-ija]azulene). *Angew. Chem. Int. Ed.* **1984**, *23*, 717–719.

Bibliography

300. Chen, Z.; Wannere, C. S.; Corminboeuf, C.; Puchta, R.; Schleyer, P. v. R. Nucleus-independent chemical shifts (NICS) as an aromaticity criterion. *Chem. Rev.* **2005**, *105*, 3842–3888.
301. Zilberg, S.; Haas, Y. Two-State Model of Antiaromaticity: The Triplet State. Is Hund's Rule Violated? *J. Phys. Chem. A* **1998**, *102*, 10851–10859.
302. Mayer, P. J.; El Bakouri, O.; Holczbauer, T.; Samu, G. F.; Janáky, C.; Ottosson, H.; London, G. Structure–Property Relationships in Unsymmetric Bis (antiaromatics): Who Wins the Battle between Pentalene and Benzocyclobutadiene? *J. Org. Chem.* **2020**, *85*, 5158–5172.
303. Zywietz, T. K.; Jiao, H.; Schleyer, P. v. R.; de Meijere, A. Aromaticity and antiaromaticity in oligocyclic annelated five-membered ring systems. *J. Org. Chem.* **1998**, *63*, 3417–3422.
304. El Bakouri, O.; Smith, J. R.; Ottosson, H. Strategies for design of potential singlet fission chromophores utilizing a combination of ground-state and excited-state aromaticity rules. *J. Am. Chem. Soc.* **2020**, *142*, 5602–5617.
305. Grimme, S.; Hansen, A. A practicable real-space measure and visualization of static electron-correlation effects. *Angew. Chem. Int. Ed.* **2015**, *54*, 12308–12313.
306. Kabuto, C.; Fujimori, K.; Yasunami, M.; Takase, K.; Morita, N.; Asao, T. Structure of methyl 10-ethylidicyclohepta [cd,gh] pentalene-5-carboxylate, C₂₀H₁₆O₂. *Acta Crystallogr., Sect. C: Cryst. Struct. Commun.* **1983**, *39*, 1245–1248.
307. Mathey, P.; Lirette, F.; Fernández, I.; Renn, L.; Weitz, T.; Morin, J.-F. Annulated Azuleno[2,1,8-ija]azulenes: Synthesis and Properties. *Angew. Chem. Int. Ed.* **2023**, *e202216281*.
308. Koseki, S.; Nakajima, T.; Toyota, A. Violation of Hund's multiplicity rule in the electronically excited states of conjugated hydrocarbons. *Can. J. Chem.* **1985**, *63*, 1572–1579.
309. Toyota, A.; Nakajima, T. Violation of Hund's multiplicity rule in the lowest excited singlet–triplet pairs of cyclic bicalicene and its higher homologues. *J. Chem. Soc., Perkin Trans. 2* **1986**, 1731–1734.
310. Toyota, A. Violation of Hund's rule in the lowest excited singlet-triplet pairs of dicyclohepta[cd,gh]pentalene and dicyclopenta[ef,kl]heptalene. *Theor. Chim. Acta* **1988**, *74*, 209–217.
311. Yoneda, S.; Shibata, M.; Kida, S.; Yoshida, Z.-i.; Kai, Y.; Miki, K.; Kasai, N. A Novel Aromatic Hydrocarbon with 16 π -Electron Periphery: "Cyclic Bicalicene". *Angew. Chem. Int. Ed.* **1984**, *23*, 63–64.
312. Sugimoto, T.; Shibata, M.; Yoneda, S.; Yoshida, Z.; Kai, Y.; Miki, K.; Kasai, N.; Kobayashi, T. Electronic structure of cyclic bicalicenes. *J. Am. Chem. Soc.* **1986**, *108*, 7032–7038.

313. Shainyan, B. A.; Fettke, A.; Kleinpeter, E. Push-pull vs captodative aromaticity. *J. Phys. Chem. A* **2008**, *112*, 10895–10903.
314. Oziminski, W.; Palusiak, M.; Dominikowska, J.; Krygowski, T.; Havenith, R.; Gibson, C.; Fowler, P. Capturing the elusive aromaticity of bicalicene. *Phys. Chem. Chem. Phys.* **2013**, *15*, 3286–3293.
315. Mandado, M.; Ramos-Berdullas, N. Tunable aromaticity in bicalicenes. *Phys. Chem. Chem. Phys.* **2015**, *17*, 16826–16834.
316. Baird, N. C. Quantum organic photochemistry. II. Resonance and aromaticity in the lowest $3\pi\pi^*$ state of cyclic hydrocarbons. *J. Am. Chem. Soc.* **1972**, *94*, 4941–4948.
317. Rosenberg, M.; Dahlstrand, C.; Kilså, K.; Ottosson, H. Excited state aromaticity and antiaromaticity: opportunities for photophysical and photochemical rationalizations. *Chem. Rev.* **2014**, *114*, 5379–5425.
318. Escayola, S.; Tonnelé, C.; Matito, E.; Poater, A.; Ottosson, H.; Solà, M.; Casanova, D. Guidelines for Tuning the Excited State Hückel–Baird Hybrid Aromatic Character of Pro-Aromatic Quinoidal Compounds. *Angew. Chem. Int. Ed.* **2021**, *60*, 10255–10265.
319. Karadakov, P. B. Ground- and excited-state aromaticity and antiaromaticity in benzene and cyclobutadiene. *J. Phys. Chem. A* **2008**, *112*, 7303–7309.
320. Karadakov, P. B. Aromaticity and antiaromaticity in the low-lying electronic states of cyclooctatetraene. *J. Phys. Chem. A* **2008**, *112*, 12707–12713.
321. Blaskovits, J. T.; Garner, M. H.; Corminboeuf, C. Symmetry-Induced Singlet-Triplet Inversions in Non-Alternant Hydrocarbons. *Angew. Chem. Int. Ed.* **2023**, e202218156.
322. Poelking, C.; Andrienko, D. Design rules for organic donor–acceptor heterojunctions: pathway for charge splitting and detrapping. *J. Am. Chem. Soc.* **2015**, *137*, 6320–6326.
323. Rühle, V.; Lukyanov, A.; May, F.; Schrader, M.; Vehoff, T.; Kirkpatrick, J.; Baumeier, B.; Andrienko, D. Microscopic simulations of charge transport in disordered organic semiconductors. *J. Chem. Theory Comput.* **2011**, *7*, 3335–3345.

J. Terence Blaskovits

✉ jacob.blaskovits@epfl.ch
ID <https://orcid.org/0000-0002-1452-5508>
☎ +41 216 93 72 45

Curriculum Vitae
June 2023

Academic Record

- 2019 – 2023 ■ **PhD in Computational Chemistry**, Swiss Federal Institute of Technology/EPF Lausanne (Switzerland)
Thesis title: *Data-driven design of organic electronic materials*.
Thesis supervisor: Prof. Clémence Corminboeuf
- 2016 – 2018 ■ **MSc in Polymer Chemistry and Computational Chemistry**, Université Laval (Canada)
Thesis title: *A computational study of direct (hetero)arylation polymerization*.
Thesis supervisors: Prof. Mario Leclerc, Prof. Paul Johnson
Canadian Institute for Advanced Research Bio-Inspired Solar Energy Program trainee
Research stay: Harvard University (USA) with Prof. Alan Aspuru-Guzik (6 months)
- 2012 – 2016 ■ **BSc in Chemistry with International Profile**, Université Laval (Canada)
International mobility: semester at Université de Strasbourg (France)
Research projects: radioanalytical chemistry (Prof. D. Larivière), frustrated Lewis pair chemistry (Prof. F.-G. Fontaine), polymer chemistry (Prof. M. Leclerc)

Selected Publications

Please consult the attached publication list for full details.

- 1 Blaskovits, J. T., Garner, M. H., & Corminboeuf, C. (2023). Symmetry-induced singlet-triplet inversions in non-alternant hydrocarbons. *Angewandte Chemie International Edition*, e202218156.
- 2 Blaskovits, J. T., Laplaza, R., Vela, S., & Corminboeuf, C. (2023). Data-driven discovery of organic electronic materials enabled by hybrid top-down/bottom-up design. *ChemRxiv preprint*.
- 3 Blaskovits, J. T., Fumanal, M., Vela, S., & Corminboeuf, C. (2020). Designing singlet fission candidates from donor-acceptor copolymers. *Chemistry of Materials*, 32(15), 6515–6524.
- 4 Blaskovits, J. T., & Leclerc, M. (2019). Direct (hetero)arylation polymerization for the preparation of conjugated polymers. *The Handbook of Conducting Polymers, 4th Edition*, 195–238.

Selected Presentations

- 16th International Materials Chemistry conference, Dublin, Ireland, 2023 – Oral presentation
- University of Alberta Department of Chemistry seminar, Edmonton, Canada, 2023 – Invited oral presentation
- European Materials Research Society spring meeting, Strasbourg, France, 2023 – Oral presentation
- Croatian Chemical Society – Section for Theoretical and Computational Chemistry seminar, Zagreb, Croatia, 2023 – Oral presentation
- International Thermally-Activated Delayed Fluorescence workshop, Fukuoka, Japan, 2022 (Online) – Oral presentation
- World Association of Theoretical and Computational Chemists (WATOC) triennial congress, Vancouver, Canada, 2022 – Poster
- American Chemical Society fall meeting, Atlanta, USA, 2021 (Online) – Oral presentation
- Theoretical Physical Organic Chemistry meeting, Houston, USA, 2021 (Online) – Oral presentation
- Swiss Chemical Society fall meeting, Geneva, Switzerland, 2020 (Online) – Oral presentation
- Materials Research Society spring meeting, Phoenix, USA, 2018 – Oral presentation

115

Selected Presentations (continued)

- *Canadian Institute for Advanced Research (CIFAR) Bio-Inspired Solar Energy* program meeting, Toronto, Canada, 2018 – Invited oral presentation
- *Québec Center for Advanced Materials* annual conference, Sherbrooke, Canada, 2017 – Oral presentation
- *CIFAR Bio-Inspired Solar Energy* program meeting, Montréal, Canada, 2016 – Invited oral presentation
- *CIFAR Bio-Inspired Solar Energy* program meeting, Vancouver, Canada, 2016 – Invited oral presentation

Other Merits

Selected Scholarships and Prizes

- 2022 Finalist, *Three-minute thesis* competition for scientific popularization (EPFL)
- 2018 Department of Chemistry Award for Excellence in a Master's thesis defense, Université Laval
Travel Grant, Natural Sciences and Engineering Research Council of Canada (NSERC, \$1,755)
- 2017 Richard J. Schmeelk Canada Fellowship, Schmeelk Foundation
full graduate funding for anglophone students studying at a francophone university (\$25,000)
Scholarship for Canadian Francophonie, Fonds de recherche du Québec (\$15,000)
Canadian Graduate Scholarships Master's Program, NSERC (\$17,500)
- 2016 Michael Smith Foreign Study Supplement for research stay abroad, NSERC (\$6,000)
German Academic Exchange Service Study Scholarship, TU Dresden (€20,000, declined)
Medal of the Lieutenant-Governor of Québec for Youth, Government of Québec
Canadian Society for Chemistry medal, Université Laval
Lucien-Piché Foundation – Paraza Pharma Scholarship, Order of Chemists of Québec
for the top student in Quebec in the final year of a chemistry-related BSc program (\$2,000)
- 2015 Hypercube scholar award for the highest academic average, Hypercube Inc.
- 2014 – 2018 Roger-Mahé scholarship for academic excellence, Government of Alberta (\$4,000)
- 2014, 2015 Undergraduate Student Research Award, NSERC (\$12,000)
Best oral presentations, University of Sherbrooke Undergraduate Chemistry Symposium (1st place - 2015, 2nd place - 2014; \$500)
- 2012 – 2016 Inaugural Schulich Leader Scholarship, Université Laval (full funding for a four-year degree)
largest scholarship in Canada; for academic excellence and community leadership (\$60,000)
- 2012 Governor General of Canada's Academic Medal, Government of Canada

Teaching Experience

- 2023 *MSc research project* supervisor in machine learning for materials design (EPFL)
- 2022 *Organic electronic materials* teaching assistant (EPFL/ETH Zürich)
- 2021 *From Atoms to Computers* academic summer camp co-organizer and presenter (NCCR-MARVEL/EPFL)
MSc research project supervisor in computational materials design (EPFL)
- 2020 *BSc research project* supervisor in materials modelling (EPFL)
- 2019 – 2021 *Advanced general chemistry* teaching assistant (EPFL)
- 2018 – 2019 Teacher of mathematics, science and music, Gandhi Ashram School (Kalimpong, India)
- 116 *One-year volunteer teaching position at a Jesuit-run school for underprivileged youth*
- 2018 *Practical Assignments in Organic Synthesis* teaching assistant (Université Laval)

Other Merits (continued)

2017 *The Quantum World* EdX online course tester (Harvard University/HarvardX)

Scientific Mobility

2018 Visiting student at Stanford University (USA) with Prof. Todd Martinez (2 months)

Organizational Contributions

- 2019 – 2023 Organizer of lab visits and presentations for undergraduate and school students (EPFL, Switzerland)
- 2016 Session organizer and co-chair, CIFAR Bio-Inspired Solar Energy Program Meeting (Montréal, Canada)

Other Activities and Social Engagement

- 2009 – *ongoing* First violinist in 9 symphony and chamber orchestras (Canada, France, Belgium, USA, India, Switzerland)
- 2008 – *present* 11 half-marathons, marathons and mountain half-marathons (Canada, USA, Switzerland)
- 2000 – *present* Hiking, cycling, canoeing, and mountain-trekking (Canada, India, Nepal, Switzerland)

References

Prof. Clémence Corminboeuf

Professor

École polytechnique fédérale de Lausanne
BCH 5312, Av. F.-A. Forel 2,
CH-1015 Lausanne, Switzerland.

✉ clemence.corminboeuf@epfl.ch

Prof. Mario Leclerc

Professor

Université Laval
Pav. A.-Vachon 2240-C, 1045 Av. de la médecine,
Québec G1V 0A6, Canada.

✉ mario.leclerc@chm.ulaval.ca

Prof. Paul A. Johnson


Associate professor

Université Laval

Pav. A.-Vachon 1203, 1045 Av. de la médecine,
Québec G1V 0A6, Canada.

✉ paul.johnson@chm.ulaval.ch

J. Terence Blaskovits - Publication list

 <https://orcid.org/0000-0002-1452-5508>

Google Scholar: [hJgesv4AAAAJ](https://scholar.google.com/citations?user=hJgesv4AAAAJ)

PUBLICATION SUMMARY

Peer-reviewed journal publications: 15

Peer-reviewed book chapters: 1

First-authored publications: 12

Manuscripts submitted or in preparation: 3

h-index (Google Scholar): 11

PEER-REVIEWED JOURNAL PUBLICATIONS

† These authors contributed equally.

15. **Blaskovits, J. T.**†; Garner, M. H.†; Corminboeuf, C. Symmetry-induced singlet-triplet inversions in non-alternant hydrocarbons. *Angewandte Chemie International Edition*, **2023**, e202218156. <https://doi.org/10.1002/anie.202218156>
14. **Blaskovits, J. T.**; Fumanal, M.; Vela, S.; Cho, Y.; Corminboeuf, C. Heteroatom oxidation controls singlet-triplet energy splitting in singlet fission building blocks. *Chemical Communications*, **2022**, 58 (9), 1338–1341. <https://doi.org/10.1039/d1cc06755a>
13. Das, S.; Laplaza, R.; **Blaskovits, J. T.**; Corminboeuf, C. Mapping active site geometry to activity in immobilized frustrated Lewis pair catalysts. *Angewandte Chemie International Edition*, **2022**, 134 (32), e202207938. <https://onlinelibrary.wiley.com/doi/10.1002/anie.202207938>
12. **Blaskovits, J. T.**†; Lin, K.-H.†; Fabregat, R.; Swiderska, I.; Wu, H.; Corminboeuf, C. Is a single conformer sufficient to describe the reorganization energy of amorphous organic transport materials? *The Journal of Physical Chemistry C*, **2021**, 125 (31), 17355–17362. <https://doi.org/10.1021/acs.jpcc.1c04067>
11. Dong, Z.; **Blaskovits, J. T.**; Fadaei-Tirani, F.; Scopelliti, R.; Sienkiewicz, A.; Corminboeuf, C.; Severin, K. Tuning the π -accepting properties of mesoionic carbenes: A combined computational and experimental study. *Chemistry – A European Journal*, **2021**, 27 (46), 11983–11988. <https://doi.org/10.1002/chem.202101742>
10. **Blaskovits, J. T.**; Fumanal, M.; Vela, S.; Fabregat, R.; Corminboeuf, C. Identifying the trade-off between intramolecular singlet fission requirements in donor-acceptor copolymers. *Chemistry of Materials*, **2021**, 33 (7), 2567–2575. <https://doi.org/10.1021/acs.chemmater.1c00057>
9. **Blaskovits, J. T.**; Fumanal, M.; Vela, S.; Corminboeuf, C. Designing singlet fission candidates from donor-acceptor copolymers. *Chemistry of Materials*, **2020**, 32 (15), 6515–6524. <https://doi.org/10.1021/acs.chemmater.0c01784>
8. **Blaskovits, J. T.**; Johnson, P. A.; Leclerc, M. Mechanistic origin of β -defect formation in thiophene-based polymers prepared by direct (hetero)arylation. *Macromolecules*, **2018**, 51 (20), 8100–8113. <https://doi.org/10.1021/acs.macromol.8b01142>
7. **Blaskovits, J. T.**; Leclerc, M. C-H activation as a shortcut to conjugated polymer synthesis. *Macromolecular Rapid Communications*, **2018**, 40 (1), 1800512. <https://doi.org/10.1002/marc.201800512>
6. Zindy, N.; **Blaskovits, J. T.**; Beaumont, C.; Michaud-Valcourt, J.; Saneifar, H.; Johnson, P. A.; Bélanger, D.; Leclerc, M. Pyromellitic diimide-based copolymers and their application as stable cathode active materials in lithium and sodium-ion batteries. *Chemistry of Materials*, **2018**, 30 (19), 6821–6830. <https://doi.org/10.1021/acs.chemmater.8b02862>
5. Sun, J.-P.; **Blaskovits, J. T.**; Bura, T.; Beaupré, S.; Leclerc, M.; Hill, I. G. Photovoltaic device performance of highly regioregular fluorinated poly(3-hexylthiophene). *Organic Electronics*, **2017**, 50, 115–120. <https://doi.org/10.1016/j.orgel.2017.07.033>
- 14.8 Bura, T.; Beaupré, S.; Légaré, M.-A.; Quinn, J.; Rochette, E.; **Blaskovits, J. T.**; Fontaine, F.-G.; Pron, A.; Li, Y.; Leclerc, M. Direct heteroarylation polymerization: Guidelines for defect-free conjugated polymers. *Chemical Science*, **2017**, 8 (5), 3913–3925. <https://doi.org/10.1039/c7sc00589j>

3. **Blaskovits, J. T.**†; Bura, T.†; Beaupré, S.; Lopez, S. A.; Roy, C.; de Goes Soares, J.; Oh, A.; Quinn, J.; Li, Y.; Aspuru-Guzik, A.; Leclerc, M. A study of the degree of fluorination in regioregular poly(3-hexylthiophene). *Macromolecules*, **2016**, *50* (1), 162–174. <https://doi.org/10.1021/acs.macromol.6b02365>
2. Pouliot, J.-R.; Grenier, F.; **Blaskovits, J. T.**; Beaupré, S.; Leclerc, M. Direct (hetero)arylation polymerization: Simplicity for conjugated polymer synthesis. *Chemical Reviews*, **2016**, *116* (22), 14225–14274. <https://doi.org/10.1021/acs.chemrev.6b00498>
1. Bura, T.†; **Blaskovits, J. T.**†; Leclerc, M. Direct (hetero)arylation polymerization: Trends and perspectives. *Journal of the American Chemical Society*, **2016**, *138* (32), 10056–10071. <https://doi.org/10.1021/jacs.6b06237>

PEER-REVIEWED BOOK CHAPTERS

1. **Blaskovits, J. T.**; Leclerc, M. Direct (hetero) arylation polymerization for the preparation of conjugated polymers. In T. A. Skotheim, B. C. Thompson J. R. Reynolds (Eds.), *The handbook of conducting polymers, 4th edition* (pp. 195–238). CRC Press, **2019**. <https://doi.org/10.1201/b22233>

MANUSCRIPTS SUBMITTED OR IN PREPARATION

3. **Blaskovits, J. T.**; Laplaza, R.; Vela, S.; Corminboeuf, C. Data-driven discovery of organic electronic materials enabled by hybrid top-down/bottom-up design. **2023**, *Submitted*. *ChemRxiv preprint*: <https://doi.org/10.26434/chemrxiv-2022-88t32>
2. Garner, M. H.†; **Blaskovits, J. T.**†; Corminboeuf, C. Double-bond delocalization in non-alternant hydrocarbons induces inverted singlet-triplet gaps. **2023**, *Submitted*. *ChemRxiv preprint*: <https://doi.org/10.26434/chemrxiv-2023-568ks>
1. Das, S.; Laplaza, R.; **Blaskovits, J. T.**; Corminboeuf, C. Engineering frustrated Lewis pair active sites in metal-organic frameworks for catalytic CO₂ hydrogenation. **2023**, *Submitted*. *ChemRxiv preprint*: <https://doi.org/10.26434/chemrxiv-2023-09mdd>